STUDY OF ReBCO AND BSCCO SUPERCONDUCTORS AT RADIO AND MICROWAVE FREQUENCIES

THESIS SUBMITTED FOR THE DEGREE OF
DOCTOR OF PHILOSOPHY

BY
P. V. PATANJALI

SCHOOL OF PHYSICS
UNIVERSITY OF HYDERABAD
HYDERABAD - 500 046
INDIA

DECLARATION

I hereby declare that the work presented in the thesis entitled **"Study of ReBCO and BSCCO Superconductors at Radio and Microwave Frequencies",** has been carried out by me under the supervision of Dr. V.Seshu Bai, at the School of Physics, University of Hyderabad. I also declare that no part of the thesis or the thesis as a whole has not been submitted to any university or institution for the award of any degree or diploma.

Place: Hyderabad **P.V.PATANJALI**

Date : 15-3-97

CERTIFICATE

This is to certify that the research work compiled in this thesis entitled " **Study of ReBCO and BSCCO Superconductors at Radio and Microwave Frequencies** " has been carried out by Mr. P.V.Patanjali under my supervision and the same has not been submitted elsewhere for the award of any degree.

V. Seshu Bai

Date: March 15, 1997

Dr. V.Seshu Bai

Dean

School of Physics

ACKNOWLEDGMENT

I wish to thank my supervisor, Dr. Mrs. V.Seshu Bai, for introducing me to high frequency studies and for her guidance during the course of my Ph.D work.

I thank Prof. K.N.Srivastava and Prof. A.P.Pathak, the present and former Deans of the School of Physics, for providing me with necessary infrastructural facilities, and the technical staff for their help.

I thank Dr. M.D.Sastry, Prof. S.M.Bhagat and Dr. T.Rajasekaran for helpful discussions and the latter, especially, for providing me with melt textured superconductors.

I thank my colleagues Ravi, Harish Kumar, Sudhakar Reddy, Visvanath, Hari Babu, Isaac and Radhika for their cooperation during various stages of my work. I thank my parents, siblings and friends for their deep understanding and constant encouragement.

I thank the members of the Andhara Pradesh Photographic Society, the Bird Watcher's Society of Andhra Pradesh and the University of Hyderabad Adventure Club for making my stay in Hyderabad enriching and pleasurable. 1 thank the University grants Commission (UGC) for providing me with fellowship to carry out the thesis work.

Preface

The high T_c cuprate superconductors are highly anisotropic, layered type-II superconductors with very short coherence lengths of the order of cell dimensions. This makes it possible for the ceramic superconductors to have a variety of inter- and intra grain defect structures which form weaklinks in these materials at various levels. The presence of such extrinsic but ubiquitous defects makes the electromagnetic response of these materials very sensitive to the applied field and temperature. Measurement of surface resistance of HTSCs has attracted maximum attention in literature and by and large this is the most thoroughly investigated property at microwave frequencies. This is because R_s is an important parameter as it determines power dissipation. Surface reactance, on the other hand, gives a wealth of information on the penetration depth (A) charaterising the HTSCs and the magnetic properties.

Magnetically modulated microwave absorption as a function of temperature and low field are two important techniques which can be used to determine the transition temperatures and loss mechanisms, respectively. However, because there is considerable hysteresis in the power absorption and the sample is in a nonequilibrium state during field cycling, the above two techniques, though very sensitive, suffer from a few disadvantages. Direct power absorption is a simple and better tool to study the virgin response of HTSCs. Several authors have used these techniques to study the loss mechanism in these superconductors at microwave frequencies. But to the best of our knowledge, but for a few brief reports, no detailed study has been carried out at radio frequencies.

In the present thesis a detailed study of the high frequency loss mechanisms, penetration depth and the associated novel features such as paramagnetic Meissner effect are presented. The thesis is divided into seven chapters of which chapter 1 consists of a general introduction to HTSCs and high frequency study. It also summarizes the work done in literature relevant to non-resonant microwave absorption. Chapter 2 describes the experimental techniques developed for rf (MHz) measurements. The construction of a rf marginal oscillator for the measurement of change in power absorption and frequency is described.

Chapter 3 consists of a systematic study of rf (11.9 MHz) absorption in sintered BSCCO and GdBCO samples. In the case of BSCCO the results are discussed in the frame work of resistively shunted Josephson junction (RSJ) model. It is also found that the junctions responsible for the absorption are of SIS type. In the case of GdBCO sample the field induced loss is found to be following a combination of RSJ and decoupled junction models. The temperature variation of rf absorption of BSCCO and GdBCO are found to follow the London's two fluid equation.

Chapter 4 describes the results of rf and microwave absorption at high fields obtained on various HTSC, namely, sintered GdBCO and melt textured GdBCO with various percentages of Re_2BaCO_5(211), sintered and press sintered BSCCO samples. The results are explained by invoking flux flow model. It is found that melt textured samples do not show any appreciable microwave and rf absorption at low fields and thus are best suited for bulk device applications at these frequencies. At high fields the increase in the percentage of 211 is found to enhance pinning in these materials.

In chapter 5 the results of field modulated microwave absorption at 9.98 GHz on sintered pellet, powder and melt textured samples of GdBCO are presented. In the case of GdBCO powder, an anomalous zero filed maximum followed by minima at ± 0.6 has been observed which has been attributed to the π junctions and the paramagnetic Meissner effect. Various possible origins of π junctions from $d_{x^2-y^2}$ symmetry consideration and Gd^{3+} impurity moments are discussed.

In Chapter 6 the results of temperature and field variation of frequency shift of the rf oscillator are reported. Generally, for any superconductor the frequency of oscillator increases as the sample is cooled to below its transition temperature. However, in the case of BSCCO samples an anomalous frequency decrease is observed in the tail region as the sample is cooled. The anomaly is attributed to a change over from intra to inter grain contribution to the penetration depth. In the case of GdBCO sintered pellet an extremely unusual frequency decrease is observed as the sample is cooled which is discussed in relation to the temperature dependent frequency shift of the DyBCO sintered pellet, which also has 3+ moments. The possibility of Gd^{3+} moments interacting with the Josephson currents thus giving rise to such an anomaly is also discussed. Chapter 7 summarizes the results reported in 2,3,4,5 and 6 chapters and gives an overall picture of the rf response in relation to that at microwave frequencies.

CONTENTS

Chapter 1

INTRODUCTION

1.1. General History

In 1911 Kamerlingh Onnes [1] discovered that the electrical resistivity of mercury became zero at 4.2 K and called the unusual phenomenon superconductivity. He also discovered that there was a threshold value of the current density that can be carried by a superconducting sample before it reverts to its normal state and that a magnetic field could destroy superconducting effect as well [2J. In 1933 Meissner and Ochenfeld [3] found another important property, that the superconductor expels the flux inside it and becomes diamagnetic, when cooled to below its transition temperature. The effect has since been called Meissner effect. Thus, superconductors represent a class of materials whose electrical resistivity goes to zero and which exhibit diamagnetism below a certain temperature called the transition temperature, T_c.

The application of magnetic field on a superconductor generates a spontaneous diamagnetic current on the surface of the superconductor. The applied magnetic field penetrates into the superconductor through a thin layer decaying in intensity exponentially. The distance at which the applied field decays to $1/e$ of the field at the surface is called London penetration depth λ_L and the magnetic field inside a superconductor is

$$B = B_0 e^{-x/\lambda_L}$$

where, B_0 is the magnetic induction at the surface. London [4] modified Maxwells electrodynamic equations to explain the flux expulsion and the equations are given by

$$curl J_s = \frac{-1}{\mu_0 \lambda_L^2 B}$$

and

$$J_s = \frac{1}{\mu_0 \lambda_L^2}$$

where J_s is the supercurrent density, B is the magnetic field induction and E is the electric field inside the superconductor. In terms of mass m and charge e of electrons λ_L is given by

$$\lambda_L = \sqrt{\frac{m}{\mu_0 n_s e^2}}$$

where, n_s is the superelectron density. In 1949 Pippard [5] introduced another characteristic length of a superconductor, the coherence length, ξ, which is the distance through which cooper pair electrons are correlated or superconductor order parameter does not vary appreciably.

Depending on the magnetic properties, superconductors are classified as type I and type II superconductors [6]. Type I materials are perfectly diamagnetic upto a critical field $H_c(T)$ above which they are normal. Whereas, type II materials exhibit perfect diamagnetism upto a lower critical field $H_{c1}(T)$ above which they enter

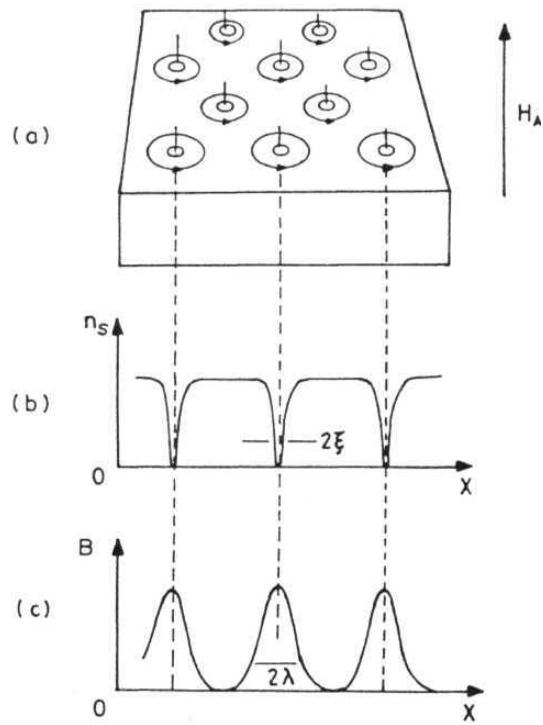

Fig. 1 Mixed state of a type II superconductor when the applied magnetic field is greater than H_{c1}, (a) triangular vortex lattice, (b) variation of superelectron density and (c) variation of flux density. (ref. 6)

a mixed state up to an upper critical field $H_{c2}(T)$ beyond **which they reach normal** state. In the mixed state the flux enters the superconductor partially though the sample is electrically superconducting. Some type II superconductors may show surface superconductivity above H_{c2} up to a field H_{c3}. The existence of mixed state is explained by Abrikosov on the basis of surface energy considerations. He showed that the surface energy of a superconductor-normal interface which is proportional to $\mu_0 H_c^2(\xi - \lambda)$, can be positive or negative depending on whether ξ > A or A > ξ and in the latter case it is energetically favorable for the material to go into a mixed state with alternate superconductor and normal regions than turning completely normal above H_{C1}. The normal regions form vortex tubes with each vortex tube carrying one flux quantum ϕ_0. The vortex tubes thus formed repel each other and arrange themselves into a triangular lattice as shown in the Fig. 1.

1.2. High Temperature Superconductivity.

Discovery

The discovery of superconductivity in La-Ba-Cu-0 system at 30K by Bednorz and Muller [7] catapulted the research in superconductivity, which was otherwise thought to be saturated. BCS theory predicts that for a phonon mediated pairing mechanism, such as that existing in metals, the critical temperature cannot be higher than 20-30K. Scientists therefore had a little hope of reaching 30K upper bound. Soon after their discovery several oxide superconductors have been made. Chu *et. al* [8] found that T_c of $La_{2-x}Ba_xCuO_{4-y}$ can be increased up to 42.5K by the application of pressure. The replacement of Ba with Sr was found to be enhancing the T_c by

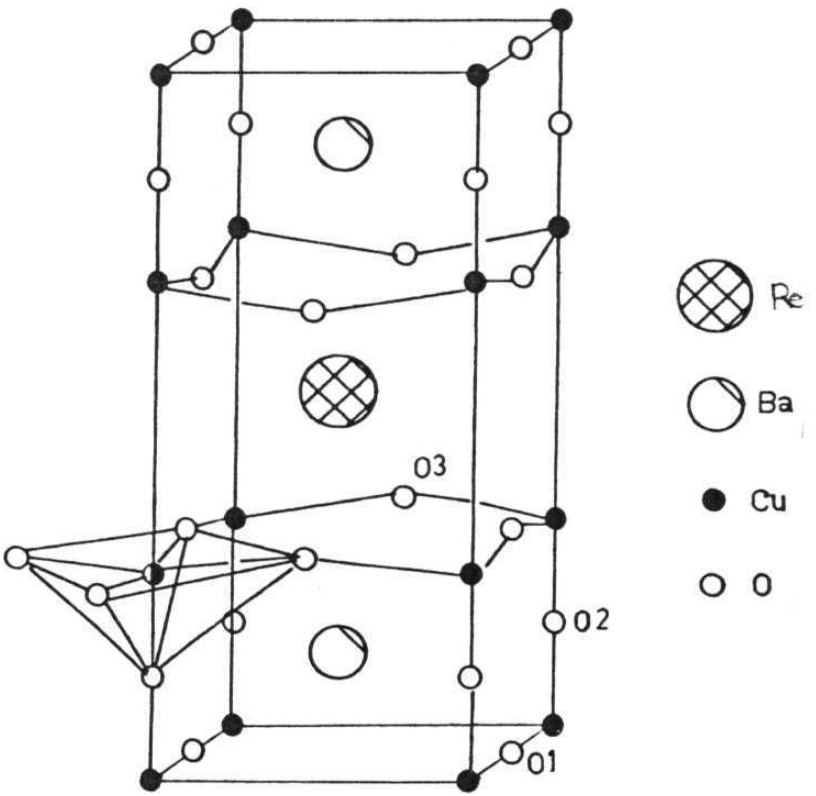

Fig. 2 Structure of ReBCO, the orthorhombic unit cell.

about 6K. Wu *et. al* [9] discovered superconductivity in $YBa_2Cu_3O_{7-\delta}$ (YBCO) at 92K. The replacement of Yittrium by most of the rare earth elements (except Pr, Ce and Tb) resulted in no change in the T_c and the structures of all the compounds are orthorhombic (except Pr which favors tetragonal) at room temperature. The superconducting properties of YBCO are very sensitive to oxygen content. The T_c can be varied from 92K to 45K by increasing *6* from 0 to 0.5; the compounds with *6* > 0.5 do not superconduct. At the beginning of 1988 Maeda *et. al* [10] reported superconductivity in Ba-Sr-Ca-Cu-0 (BSCCO) at 110K. The drawback of this material is the presence of lower T_c phases which always appeared in the final product. The search for better materials continued actively; in the same year Sheng and Hermann [11] presented a new material Tl-Ba-Ca-Cu-O with T_c of 120K, in 1993 Putilin *et. al* [12] found superconductivity in Hg-Ba-Cu-0 system with T_c of 94K. Chu obtained T_c of150K in this material by applying high pressure. Lately, there have been many reports of increase in T_c up to 250K, however, the results are not reliable as they are not reproduced.

Structure

Two of the well studied HTSC systems are the rare earth ReBCO (Re=Y, Gd, Dy, Sm, Er, Ho and Nd) and BSCCO. The crystal structure of $ReBa_2Cu_3O_7$ (*ReBCO*) has been reported by several authors [13-16]. The orthorhombic structure of YBCO compound is shown in Fig. 2. The four cations (Re, Ba, Cu1 and Cu2) and 02 are in positions identical to those of the tetragonal form yielding the identical 1-2-2 structural module. Tetragonal 03 at (0, 1/2. 0.38) splits into two fully occupied *O3A* at (0, 1/2, 0.38) and *O3B* at (1/2, 0, 0.38) in the orthorhombic form. Similarly the

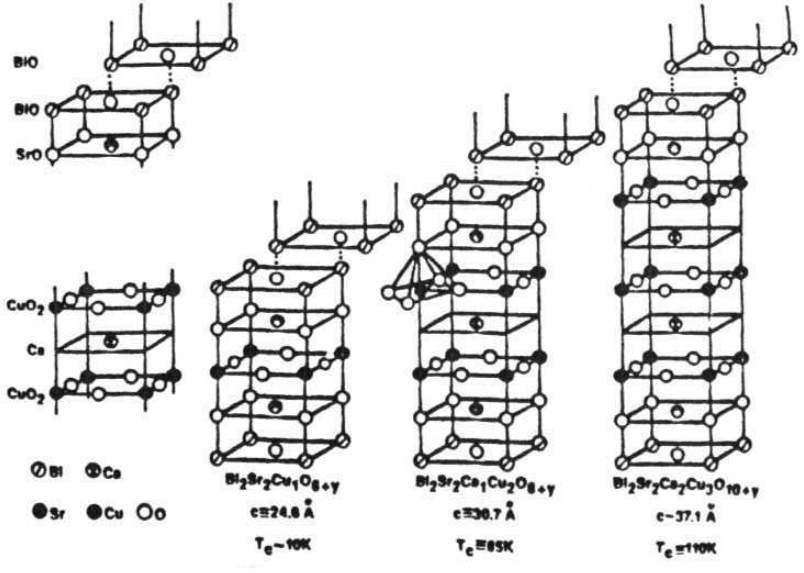

Fig. 3 Structures of Bi-Sr-Ca-Cu-O superconductors.

partially tetragonal 01 splits into *OlA* and *OlB* positions between the adjacent 1-2-2 slabs. In the tetragonal structure, these sites are symmetrically equivalent and must be equally occupied. In the orthorhombic structure, oxygen concentrates in *OlA* halfway along b-axis making b slightly larger than a. As a result, in ideal ReBCO the *OlA* is fully occupied while *OlB* is empty leading to distinct *Cu — 03* chains oriented parallel to b-axis. The lattice parameters of the orthorhombic YBCO are a = 3.82 A , b=3.88 A and c = 11.67 A.

The crystal structures of $Bi_2Sr_2CuO_y$(2201), $Bi_2Sr_2Ca_1Cu_2O_y$(2212) and $Bi_2Sr_2Ca_2Cu_3O_y$(2223) are shown in Fig. 3 as reported by Tarascon *et.al* [17]. The 2201 structure, shown in the Fig. 3a, consists of a Cu-02 layer sandwiched between two Sr-02 layers. The Cu is square coordinated by four $O1$ oxygens with Cu-O1 distances $\sim 1.94\mathring{A}$. The 02 oxygens lie immediately above and below each copper (Cu-02 = 2.6 A), thus forming an extremely elongated CuO_6 octahedron. Strontium has nine nearest oxygens with an average Sr-0 distance $\simeq 2.7A$. Four Bi-O3 bonds near the (001) plane range from 2.2 to 2.9 A , while the Bi-02 bond linking Bi to the Sr-02 layer is much shorter ($\approx 2.0\mathring{A}$). In contrast, the Bi-03 bond which joins adjacent sheets in $Bi_2\ O_2$ bilayers is longer than $3.0\mathring{A}$. This long and weak Bi-O3 bond parallel to the c-axis results in very weak interlayer bonding and mica-like mechanical behavior in all the Bi based superconductors.

The 2212 structure as shown in Fig. 3b is related to 2201 structure. The Cu-0 sheet in 2201 is replaced by CuO_2 /Ca/CuO_2 sandwiches in 2212. Calcium adopts eight coordination, similar to the Re environment in ReBCO. There are no oxygens at the Ca level. So copper atoms have only five neighbors in square pyramidal coor-

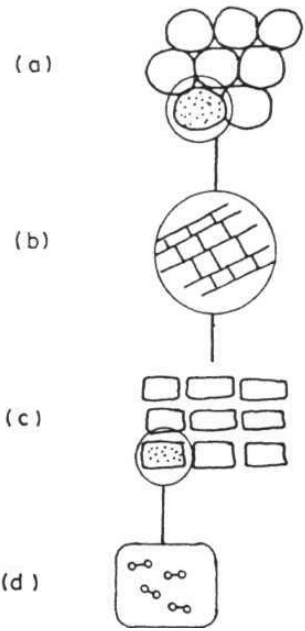

Fig. 4 Schematic display of physical situation in a ceramic pellet. (a) cluster of grains, (b) 2-D planes inside each grains, (c) 2-D array of domains and (d) microscopic mechanism (defects) inside a domain (ref.25).

dination rather than elongated octahedral coordination in 2201. The structural **slab** containing $SrO/CuO_2/Ca/CuO_2/SrO$ topologically identical to the $YBa_2Cu_2O_6$ (122) module portion of the YBCO structure.

The 2223 structure is related to the 2212 structure with additional Ca and $Cu-O2$ layers as shown in Fig 3c. The structural details of Bi — Sr — Ca — Cu — O system are very much complicated because of stacking faults, superstructural modulations, and oxygen and cation disorder. Different types of unit cells have been reported in literature [18-23] with different unit cell parameters. Tarascon *et.al* [17] reported pseudo-tetragonal symmetry for the 2201, 2212 and 2223 structures with unit cell parameters a = b = 5.4 A and c values 24.6, 30.6 and 37.1 A, respectively.

Granularity

The HTSCs are known to show many interesting physical properties which are qualitatively different when compared with the conventional superconductors. Unavoidable defects present in these materials can act as weaklinks because of very short coherence lengths ($\approx 10A$) [24]. This leads to granularity in these superconductors on different length scales, namely, intragrain, intergrain, interdomain etc. The ceramic samples have a disordered array of grains, shown in the Fig. 4a [25]. Inside each grain, there are weakly coupled two dimensional planes (Fig 4b). Each plane again has an array of domains (Fig. 4c) because of the heavy twinning or stacking faults in the system. And the other defects are within the lattice, oxygen vacant sites and the stacked arrays of alternate superconducting (CuO planes) and nonsuperconducting layers. Due to phase locking weak superconducting links may be formed at all these

defect sites leading to a glassy behavior of the material. These weaklinks greatly influence the transport, magnetic and electrodynamic properties.

1.3 Josephson junction

A superconductor can be described as a whole by a microscopic wave function $\psi = n_s^{1/} e^{\iota\theta}$ where 9 is the phase of the wave function. For a number of pairs N, the phase is undefined due to the uncertainty $\Delta N \Delta\theta > 2\pi$. But, if the phase is fixed at a point it is automatically fixed at all other points due to long range order. When two different superconductors are placed very close to each other or separated by a thin insulating layer, then their macroscopic wave functions overlap to form a weak coupling. If the coupling energy is greater than the thermal energy then Cooper pairs tunnel from one superconductor to the other with a phase correlation or phase locking. In such a case these weakly coupled superconductors behave as a single superconductor with [26] / = $I_c sin(\theta)$ and $d\theta/dt = (2eV/\hbar)$. Here, I_c is the critical current and V is the voltage across the junction. The coupling energy is given by $E_j = (-I_c\phi_0/2\pi)\cos\theta$. If V=0 then $ is constant therefore a finite zero-voltage current flows through the gap with maximum value of the current I_c. This is the dc Josephson effect. When $V \neq 0$ across the junction the current / = $I_c sin(\theta + (2eV/\hbar)t)$ oscillating with an angular frequency $\omega = 2eV/\hbar$. This is the ac Josephson effect.

Apart from the quantum mechanical tunneling of Cooper pairs across an insulating or normal barrier, Josephson junctions can be realized by various other means. A point contact or a constriction in the superconductor or a normal metal layer between two superconductors can form a Josephson junction. The metallic barrier gives

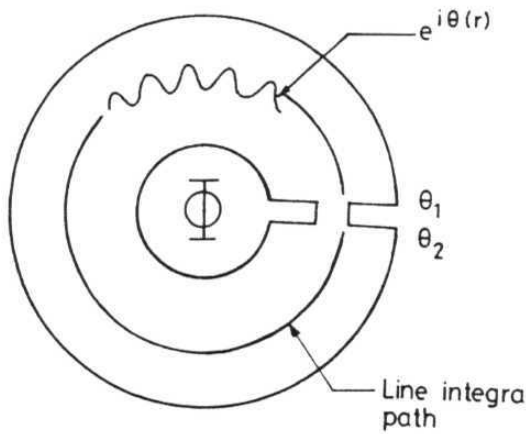

Fig. 5 Superconducting ring containing a weaklink (ref. 27).

a superconductor-normal-superconductor (SNS) junction and insulating **barrier gives** superconductor-insulator-superconductor (SIS) junction. Contrary to the conventional low T_c superconductors, in the HTSCs even single crystal possesses weaklinks. In the case of conventional low T_c superconductors where the coherence length is very large($\approx 1\mu$m), the atomic size defects have essentially no influence on superconductivity.

When a current flows through a network of Josephson junctions flux gets trapped. **One** such loop is shown in Fig. 5. In the absence of external field, the current I in the loop of inductance L gives rise to a flux enclosed by the loop as $\Phi = LI$, with $I = I_c sin(2\pi\Phi/\phi_0)$. The total energy of the Josephson junction loop is

$$E_J = \frac{1}{2}LI^2 - \frac{I_c\phi_0}{2\pi}cos\theta.$$

Writing $2\pi LJ_c/\phi_0 = 0$ one can readily see that if $0 < 1$ the ring cannot trap the flux. The loop is then nonhysteretic. For $0 > 1$ however, the loop can trap flux in a metastable state and becomes hysteretic. Thus the magnetic behavior of the loop is determined by the parameter β, which is generally called Stewart Mc Cumber parameter [27].

Lower critical field of a Josephson junction

The lower critical field of Josephson junction, H_{c1j} is much smaller than that of intrinsic H_{c1}. When the applied field exceeds $H_{c1J}=\phi_0/2\pi\lambda_J(2\lambda_L + d)$ [28] fluxons enter the junction. Here d is the thickness of the barrier and λ_J is the Josephson penetration depth (discussed below). The entry of fluxons is quantized as in the case

of bulk superconductor.

Josephson penetration depth

In a superconductor without any weaklinks, the magnetic field penetrates into the bulk of the superconductor to a depth equal to the London penetration depth. But in a superconductor with weaklinks present magnetic field penetrates first into the Josephson junctions since the lower critical field of the junctions is orders of magnitude smaller than that of the grains. This penetration depth is much larger than London penetration depth and is given by [28]

$$\lambda_J = \sqrt{\frac{\hbar c^2}{16\pi e J_c \lambda_L}}$$

where J_c is the critical current density across the junction, which is, again, orders of magnitude smaller than the bulk critical current density, so naturally λ_J is of macroscopic size.

1.4 Magnetization in HTSC

The partial penetration of flux in Type II superconductors for $H_{c1} < H_a < H_{c2}$ leads to characteristic magnetization behavior according as the flux is pinned or unpinned. When the applied field equals H_{c2} the fluxon cores begin to overlap and superconductivity is destroyed [6]. Fig. 6a shows the magnetization behavior of type II materials which are perfectly homogeneous without any defects or weaklinks. The curve is the same for both increasing and decreasing fields showing reversibility of

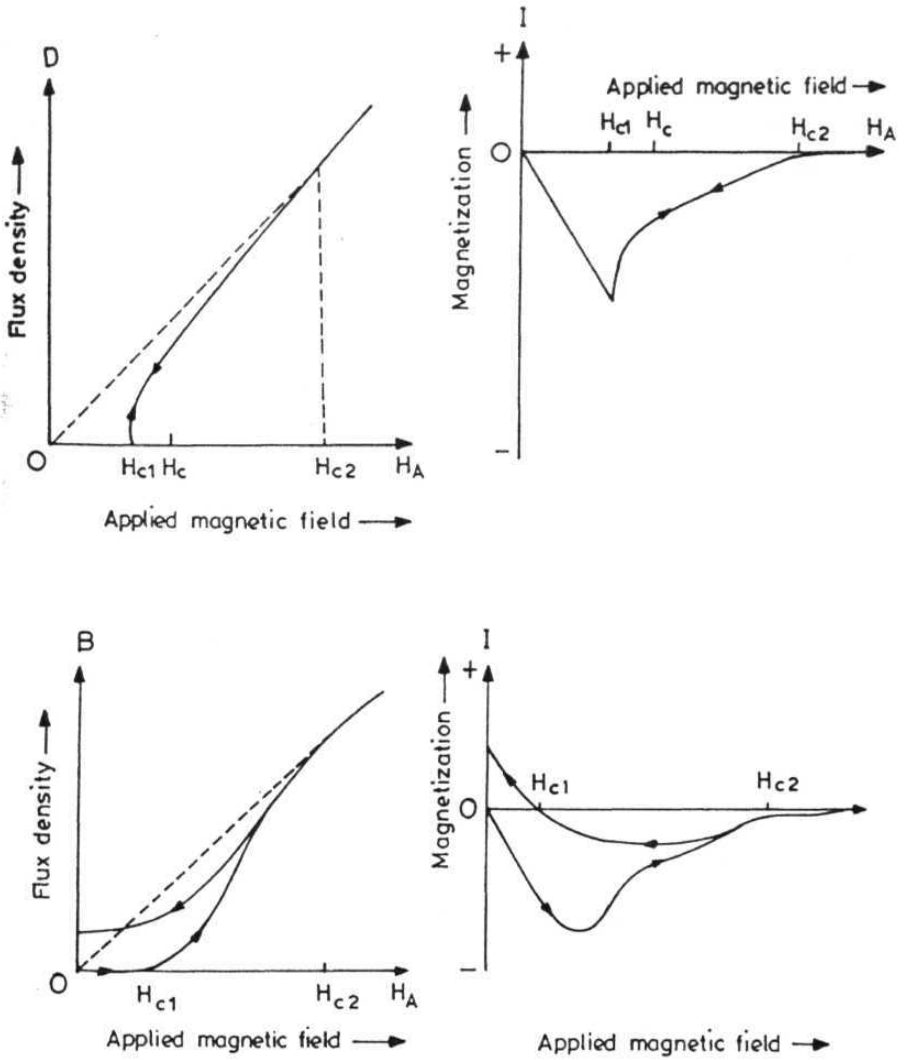

Fig. 6 Magnetization of a type II superconductor, (a) reversible magnetization and (b) irreversible magnetization.

magnetization. In a practical superconductor with lot of imperfections, fluxons get pinned at defect sites leading to irreversibility and hysteresis in the magnetization. When the applied field is increased, flux cannot enter suddenly at H_{c1} as fluxons pinned at the surface are not allowed to move into the interior of the sample freely. The same pinning centres do not allow the fluxons to leave the sample [6]. Fig. 6b shows the irreversible magnetization curves. The pinning energy is given by

$$U_p = \xi^3 H_c^2/(2\mu_0).$$

In HTSCs the very small value of ξ causes intrinsic pinning due to the discreteness of the lattice. Flux can also be held in its place when there is a strong interaction between the flux lines. In such a case, the force with which the entire flux lattice (flux bundle) is pinned determines the I_c (the macroscopic extrinsic critical current). The extrinsic I_c is orders of magnitude smaller than the intrinsic depairing current that arises from the unbinding of the Cooper pair at high superfluid velocity.

1.5 Flux flow

When a transport current passes through a superconductor whose state comprises of an arrangement of normal regions containing magnetic flux, the Lorentz interaction between the current and magnetic field produces a force which sets the flux in motion. Kim et. al [29] proposed a phenomenological picture with three forces acting on a moving vortex: the Lorentz force between the current J and the magnetic flux inside the vortex Φ_0; the pinning force F_P, and a viscous force proportional to a viscosity coefficient η and the flux tube velocity *v*. The forces satisfy the following condition for a steady motion of vortices

$$J \times \Phi_0 - \eta v - F_P = 0$$

The origin of the viscous term was explained by Bardeen and Stephen [30] and Vijfeijken and Niessen [31] who treated it theoretically with a generalized London model. When Lorentz force exceeds *Fp* fluxons will start moving and an e.m.f. $E = -v \times B$, is generated in the direction of the current which leads to dissipation. The minimum value of current to initiate the flux movement is $J_{min} = J_c = \frac{F_p}{\Phi_0}$.

Any current higher than the J_c gives rise to flux flow and therefore to losses. Thus for one dimensional motion, the emf

$$E = \frac{\phi_0 B}{\eta}(J - J_c).$$

Defining the **flux flow** resistivity ρ_f as the coefficient of proportionality between E and J, and considering that it must take the normal state value ρ_n when $B = B_{c2}$,

$$\rho_f = \rho_n \frac{B}{B_{c2}}$$

where the viscosity coefficient is related to the normal state resistivity **through**

$$\eta = \frac{\phi_0 B_{c2}}{\rho_n}.$$

The power dissipated by the viscous forces per unit volume, $p = J.E$ gives

$$p = \rho_n \frac{B}{B_{c2}} J(J - J_c)$$

and the speed of flux penetration is given by

$$v = \frac{\rho_n}{B_{c2}}(J - J_c)$$

which is constant in the case of applied current much higher than the shielding current. For the depinned fluxon state, the macroscopic critical current is zero even though thermodynamically the system has a condensate [32].

Apart from Lorentz force, the thermal energy kT can also make the fluxons hop from one pinning centre to the other (activated motion) [29]. Such hopping again, gives rise to losses in the material. The hopping rate is given by

$$R_{hopp}(T) = f_a exp(\frac{-U_p^{eff}(T)}{kT}),$$

where $U_p^{eff}(T) = U_p(T)(1 - J(T)/J_{c0})$ is the effective pinning potential, J_{c0} is the critical current without thermal depinning and f_a is the attempt frequency with which the fluxon tries to escape the pinning centre.

An important parameter influencing the mechanism of flux motion is the frequency of the current. At low frequencies the pinning forces dominate the dynamics while at higher frequencies there occurs depinning of the vortices and a transition to a viscous regime with dissipation. The depinning frequency is given by $f_c = \frac{\eta}{k}$, where η is the viscosity coefficient and k is the elastic constant associated with pinning forces.

Several studies of HTSC ceramics [33-35] have shown that Ω_c is in the microwave range for thin films and single crystals, and in the range 10^7 to 10^8 Hzs for sintered ceramics with Josephson junctions. At any temperature $T > 0$, there exists a fraction of free fluxons depinned which can move about slowly and can cause losses for even small currents in a thermally activated superconductor. This flux creep leads to quasi critical state. However, at low temperatures the effect of flux creep is negligible and J_c is determined by the voltage criterion.

1.6 High Frequency Response

The drawback of the dc electrical resistance measurement is, it needs a continuous sample. Alternatively, one can study the superconductors at high frequencies . Though a superconducting transition becomes less abrupt with increasing frequency , the high frequency method has a number of advantages since it probes the entire sample, at least within the penetration depth, and provides a tool for investigating superconductivity even in discontinuous samples which cannot be studied by conventional resistance measurements. In contrast to the dc resistance of superconductors, the ac resistance is non zero, because an alternating field can cause transitions between neighbouring states. The ac losses increase with temperature and angular frequency ω for small periodic fields, $H(t) = He^{i\omega t}$, here $H \ll H_c$, the thermodynamic critical field. These losses are determined by surface resistance R_s through the relation $P = \frac{R_s}{2} \int\int dS H^2$, where surface resistance R_s is the real part of the surface impedance Z. Z is the ratio of E and H components of the high frequency radiation [36].

The zero dc resistance and the **ac loss can be explained** using **the two fluid model for the** superconducting state. So long as $T > 0$, there will be quasi **particles or normal** electrons present, and Cooper pairs, condensed into a macroscopic quantum state. The charge carries are both the superconducting Cooper pairs and normal electrons. **The** Cooper pairs do not absorb the energy quanta less than a particular gap energy ($\approx$ 100 GHz) and therefore carry loss less currents which expel the magnetic field from the interior of the superconductor. Because the current density is finite the magnetic field penetrates into the superconductor. Because the magnetic field H penetrates into the superconductor the accompanying electric field, $E = \omega\mu_0\lambda_L H$, accelerates normal conducting electrons, which dissipate the gained energy in interaction with the lattice. The losses are then described by [37]

$$P = \frac{n_n}{2}\sigma \int dz E^2(z) = n_n\sigma\omega^2\mu_0^2\lambda_L^3 H^2$$

Surface Impedance

Surface impedance is an important parameter and has been the object of many measurements of HTSC. For superconductors obeying BCS theory the surface impedance has been examined by Carini *et. al* [38]. It is defined as $Z_s = R_s + \imath X_s$, R_s being surface resistance and X_s the surface reactance. In terms of complex conductivity $\sigma - \sigma_1 - \imath\sigma_2$, the surface impedance is

$$Z_s = \sqrt{\frac{\imath\mu_0\omega}{\sigma_1 - \imath\sigma_2}}.$$

If $\sigma_1 << \sigma_2$ (that is, if $\hbar\omega << k_B T$ and T is significantly below T_c), then the surface reactance and resistance are given by the following relations,

$$X_s = \omega\mu_0\lambda$$

$$R_s = \frac{1}{2}\sqrt{\frac{\mu_0\omega}{\sigma_2}}\left(\frac{\sigma_1}{\sigma_2}\right)$$

where A is the penetration depth whose temperature dependence is given by

$$\lambda = \frac{\lambda_0}{\sqrt{1-\left(\frac{T}{T_c}\right)^4}}$$

and

$$\sigma_2 = \frac{1}{\omega\mu_0\lambda^2}$$

The overall temperature and frequency dependence of R_s at low temperatures ($k_B T <<$ A) is

$$R_S = A\frac{\Delta}{T}\left(\frac{\omega^2}{\Delta}\right)ln\left(\frac{\Delta}{\hbar\omega}\right)exp\left(\frac{-\Delta}{kT}\right)$$

where, A is a numerical factor, reflecting the properties of the normal state at $T > T_c$ and A is the energy gap parameter. The exponential behavior is due to an isotropic BCS gap. In the normal conducting state of the superconductor the values of R_s and δ_n are connected to the conductivity σ by the relations

$$R_s = \sqrt{\frac{\mu_0\omega}{2\sigma}}$$

and

$$\delta_n = \sqrt{\frac{2}{\mu_0 \omega \sigma}}$$

The above relations represent a marked variation of frequency and temperature dependence of R_s and X_s in the normal and superconducting states.

Microwave absorption studies in normal metals and conventional superconductors have long been used [39-44] to get information about the superconducting state below T_c. For phonon mediated type II superconductors, the microwave surface resistance provides a well established method for studying flux flow surface losses in bulk planar samples. As the skin depth at microwave frequencies is very small in these materials, the measurement had to be carried out on thin films. In high T_c superconducting oxides, however, the skin depths are rather large ($\approx 1 - 10 \mu m$) often, typically of the order of the grain size.

High frequency impedance is a widely useful tool for the study of type II superconductors. Impedance measurements on the mixed state can give information on both ideal mixed state and on the nature of flux pinning mechanisms in the nonideal mixed state. At microwave frequencies almost all effects of flux pinning fall away, and one can readily study the the properties of the ideal mixed state even in the most strongly pinned state [43]. However at radio frequencies (MHz) flux lattice may be rigid and one can study a nonideal mixed state.

On the application side, a superconductor makes a best high frequency cavity because its dissipation is far less than that in a best normal conductor. This allows

the construction of superconducting microwave cavities with Q's up to 10^9, compared to Q $\approx 10^3$ - 10^5 for normal metal cavities [36].

1.7 Literature Survey of Non Resonant High Frequency Absorption in HTSCs

Soon after the discovery of HTSC several methods have been employed to study the high frequency response. The observation of non-resonant field modulated microwave absorption as a function of dc field was reported by Bhat et.al [45]. This was followed by a large number of reports [46-65] and by now the technique is well established to be very useful in the study of HTSC. On the other hand, Moorjani et. al *[66]* have developed magnetic field modulated microwave absorption as a function of temperature to determine the superconducting transition and, intragrain and intergrain responses. The details of this technique are discussed in chapter 2. These two techniques have their own limitations, in the sense, the sample is never in the equilibrium state during the field modulation and secondly, the hysteresis present in the power absorption of the HTSC does not allow the study of virgin response. Direct power absorption is a simple and a better tool to study the virgin response of the HTSCs and has been used by some authors [67-74] to study the power absorption as a function of field and temperature. In the following a summary of the important work done and the models used are given.

To explain the low field modulated microwave absorption response Dulcic et. al [75] proposed a model based on resistively shunted Josephson junctions (RSJ). The magnetic field sweep induces a boundary current I_0 superimposed on the microwave

induced current $I_{mw}cos(\omega_{mw}t)$. These currents act as transport currents for the Josephson junctions, so that the differential equation for a typical junction on the surface is given by

$$\frac{C\hbar}{2e}\frac{d^2\phi}{dt^2} + \frac{1}{R}\frac{\hbar}{2e}\frac{d\phi}{dt} + I_c sin\phi = I_0 + I_{mw}cos(\omega_{mw}t)$$

where the junction parameters are given by the capacitance C, normal resistance R, critical current I_c and the difference of the phases in the two grains forming the junction ϕ [76]. In the absence of microwave field, the phase would adjust to an equilibrium value ϕ_0. The microwave current will induce small oscillations in the phase around ϕ_0, *i.e.* $\phi(t) = \phi_0 + \phi_{mw}(t)$. Neglecting the capacitive term, the power absorbed in the junctions takes a simple form

$$P = P_n \frac{1}{1+\eta}$$

where $P_n = \frac{1}{2} I_{mw}^2$ R is the absorption in the limit of high fields when the junction becomes normal, and the parameter 77 is given by

$$\eta = \frac{I_c^2 cos^2\phi_0}{[(1/R)(\hbar/2e)\omega_{mw}]^2}.$$

Magnetic field reduces the critical current of a junction and the reduction factor, F(H) is given by the well known diffraction formula $\frac{sin(\pi H/H_0)}{\pi H}$, where H_0, the field at which the junction contains one quantum of flux, depends on the size of the junction. The total microwave absorption is affected by a large number of junctions with a distribution

in H_0. Hence the envelope F(H) of the diffraction formula should be considered as reduction factor for I_c. One can write $\eta = \eta_0 F^2(H)$, where η_0 is the value of η at zero field. Temperature dependence of the field dependent loss comes from I_c and therefore through η_0.

Bhagat's group has done extensive work on direct microwave power absorption as a function of temperature and field [67,77-82]. In the microwave loss near T_c the large peak observed [77] in micron sized YBCO and BSCCO superconductors is accounted for in terms of distribution in T_c. The onset of superconductivity enhances the rf field seen by their neighbors leading to a net increase in absorption. The temperature regime of enhanced loss spans the extrema of the transition temperature. In the field induced microwave absorption the initial monotonic increase [78,79] has been expressed by the empirical form $\frac{1}{H^2}$. A simple model in which the defects on the grain surfaces are visualized as forming rf SQUIDS is suggested as a plausible explanation. It is also reported that the field induced loss in c-axis oriented YBCO thin films [80] arises from coupling to damped fluxons and yields first determination of the ratio of restoring to viscous forces. The RSJ model, proposed by Dulcic *et.al* is further developed and is effectively used to analyze filed induced losses. The magnetic hysteresis observed [82] is shown to be a strong function of temperature and frequency.

Guira's group has concentrated on the low and high field absorption [83,84]. The results of the low field absorption are explained in terms of decoupled junction model [83] in which the absorption goes as $(1 - e^{-H/H_d})$, where, H_d is the dephasing field of the junctions. However, the high field absorption is explained in terms of flux flow model [84].

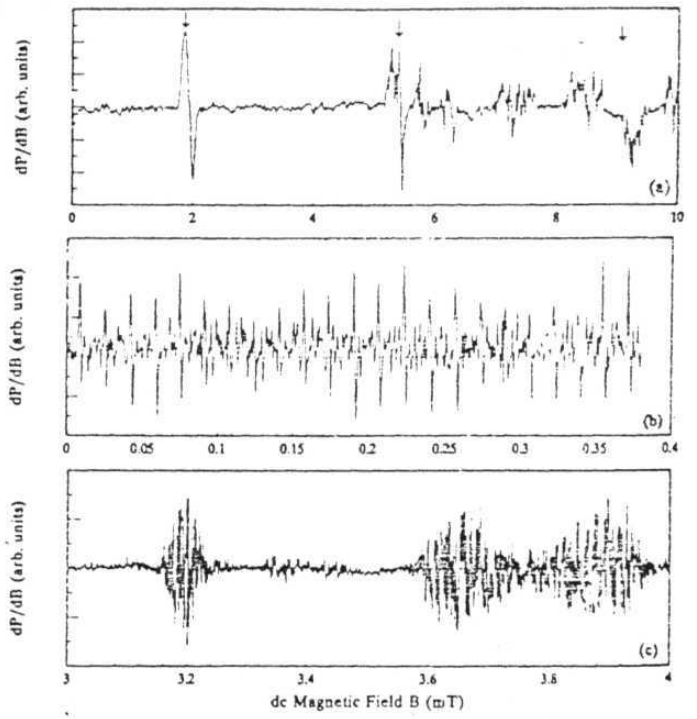

Fig. 7 Periodic line spectra observed in the modulated microwave magnetoabsorption of YBCO, a,b and c represent three different configurations. The origin of such spectra are explained in terms of flux quantization in the weaklinks (ref. 95)

Employing modulation technique, Portis et. al [54] studied the low field absorption and attributed it to fluxon motion driven by microwave currents. In HTSCs a fraction of these fluxons are weakly pinned and are driven by microwave currents and at the same time damped by viscosity, giving rise to field dependent microwave loss. The surface resistance and reactance are expressed as [85],

$$R = X_0\sqrt{-1+\sqrt{\frac{1+\frac{4f^2B^2}{B_0^2}}{2}}}$$

$$X = X_0\sqrt{1+\sqrt{\frac{1+\frac{4f^2B^2}{B_0^2}}{2}}}$$

In single HTSC crystals, the absorption as a function of field is found to show line spectra [86-88,95]. Fig. 7 shows typical line spectra observed in YBCO. Such line spectra have also been observed [89,90] in the conventional superconductors. The explanation for this phenomenon was given by Owens [91]. Since the flux is quantized in the superconducting loop, phase jumps occur when the field enclosed by the loop changes by integral multiples of flux quanta, as the applied field is increased. These flux jumps occur in a very short time and produce large voltage pulses given by $V(t) = -(\hbar/2e)d\theta/dt$ because of which the current in the loop exceeds the critical current and hence microwave power is absorbed. However, Martinek and Stankowski [92] have proposed a different approach in which the rf SQUID with thermal fluctuations has been used to explain the periodic line spectra.

Ji et al [93] have proposed two - level critical state model to account for the unconventional hysteresis, i.e. the minimum in the reverse field sweep occurring at fields well below the zero of the applied field, observed in the low field microwave absorption. Using this model and flux flow like dissipation, the surface resistance was very well described by [94]

$$R_s = \sqrt{\frac{2\pi\omega\phi_0^2 n_j}{c^4\eta_j}}$$

where n_j is the intergranular fluxon number density, η_j is the coefficient of viscous drag in the intergranular region and ω is the angular frequency. Wosik *et. al* [95] studied the flux quantization in weaklinks of melt textured YBCO using the field modulated microwave absorption method. From the line spectra observed they have identified the types and locations of Josephson junction weaklinks in the sample.

Despite a large number of reports on the surface resistance or absorption study of HTSC at microwave frequencies, very little work has been undertaken on surface reactance and high frequency penetration depth [96-100]. At radio frequencies (MHz) a very few researchers [101-104] have studied the surface resistance and reactances. A summary of the little work reported at radio frequencies is given below.

Sridhar's group has effectively made use of rf impedance measurements to determine various features of HTSC including the verification of the basic superconductivity theories and the symmetry of the wave function. The overall response of R_s and δ_s (screen depth) as a function of temperature was well described by the BCS theory in the dirty limit, but some additional features in R_s and δ_s suggest detailed

deviation from the BCS s-wave state [101]. The rf penetration depth was found to increase quad rat ically, $\Delta\lambda_{eff} = k(T)B^2$, with applied magnetic field in samples of ceramic YBCO. The B^2 dependence and large values of k(T) (Ginzburg-Landau parameter) are quantitatively explained [105] in terms of dc flux dependence of the high frequency response of the Josephson junction network. Measurements of field dependent rf penetration depth are used to delineate the lower critical field H_{c1} — T phase boundary and to study the fluxon dynamics in YBCO single crystals, and H_{c1} was found to be obeying BCS temperature dependence [106].

1.8 Aims and objectives of the present work

As discussed above the high frequency response of HTSCs is strongly dependent on the Josephson junctions and the critical vortex state, and many characteristic parameters of the superconductors can be determined from such a study. The present thesis is aimed at a detailed study of high frequency loss mechanism at MHz and GHz, the penetration depth, surface reactance and the associated novel features such as paramagnetic Meissner effect in various sintered and melt textured superconductors. For the purpose of studying rf response of superconductors a marginal oscillator is built and has been effectively used to study the rf impedance. Field induced absorption is not fully understood yet as it appears to be sample dependent. A systematic study has been carried out to understand the temperature and field (at low and high fields) dependent absorption in sintered and melt textured samples at radio and microwave frequencies to test the validity of the Josephson junction and flux flow models.

The π junctions could give rise to paramagnetic meissner effect which is observed

in some HTSCs. An attempt has been made to look for the **signature of the para**-magnetic Meissner effect in GdBCO sample in the microwave absorption. From the frequency change of the rf oscillator both penetration depth and surface reactance can be determined. However, in the literature there have been very **few** reports of such a study. It could be a powerful tool to study the vortex dynamics and order parameter symmetry because of its high sensitivity when compared to conventional magnetization measurements. However, in the case of sintered samples which have a number of weaklinks such a technique needs to be used cautiously. The usefulness of this technique to study sintered superconductors is examined.

References

[1] H.Kammerlingh Onnes, Leiden Commun, **1206,** 1226 (1911)

[2] Orlando and Delin, Foundations of Applied Superconductivity, Addison Wesley Publishing Co, 4 (1991)

[3] W.Meissner and R.Ochenfeld, Naturwiss **21,** 787 (1933)

[4] F.London and H.London, Physica, 2, 341 (1935)

[5] A.B.Pippard, Physica, **19,** 765 (1953)

[6] A.C.Rose Innes and E.H.Rhoderik, Introduction to Superconductivity, Pergmon Press (1969)

[7] J.G.Bednorz and K.A.Muller, Z. Physics B, Condensed Matter, 64, 189 (1986)

[8] C.W.Chu et. al, Phys. Rev. Lett, **58,** 405 (1987)

[9] M.K.Wu et. al, Phys. Rev. Lett, 58, 908 (1987)

[10] H.Maeda, Y.Tanaka, M.Fukutomi and T.Asano, Jpn. J. Appl. Phys, **27,** L209 (1988)

[11] Z.Sheng and A.M.Hermann, Appl. Phys. Lett, **52,** 1738 (1988)

[12] S.N.Putlin, E.V.Antipov, O.Chmaissem and M.Marezio, Nature, **362,** 226 **(1993)**

[13] R.J.Cava, B.Batlogg, R.B.Vandover, D.W.Murphy, S.Sunshine, T.Siegrist, J.P.Remeik E.A.Rietman, S.Z.ahurak and G.P.Espinosa, Phys. Rev. Lett, 58, 1676 (1987)

[14] P.M.Grant, R.B.Beyers, E.M.Engler, G.Lim, S.S.P.Parkin, M.L.Ramirez, V.X.Lee, A.Nazzal, J.E.Vazquez and R.J.Savoy, Phys. Rev. **B, 35,** 7252 (1987)

[15] R.M.Hagen, L.W.Finger, R.J.Angel, C.T.Prewitt, N.L.Ross, H.K.Mao, C.G.Hadidiako P.H.Hor, R.L.Meng and C.W.Chu, Phys. Rev. B, **35,** 7238 (1987)

[16] Y.Le Page, W.R.Mc Kinnon, J.M.Tarascon, L.H.Greene, G.W.Hull and D.M.Huang, Phys. Rev. B, 35, 7245 (1987)

[17] J.M.Tarascon, W.R.McKinnon, P.Barboux, D.M.Huang, B.G.BADLEY, L.H.Green, G.W.Hull, Y.LePage, N.Stoffel and M.Giroud, Phys. Rev. B, 38, 8835 (1988)

[18] C.C.Torardi, M.a.Subramanian, J.C.Cclabrese, J.Gopalakrishnan, E.M.McCarron, K.J.Morrissey, T.R.Askew, R.B.Flippen, V.Chowdhary and A.W.Sleight, Phys. Rev. B, 38, 225 (1988)

[19] K.Imai, I.Nakai, T.Kawashima, S.Suero and A.Ono, Jpn. J. Appl. Phys, **27,** L1661 (1988)

[20] M.Onodo and M.Sato, Solid State Commun. **67,** 799 (1988)

[21] R.M.Hazen, C.T.Prewitt, R.J.Angel, N.L.Ross, L.W.Finger, C.G.Hadidiacos, D.R.Veblon, P.J.Heaney, P.H.Hor, Z.J.Huang, L.Gao, J.Bechtold and C.W.Chu, Phys. Rev. Lett. 60, 1174 (1988)

[22] J.M.Tarascon, Y.Le Page, P.Barboux, B.GBagley, L.H.Greene, W.R.McKinnon, G.W.Hull, M.Giroud and D.M.Huang, Phys. Rev. B, 37, 9382 (1988)

[23] J.K.Liang, S.S.Xie, G.C.Che, J.Q.Huang, Y.L.Zhang and Z.X.Z.Hao, Mod. Phys. Lett B, 2, 483 (1988)

[24] G.Deutscher and K.A.Muller, Phys. Rev. Lett, 59, 1745 (1987)

[25] I.Morgenstern, Earlier and Recent aspects of Superconductivity, ed. J.G.Bednorz and K.A.Muller, Springer Verlag, p. 240 (1990).

[26] A.Barone, ibid, page 163

[27] C.E.Gough, ibid, page 147

[28] A.M.Portis, ibid, page 240

[29] Y.B.Kim et.al., Phys. Rev. **139,** A 1163 (1965)

[30] J.Bardeen and M.J.Stephen, Phys. Rev. **140,** A1197 (1965)

[31] A.G.van Vijfeijken and Niessen, Phys. Lett. 16, 23 (1965)

[32] J.Manhart, ref. 16, page 211

[33] M.Golosovski et. al., Phys. Rev. B, 43, 10390 (1991)

[34] D.H.Wu et.al., Phys. Rev. Lett. 65, 2074 (1990)

[35] F.Zuo et al., Phys. Rev. B, 41, 6600 (1990)

[36] M.Tinkham, Rev. Mod. Phys, **46,** 587 (1974)

[37] J.Halbritter, Z.Physik **266** , 209 (1974)

[38] J.Carini, L.Drabeck and G.Gruner, b3, 5 (1989) Mod. Phys. Lett.

[39] B.Rosenblum and M. Cordona, Phys. Rev. Lett, **12,** 657 (1964)

[40] M.Cordona, J.Gittleman and B.Rosenblum, Physics Letters, **17,** 92 (1965)

[41] J.LGittleman and B.Rosenblum, Physics Letters, 20, 453 (1966)

[42] Y.B.Kim and M.J.Stephen, Superconductivity Vol I,Ed. R.D.Parks, Marcel Dekker, New York, 1969

[43] J.LGittleman and B.Cordona, Journal of App. Phys., 39, 2617 (1968)

[44] K.A.Muller, M.Pomeranz, C.M.Knoedler and D. Abraham, Phys. Rev. Lett, 45, 832 (1990)

[45] S.V.Bhat, P.Ganguly, T.V.Ramakrishnan and C.N.R.Rao, J. Phys C 20, L 539 (1987)

[46] K.W.Blazey, K.A.Muller, J.G.Bednorz, W.Berlinger, G.Amoretti, E.Buluggiu, A.Vera and F.C.Matacotta, Phys. Rev **B, 36,** 7241 (1987)

[47] K.Kachaturyan, E.R.Weber, P.Tejedor, A.M.Stacy and A.M.Portis, Phys. Rev. B, **36,** 8309 (1987)

[48] J.Stankowski, P.K.Kahol, N.S.Dalai and J.S.Moodera, Phys. Rev B, **36** 7126 (1987)

[49] R.Durny, J.Hautala, S.Ducherme, B.Lee, O.G.Symko, P.C.Taylor, D.J.Zhang and J.A.Xu, Phys Rev B, 36, 2361 (1987)

[50] C.Rettori, D.Davidov, I.Blelaish and I.Feluer, Phys. Rev B, **36,** 4028 (1987)

[51] M.D.Sastry, A.G.I.Dalvi, Y.Babu, R.M.Kadam, J.V.Yakmi and R.M.Iyer, Nature, **330,** 49 (1987)

[52] K.N.Srivastava, J.Phys C, 30, L789 (1987)

[53] E.J.Pakulas, T.Osada, F.Holtzberg and D.Kaiser, Physica C, **153-155,** 510 (1988)

[54] A.M.Portis, K.W.Blazey and F.Waldner, Physica C, **153-155,** 308 (1988)

[55] M.Puri, J.T.Masiakowski, S.Marrelli, J.Bear and L.Kevan, J. Phys. Chem 94, 6094 (1990)

[56] P.Orlandi and A.Rigamonti, Physics C, **178,** 197 (1991)

[57] R.Karim, S.A.Oliver, C.Vittiria, A.Widom, G.Balestrino, S.Barbarena and P.Paroli, Phys. Rev. B, 39, 797 (1988)

[58] R.Karim, H.How, R.Seed, C.Vittoria, G.Balestrino, A.Paoletti and P.Paroli, J. Mag. Magnetic Mate. 83, 511 (1990)

[59] B.L.Ramakrishna, E.W.Ong and Z.Iqbal, J. Appl. Phys. 64, 5803 (1988)

[60] R.Karim, R.Seed, S.A.Oliver, A.Widom and C.Vittiria, IEEE Trans. Mag, 25, 3221 (1989)

[61] M.D.Sastry, K.S.Ajaykumar, R.M.Kadam, G.M.Phatak and R.M.Iyer, Physica C, 170,41 (1990)

[62] M.Puri, R.Durny and L.Kevan, Physics **C,** 190, 210 (1992)

[63] W.E.Carlos, R.Kaplan, D.H.Lowndes and D.P.Norton, PhysicaC, **198,** 247 (1992)

[64] S.H.Glarum, J.H.Marshall and L.F.Schneemeyer, Phys. Rev. **B,** 37, 7491 (1988)

[65] M.Mahel and S.Benaka, Solid State Communi, 83, 615 (1992)

[66] K.Moorjani, J.Bohandy, F.J.adrian, B.F.Kim, R.D.Schull, C.K.Chiang, L.J.Swartzend and L.H.Bennett, Phys. Rev. B, 36, 4036 (1987)

[67] S.Tyagi, A.Gould, G.Shaw, S.M.Bhagat and M.A.Manheimer, Physics Letters A, **136** ,499 (1989)

[68] T.L.Hylton, A.Kapitulnik, M.R.Beasley, J.P.Carini, L.Drabeck and G.Gruner, Appl. Phys. Lett, 53, 1343 (1988)

[69] M.Guira, R.Marcon and R.Fastampa, Phys. Rev. , 40, 4437 (1989)

[70] J.Halbritter, J. Appl. Phys. 68, 6315 (1990)

[71] J.Wosik, L.M.Xie, J.Halbritter, R.Chu, A.Salama, J.C.Wolfe, V.Selvamanikam and K.Salama, IEEE Trans. on Appl. Supercon, 3, 1432 (1993), G.Godel, N.Gold, J.Hasse, J.Bock and L.Halbritter, Supercond. Sci Technol, 7, 745 (1994)

[72] **J.Halbritter,** J.Appl. Phys, **71,** 339 (1992)

[73] A.M.Portis, D.W.Cooke, E.R.Gray, P.N.Arendt, C.L.Bohn, J.R.Delayen, C.T.Roche, M.Hein, N.Klein, G.Muller, S.Orbach and H.Piel, Appl. Phys. Lett, **58, 307 (1991)**

[74] B.Czyzak, Physics **C, 243,** 327 (1995)

[75] A.Dulcic, B.Rakvin and M.Pozek, Europhys Lett, **10,** 593 **(1989)**

[76] A.Barone and G.Paterno, Phys. and Applications of the Josephson Effect, Wiley J., New York, N.Y. (1982)

[77] M.A.Manheimer, S.Lofland, A.Gould, S.M.Bhagat, B.Halsey, S.M.Green and S.Tyagi, Physica **C, 183,** 324 (1991)

[78] A.Gould, M.Huang and S.M.Bhagat, J. Appl. Phys 69, 4880 (1991)

[79] A.Gould, S.M.Bhagat **and** F.C.Wellstood and S.Tyagi, Solid State Commu. **81,** 339(1992)

[80] M.X.Huang, S.M.Bhagat, A.T.Findikogulu and T.Venkatesan, M.A.Manheimer and S.Tyagi, Physica C, 193 (1992)

[81] J.S.Ramachandran, M.X.Huang, K.Kish and S.Tyagi, Physica C, **202,** 151 (1992)

[82] A.Gould, S.M.Bhagat, M.A.Manheimer and S.Tyagi, J. Appl. Phys **67,** 5020 (1990)

[83] R.Fastampa, M.Guira and C. Matacotta, Europhys. Lett. 6, 265 (1988)

[84] R.Marcon, R.Fastampa, M.Guira and E.Silva, Phys. Rev.B, 2940 **(1991)**

[85] A.M.Portis, K.W.Blazey, K.A.Muller and J.G.Bednorz, Euro. Phys. Lett, 5, 467 (1988)

[86] K.W.Blazey, Z.Phys, B, 64, 268 (1986)

[87] A.Dulcic, R.H.Crepeau and J.H.Freed, Phys. Rev. **B,** 39, 4249 (1989)

[88] A.Dulcic, R.H.Crepeau, J.H.Freed, L.F.Schneemeyer and J.V.Waszczak, Phys. Rev. B, 42,2155 (1990)

[89] K.W.Blazey, A.M.Portis, K.A.Muller and F.H.Holtzberg, Europhys. Lett, 6, 457 (1988)

[90] K.W.Blazey, A.M.Portis and F.H.Holtzberg, Physica C, 157 (1989)

[91] F.J.Owens, Physica C, 171, 25 (1990)

[92] J.Martinek and J.Stankowski, Phys. Rev. B, **50**, 3995 (1994)

[93] L. Ji, M.S.Rzchowski, N.Anand and M.Tinkham, Phys. Rev B, 47, 470 (1993)

[94] L. Ji, M.S.Rzchowski and M.Tinkham, Phys. Rev. B, 42, 4838 (1990)

[95] J.Wosik, L.M.Xie, J.C.Wolfe, X.Ren and C.W.Chu, Phys. rev. B, 51, 16289 (1995)

[96] S.Sridhar and W.L.Kennedy, Rev. of Sci. Instrumen., 59, 531 (1988)

[97] S.K.Remillard, M.E.Reeves, F.J.Rachford and S.A.Wolf, J. Appl. Phys, 75, 4103 (1994)

[98] M.Hein, H.Piel, M.Strupp, M.R.Truinn and A.M.Portis, J. Mag. Magnetic Mate. 104-107,529 (1992)

[99] T.Jocabs, S.Sridhar, Qiang Li, G.D.Gu and N.Koshizuku, Phys. Rev. Lett. 75, 4516 (1995)

[100] S.Sridhar, J. Appl. Phys, 63, 159 (1988)

[101] S.Sridhar, C.A.Shiffman and H.Hamdeh, Phys. Rev. B, 36, 2301 (1987)

[102] Stephen Ducherme, R.Durny, J.Hautala, D.J.Zeng, P.C.Taylor, O.G.Symko and S.Kulakarni, J. Appl. Phys, 66, 1252 (1989)

[103] D.sen, S.K.Ghatak, K.L.Chopra, G.Markandeyulu and D.Bhattacharya, Solid State. Communi, 79, 935 (1991)

[104] P.Drotbohm, G.J.Russell, A.Bailey, G.Alvarez and K.N.R.Taylor, Physica C, 195, 28 (1992)

[105] Dong-Ho Wu, C.A.Shiffman and S.Sridhar, Phys. Rev. B, 38, 9311 (1988)

[106] Dong-Ho Wu and S.Sridhar, Phys. Rev. Lett, 65, 2074 (1990)

Chapter 2

r.f. INSTRUMENTATION, MEASUREMENT TECHNIQUES AND SAMPLE PREPARATION

2.1 Introduction

The high frequency measurement techniques as that of magnetic susceptibility have an advantage of being able to detect superconductivity in samples which are discontinuous. Such studies are of particular importance because electromagnetic probes are sensitive only to the electronic state while other conventional probes like specific heat, ultrasonic attenuation etc. are strongly influenced by the phonon system, which is heavily populated at the high temperatures involved in HTSCs. Several techniques have been developed at microwave frequencies to study the surface impedance $Z_s = R_s + X_s$. Continuous wave (CW) electron paramagnetic resonance (EPR) and to a much lesser extent nuclear magnetic resonance (NMR) spectrometers are used for studying high frequency absorption. While EPR and NMR are resonant techniques the present work is on the nonresonant high frequency studies. In the cavity perturbation technique (described in the following) from the microwave power reflected by the cavity , surface resistance is determined by many groups [1-7]. To determine the microwave surface resistance in thin films microstrip resonators are developed and are effectively used by many groups [8,9].

Contrary to the vast amount of literature available on power absorption at mi-

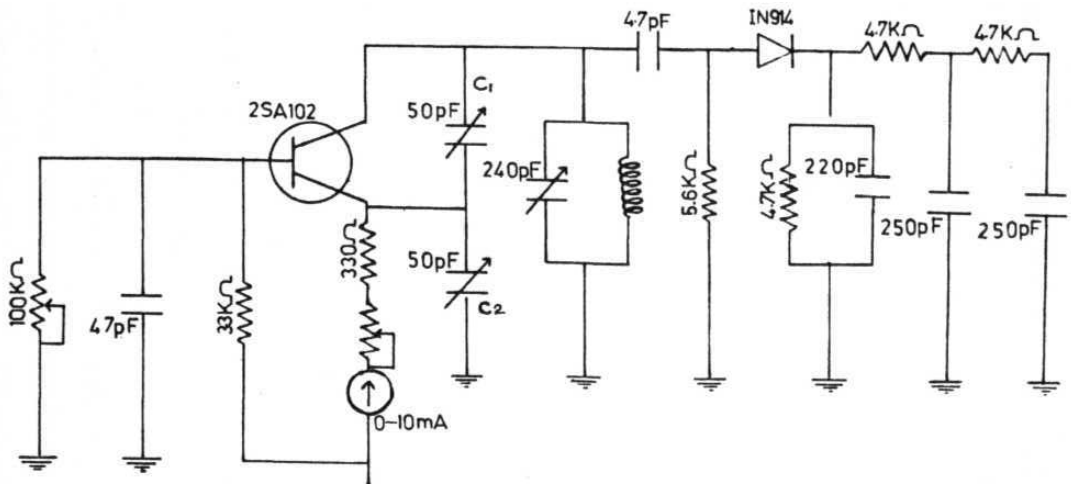

Fig. 1 Circuit of the marginal oscillator used for the radio frequency study.

crowave frequencies there have been very few reports on similar studies at radio frequencies. Stephen Ducharme et al. [10] studied the non - resonant absorption at radio frequencies by using the modulated detection method by employing a Varian model crossed coil NMR spectrometer. Omary et. al [11] and Sridhar et, al [12] have employed a tunnel diode oscillator using which they studied field and temperature dependence of penetration depth and surface resistance. In the present work we have made use of a marginal oscillator to investigate radio frequency impedance at MHz . Magnetically modulated radio frequency absorption (MMRA) technique is developed in analogy with MMMA technique at microwave frequencies. To study the microwave response cavity perturbation technique is used. The details of these techniques are given below.

2.2 Circuit Details of the Marginal Oscillator and rf Measurement Techniques

For the present work we have built a marginal oscillator [13] whose circuit diagram is shown in the Fig. 1. The present circuit is different from that of the marginal oscillators [14-17] which are of Colpitts type and has two controls for feedback and emitter current, while the other circuits have only one or no control. The use of two controls not only gives rise to stable signal but also makes the circuit suitable for studying radio frequency absorption, penetration depth etc. of different kinds samples. Since a FET amplifier in common drain configuration has high input impedance and low output impedance [11], the output of the oscillator is fed to it in the common drain configuration to decouple the possible interdependence of power output and frequency of oscillations, and to improve stability . Because direct tapping of the signal, for

the measurement of the frequency shift, from any part of the oscillator affects the performance of the oscillator, an additional pick up coil wound on the primary tank coil is used to monitor the frequency shift without disturbing oscillations.

Coil selection for sensitive power and frequency measurements.

We have tested different coils with different no. of turns and gauges for frequency and power absorption measurements and found the following. The observations are made for coil A (35 turns, 18 SWG), coil B (20 turns, 18 SWG), coil C (35 turns, 16 SWG), coil D (30 turns, 18 SWG). Coil A resulted in less frequency change than that of coil B when the sample is warmed through transition. Coil A and Coil C resulted in approximately same power and frequency changes through transition. Coil B resulted in less power change and almost equal frequency change when compared to coil D, which has more no. of turns than coil B. And hence for sensitive power and frequency measurements different coils have to be used. To counter the problem and for other reasons discussed below we have made a multi-purpose coil.

The sustenance of oscillations is decided by capacitor Cl and C2 in the feedback circuit. Once Cl and C2 are tuned to marginal conditions the working of the oscillator wholly depends on the tank coil and the sample inside it. We used samples of various dimensions and densities. The loading and power in the coil depend on the sample material, dimensions and density. When the loss is more than the power delivered by the coil, oscillations seize. It is not practical to open the oscillator circuit and tune Cl and C2 for sustained oscillations for any particular sample. Therefore, we have made a variable pitch coil, shown in Fig. 2b. Such a coil facilitates one to use wide variety

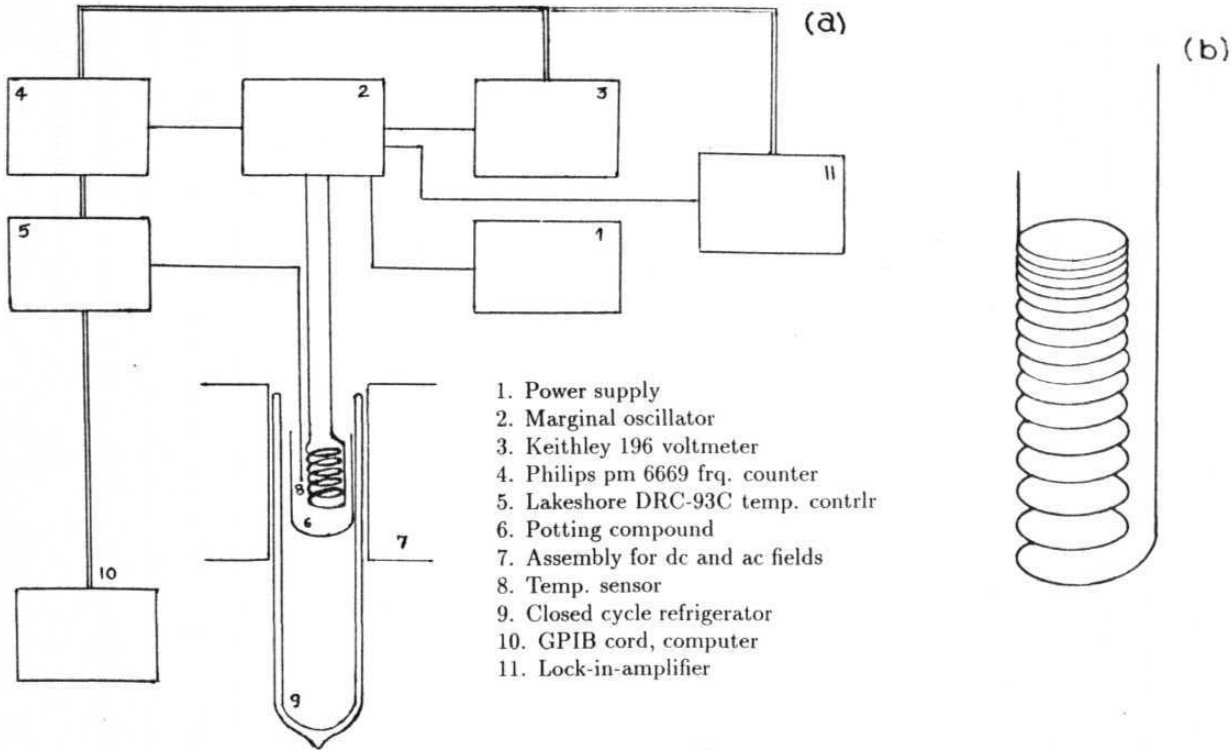

Fig. 2 (a) Block diagram of the radio frequency absorption set up, (b) Varying pitch coil made to accommodate samples of various dimensions and densities.

of samples and because of its higher inductance permits sustained oscillations even when the sample is in the normal state. A sample with large dimensions and higher density can be inserted in the upper half of the coil and a sample with smaller dimensions and low density can be inserted at the bottom half of the coil. And accordingly, different positions can be tested for better frequency and power measurements.

The inductance (L) of the coil with varying pitch can be written as

$$L = L_1 + L_2 + ...L_n + \sum_{1}^{n} M$$

where $L_1, L_2, \ldots L_n$ are inductances of each turn and M is the mutual coupling between the turns. As the temperature or field is varied change in the penetration depth in the sample causes a change in the inductance in some part of the coil depending on where the sample is kept. This change in inductance is reflected in the total inductance change.

Sample coil assembly

Sample coil forms the tank coil of the oscillator and is connected to the oscillator through a long coaxial transmission line which goes into a dewar or the sample chamber of the closed cycle refrigerator, Fig. 2a. The coil is fixed in a highly thermally conducting and electrically insulating potting compound mould to arrest the vibrations of the turns and to achieve uniform temperature along the length of the coil. Both the sample and temperature sensor are kept in thin walled glass tube which is kept inside the coil. A heater wire is wound astatically on the potting compound to facilitate temperature variation.

Principle

The basic difference of high frequency absorption at microwave and **radio** frequencies is that at microwave frequencies absorption is detected maintaining the cavity at resonance by continuously controlling either cavity dimension or klystron reflector voltage so that frequency is always kept constant. Whereas, in the present marginal oscillator the feed back circuit maintains a constant current through parallel resonance circuit. The inherent feed back ensures that the oscillator is at resonance even while the frequency of oscillation changes continuously due to the variation in the inductive impedance of the load. The oscillation level is sensitive only to the resistive losses but not to the inductive losses and hence pure absorption signal is detected.

The absorption in the sample surrounded by a coil forming part of the tuned circuit affects the quality factor Q of the resonance circuit and is given by the absorption of energy of the coil field h. Power dissipated in the coil is given by $P = (R_s/2)\int h^2 dA$. Time averaged energy stored in the coil is $W = (1/2)\mu\int h^2 dV$. Therefore, Q factor

$$\frac{1}{Q_0} = \frac{P}{\omega W} = \frac{R_s}{2}\frac{\int h^2 dA}{\omega W}$$

$$\rightarrow R_s = \tau/Q_0$$

where the field integral is cast in the geometry factor r. Thus the change in the surface resistance of the sample would reflect as a change in the quality factor and cause change in the power output. From Eq. 1 normalized power absorption $P/P_n = R_s/R_n$, where P_n and R_n are normal state power absorption and surface

resistance, respectively. Hence, studying absorption would directly give information on surface resistance.

At temperatures much less than T_c and at low applied frequencies (so that $\hbar\omega \ll kT$), the effects due to proximity of induced transition across gap is negligible. In these conditions, the high frequency screening of normal electrons (skin depth) can be assumed to be negligible. The penetration of rf field is then solely determined by the screening of superelectrons and the penetration depth can be termed as screen depth λ_s. The absolute value of λ_s at a particular temperature is difficult to measure, but its temperature variation can be studied by monitoring the change of inductance of the sample [19]. The inductance of the coil is proportional to the cross sectional area of the space occupied by the flux, that is the space between the coil and the sample plus whatever distance the flux penetrates into the surface of the sample. As the temperature or field is changed, penetration depth changes, and inductance changes with it. Then [19]

$$\frac{change\ in\ inductance}{total\ inductance} = \frac{change\ in\ \lambda \times circumference\ of\ the\ sample}{total\ cross\ section\ occupied\ by\ flux}$$

When inductance L alters, oscillator frequency shifts as

$$\frac{\delta f}{f} = -\frac{1}{2}\frac{\delta L}{L}$$

so that

$$\delta\lambda = -[\frac{A}{\pi r}]\frac{\delta f}{f}$$

where r is the radius of the sample and A is the cross sectional area between the sample and the coil. The changes in the surface reactance axe obtained from

$$\delta X_s = \mu_0 \omega \delta \lambda$$

In the materials which obey the skin-depth limit in the normal state, one can use the criterion that $R_n = X_n$ above T_c to determine X_0, the value of X at T=0K.

The frequency change could also be affected by the loss in circuit. When the resonator is lossy and Q of the resonance circuit is low there can a reasonable shift in the frequency apart from that produced by the sample. To see this effect, consider a familiar equation of motion for a damped harmonic oscillator which is sinusoidally driven [20],

$$md^2x/dt^2 + \beta dx/dt + kx = F\cos(\omega t) or$$

$$d^2x/dt^2 + \frac{\beta}{m} dx/dt + \omega_0^2 x = A\cos(\omega t)$$

where $\omega_0^2 = k/m$ is the undamped oscillation frequency and the damping parameter is β/m. If the damping is light enough ($\beta/m < \omega_0$), the system will undergo damped oscillations with an oscillation frequency reduced from its undamped value, $\omega_{res}^2 — \omega_0^2 — (\beta/m)^2$. With $Q = \omega_{res}/(\beta/m)$ the oscillation frequency in the presence of damping is

$$\omega_{res}^2 = \omega_0^2[1 + (1/2Q^2)]^{-1}$$

or $\omega_{res} - \omega_0 \sim -(1/4Q^2)$. Thus the fractional change in the oscillation frequency due to losses is

$$\frac{\omega_{res} - \omega_0}{\omega_0} \simeq -\frac{1}{4Q^2}$$

For the present Q ($\simeq$ 400) value such a shift ($\simeq$ 15) in the resonance frequency is negligible compared to the large frequency change ($\sim$ a few thousand Hzs) due to the inductance change. Hence any effect of finite losses on the resonant frequency can be neglected.

Because we are able to measure both the real and imaginary parts of the impedance Z_s, it is possible to obtain the complex conductivity $\sigma_s = \sigma_1 - i\sigma_2$ from the present measurements, using the relation $Z_s = R_n\sqrt{2i/(\sigma_s/\sigma_n)}$ where R_n and σ_n are the normal state surface resistance and conductivity, respectively [21]. σ_2 is particularly important as it gives a measure of the superfluid density n_s which is proportional to σ_2. It is also related to the penetration depth via $\sigma_2 = 1/\mu_0\omega\lambda^2$. The radio frequency resistivity $\rho_n^{rf}(T)$ in the normal state can be obtained from the surface resistance using $R_n = \sqrt{\pi\mu_0 f\rho_n^{rf}}$. Therefore, from the measurements of power at output and frequency changes of the oscillator, surface resistance, surface reactance and penetration depth of the superconductors can be obtained.

2.3 Magnetically Modulated Radio Frequency Absorption (MMRA)

Because the superconducting phase transition is a function of both field and temperature, there are many ways (corresponding to different paths in the H-T plane of

the superconducting phase diagram) in which the superconducting phase transition can be detected. All these ways are well discussed in literature [22,23]. In the present modulation technique constant dc field is applied to the sample which is modulated by much lower ac field, and the temperature is scanned through transition. As the temperature is varied through the transition the power change is detected using a lock - in analyzer at the modulation frequency. Such a field modulation is then equivalent to temperature modulation in the region of phase transition [22]. The present method is similar to the NMR technique in that the quantity directly measured is the derivative of the power with respect to the magnetic field. The difference between the MMRA and NMR methods is that in the latter technique, the field is varied as the temperature is kept constant while in the former technique the converse procedure is followed. The particular importance of field modulation is that any signal is recorded only if the rf response is magnetic field dependent, such as superconducting transition. Thus any other non field dependent phenomena like metal insulator - transitions are not detected. As described briefly in the last chapter, such a modulation technique, though more sensitive than direct power absorption, suffers from a few disadvantages and can be effectively used to determine superconducting phase transitions.

To carry out the MMRA experiments two pairs of Helmholtz coils are used for generating dc and ac fields. The applied dc field is $\sim$ 100 Oe and the ac modulation field is about 2-5 Oe. MMRA studies are carried out on various HTSCs. The results obtained are published elsewhere, they do not form part of the thesis. However, a typical MMRA signal recorded on BSCCO is shown in Fig. 3.

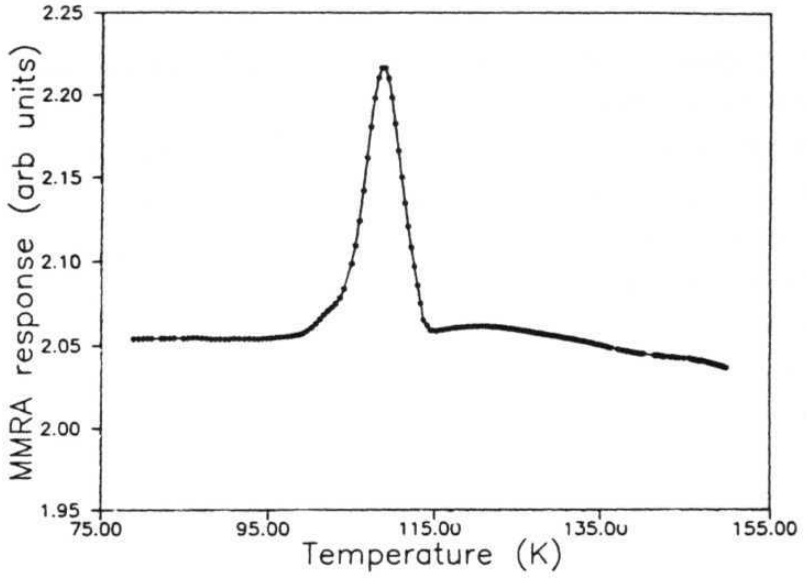

Fig. 3 A typical MMRA signal of BSCCO 11 OK phase powder.

2.4 Cavity Perturbation Technique

Cavity perturbation methods have been widely used in the measurement of dielectric parameters of a variety of samples. The perturbation theory of resonant cavities was first proposed by Bethe and Schwinger [24]. The assumptions were further redefined by Spencer [25] and Waldron [26]. In this technique the stationary microwave electric field of the resonant structure is perturbed by the small superconducting material. So there is a resultant change in resonant frequency and quality factor of the resonator. In the present Bruker ESR spectrometer automatic frequency controller is used to arrest the frequency change and the microwave current is monitored by a crystal detector.

2.5 Samples used for the present study

Sintered and press sintered $Bi_{1.2}Pb_{0.3}Sr_{1.5}Ca_2Cu_3O_y$ (BSCCO).

Sintered $GdBa_2Cu_3O_7$ (GdBCO).

Melt textured GdBCO with different percentages of Gd_2BaCuO_5 (211), namely,

GdBCO + 0 mol % 211

GdBCO + 10 mol % 211

GdBCO + 20 mol % 211 and

GdBCO + 30 mol % 211.

Sintered $DyBa_2Cu_3O_7$ (DyBCO).

2.6 Preparation of the samples

Sintered BSCCO

The 110K phase of *Bi - Sr - Ca - Cu - O* system is unstable and attempts by several groups to stabilize this phase often resulted in multiphases including a small percentage of 85K phase. Substitution of Pb for Bi in small amounts is found [27] to stabilize the 110K phase with repeated cycles of cold pressing and sintering. It has been found in our laboratory that this phase can be prepared in a stable and single phase form from a starting composition $Bi_{1.2}Pb_{0.3}Sr_{1.5}Ca_2Cu_3O_y$ without intermediate cold pressing [28]. The precursor powders required to make the BSCCO sample are prepared using a chemical route. Stoichiometric quantities of Bi_2O_3, SrO_3, $CaCO_3$ and Cu are dissolved in concentrated nitric acid while $Pb(NO_3)_2$ is dissolved in distilled water and mixed with the above solution. Then 1 gm mol. of nitric acid is added to 1 gm mol each of trivalent metal nitrates and correspondingly 2/3 gm mols of citric acid is taken for the divalent metal nitrates. The light blue color solution thus obtained is mixed with ethylene glycol. A small amount of ammonia is added to maintain the pH value around 4.5 so that the formation of precipitates can be avoided. The solution is then heated to form a jelly which eventually decomposes by an explosive reaction and yields a homogeneous black powder. The black powder was then ground well and sintered twice at 800° C with intermediate grinding. The sintered powders are pressed into pellets and annealed at 860° C for 15 days and quenched in air.

Press Sintered BSCCO

Tanaka *et al.* [29] reported that repeated cold pressing and sintering improves the critical current density of the sintered BSCCO. Press sintering results in texture in the material and higher density. The BSCCO pellets were annealed at 860°C for 5 days and quenched to room temperature in air. The air quenched pellets were subjected to uniaxial pressing under 4 tons of pressure. The pellets were then partially melted at 880°C for 50 mts, followed by annealing at 860°C for 5 days before quenching to room temperature.

Sintered ReBCO

Stoichiometric amounts of Re_2O3, $BaCo_3$ and CuO are mixed thoroughly and calcined at 800° C with intermediate mixing for 24 Hrs. The mixture is then made into pellets and and sintered at T_s (T_s = $930^0C, 935^0C, 940^0C$ for Re= Y, Gd, Dy respectively) for 24 hrs. The pellets are then oxygenated at 450° C for 72 Hrs.

Melt textured GdBCO

The four, Gd-0, Gd-10, Gd-20 and Gd-30, melt textured samples are obtained from the Defence Metallurgical Research Laboratory [30]. The process used essentially consists of melting GdBCO into the pro-peritectic $Gd_2BaCuO_5$and liquid phase at high temperature. The mixture is cooled slowly through the peritectic formation temperature ($\simeq 1000^0C$) to 900°C and then furnace cooled. The samples are then oxygenated at 450^0C for 7 days.

References

[1] E.J.Pakulis and Osada, Phys. rev. **B, 37, 5940 (1988)**

[2] A.Gould, E.M.Jackson, K.Renourd, R.Crittenden, S. M. Bhagat, **N. D. Spencer, L. F. Dolehert and** R.F.Wormsbecher, Physica C, **156,** 555 (1988)

[3] J.Halbritter, J. Appl. Phys, 71, 339 (1992)

[4] S.V.Bhat, P.Ganguly and C.N.Rao, Pramana J.Phys, **28** L 425 (1987)

[5] M. Poirier, G. Quirion, K.R.Poeppelmeier, J.P.Thiel, Phys. Rev **B, 36,** 3906 (1988)

[6] S.Sridhar and W.L.Kennedy, Rev. Sci.Instrumen. **59,** 531 (1988)

[7] K.Kato, K.Takahashi, H.Mitera, K.Minami, Jpn. J. Appl. Phys, 27, 164' (1988)

[8] S.M.Anlage, Hsuan Sze, H.J.S nortland, S.Tahara, B.Langley, C-B. Eom and M.R.Beasley, Appl. Phys. Lett, **54,** 2712 (1989)

[9] R.Pinto, N. Goyal, S.P.Pai, P.R.Apte, L.C. Gupta and R. Vijayaraghavan, J. Appl. Phys. 73,5105 (1993).

[10] Stephen Ducherme, R.Durny, J.Halbritter, D.J.Zeng, P.C.Taylor, O.G.Symko, S.Kulkarni, J. Appl. Phys, **66,** 12152 (1989)

[11] A.Omari and A.F.Khoder, Cryogenics, **33,** 1098 (1993)

[12] Dong-Ho Wu, C.A.Shiffman and S.Sridhar, Phys.Rev. B, **38,** 9311 (1988)

[13] Shin-Yu-Feng, Rev. of Sci. Instrumen. **40,** 963 (1969)

[14] J.R.Singer and S.D.Johnson, Rev. of Sci. Instrumen. **30,** 92 (1959)

[15] F.Bruin and P.C.Van Soest, ibid, **31,** 909 (1960)

[16] B.Donally and T.M.Sanders, ibid, **31,** 977 (1960)

[17] Y.T.Yang and T.C.Chen, ibid, **36,** 706 (1969)

[19] A.L.Shalow and G.E.Devlin, Phys. Rev. B, **13,** 120 (1959)

[20] B.W.Langley, S.M.Anlage, R.F.W.Pease and M.R.Beasley, Rev. Sci. Instrum. **62,** 1801 (1991)

[21] S.Sridhar, H.Hamdeh and C.A.Shiffman, Phys. Rev. B, 36, 2301 (1987)

[22] B.F.Kim, J.Bohandy, K.Moojani and F.J.Adrian, J. Appl. Phys. **63,** 2029 (1988)

[23] B.F.Kim, J.Bohandt, T.E.Phillips, F.J.Adrian and K.Moorjani, Physica **C, 161,** 76 (1989)

[24] H.A.Bethe and J.Schinger, NDRC Rre, D 1, 117 (1943)

[25] E.G.Spencer, R.C.Le Craw and A.L.Alut, J. Appl. Phys **28,** 130 (1957)

[26] R.A.Waldron , Proc. Inst. Elec. Engg, Part C, **107,** 272 (1960)

[27] H.Maeda, Y.Tanaka, M.Fukutomi and T. Asano, Jpn. J. Appl. Phys. **27** L209 (1988)

[28] V.Seshu Bai, S.Ravi, **T.Rajasekharan and R.Gopalan, J.** Appl. Phys. **70,** 4378 (1991)

[29] Y.Tanaka, T.Asano, K.Togano and H.Maeda, Appl. Phys. Lett. **54,** 1582 (1989)

[30] E.Sudhakar Reddy and T.Rajasekharan, DMRL, Kanchanbagh, Hyderabad 500058, India.

Chapter 3

TEMPERATURE AND FIELD DEPENDENCE OF RADIO FREQUENCY ABSORPTION IN BSCCO AND GdBCO

3.1 Introduction

Electromagnetic response of various HTSCs has been explored by a variety of techniques. In the case of power absorption low energy excitations are possible due to the presence of thermally excited quasi particles or due to the pair breaking caused by the magnetic flux. In the framework of the two fluid model this can be thought of as absorption by normal (dissipative) fluid, where the fraction of the normal electrons is given by $n_n = 1 - rp^2$, where ψ is the superconductor order parameter. However, there does not yet appear to be a common consensus regarding the origin of the low field absorption. In the conventional type II superconductors the mechanism of field dependent microwave losses is well understood and is believed to be due to the viscous motion of the Abrikosov fluxons [1], since almost all the effects of pinning are absent at GHz. However at radio frequencies and in HTSCs the situation may be altogether different because of the predominance of the weaklinks in these samples. Thus it calls for a detailed study of field induced loss at radio freqeuncies.

Various models have been developed to explain the phenomenon of low field absorption in HTSCs at microwave frequencies. Of the various models proposed the

resistively shunted Josephson junction (RSJ) [2-6], decoupled junction [7,8] and flux flow models [9-12] are most appealing. In this chapter a systematic study of field and temperature dependent rf absorption in BSCCO and GdBCO superconductors is presented.

3.2. Power Absorption in BSSCO Superconductor

3.2.1. Experimental

Single phase $Bi_{1.2}Pb_{0.3}Sr_{1.5}Ca_2Cu_3O_y$(BSCCO) superconductor is used for the present study. Preparation and characterization by XRD are given elsewhere [chapter2,13]. Transition to zero resistance is observed at 107 K. The temperature and field dependence of the radio frequency absorption is carried out using the marginal oscillator discussed in Chapter 2. As the temperature or field is varied power output of the oscillator is monitored. No arrangement is made to cancel earth's magnetic field. Absorption through transition is monitored while warming and cooling the sample, and both responses are found to coincide confirming zero temperature gradient between the sample and the sensor and validity of the T_c determined.

Low field radio frequency absorption (LFRA) measurements are carried out after cooling the sample to the required temperature in zero field and then applying an external dc field in steps upto about 40 mT. The external magnetic field is produced by a solenoid and is parallel to the tank coil length and thereby the rf magnetic field. Some authors [11,14] have reported a change in the absorption with time when the external field is applied or when the previously applied field is withdrawn, which is

attributed to the slow flux creep with time and therefore, the nonequilibrium state of the sample. However, we have not observed any change in the magnitude of the absorption with time at any applied field. Firstly, because the field is increased slowly in steps upto 40 mT in about 15 mts duration, and secondly, the kind of grain boundary fluxon creeping into the less dissipative parts (grains) is not seen in this sample. Hence, when the data (LFRA) are recorded the sample is assumed to be in the equilibrium state.

3.2.2. Temperature dependence of absorption

Change in the power absorption as a function of temperature is shown in Fig. 1. As can be seen from the figure critical temperature cannot be precisely determined because of the peak at the onset of the transition. The rf critical temperature, T_c^{rf}, is determined from the intersection of the extrapolated region in the sharp drop and the normal state region. For the analysis in this report $T_c^{rf} = 106.5\text{K}$ is considered the critical temperature of the sample. The peak in the vicinity of the T_c^{rf} is attributed to the distribution of T_c s and the local demagnetization factor which arises as the sample enters a mixed state (glassy) resulting in an irregular flux lattice causing an increase in the local rf field in the sample. In samples with such a distribution of T_c field is expelled from the particles which become superconducting causing an increase in the local magnetic field, as is sensed by the other particles and this gets reflected as an increase in the absorption. Though the contribution from the demagnetization factor is less, it cannot be ruled out completely. Since the sample is sintered and the effects of granularity dominate (as will be shown in the following sections) any attempt to describe the temperature dependent absorption in terms of basic BCS

theory, even in its dirty limit, may not be appropriate. Therefore, we consider the London's two fluid model. In this model the normalized power absorption is given by [15]

$$\frac{dP}{P_N} = \frac{\sqrt{2}\lambda}{\delta_n} \frac{\sqrt{[1+(\sqrt{2}\lambda/\delta_1)^4]^{1/2}-1}}{\sqrt{1+(\sqrt{2}\lambda/\delta_1)^4}}$$

where $\delta_n = [\frac{2}{\mu_0\omega\sigma_n}]^{1/2}$, $\delta_1 = [\frac{2}{\mu_0\omega\sigma_1}]^{1/2}$ are the electromagnetic skin depths. σ_n and $\sigma_1 = \mathrm{Re}(\sigma)$ are the normal state conductivity and the real part of conductivity in the superconducting state, respectively. A is the penetration depth, $\lambda = \lambda_0/\sqrt{1-t^4}$. We believe that in the case of HTSCs the A in the Eq (1) represents the effective penetration depth λ_{eff} rather than the London penetration depth. At 11.914 MHz, the frequency used in the present experiments, with $\rho_n = 25\mu\Omega - m$ and $\delta_n = 1030\mu m$ the λ_0 obtained is $233\mu m$. Obviously this value in not the London penetration depth. The penetration depth of HTSCs is large compared to the coherence length and mean free path, which is very short. The principal effect of short mean free path is to greatly reduce the superelectron screening so that $\sigma_2^{eff}/\sigma_n = (\lambda_0/\lambda_0^{eff})^2(\sigma_2/\sigma_n)$ [18]. Here σ_2 is the imaginary part of conductivity in the superconducting state. In such a case λ_0 obtained for a uniform superconductor gives an estimate of the effective penetration depth given as $\lambda_0^{eff} = g\lambda_0$, where g is the reduction factor of screening. And for a granular superconductor $\lambda^{eff} = \sqrt{(\lambda_g^{eff})^2 + (\lambda_J^{eff})^2}$. Where, λ_g^{eff} comes from the grain penetration depth (λ_g) and λ_J^{eff} from the Josephson penetration depth (λ_J). The λ_0^{eff} $(\simeq 80\mu m)$ values reported in the literature [16,17] are comparable to the present value.

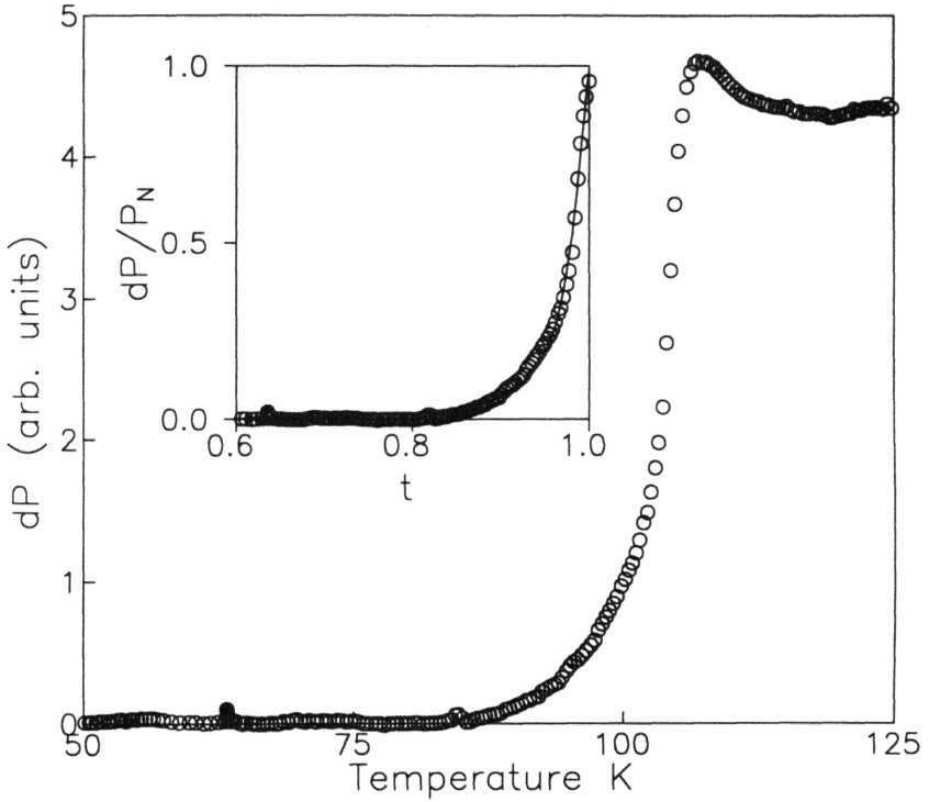

Fig. 1 Temperature dependence of rf power absorption for BSCCO sintered sample. In the inset, fit to London's two fluid Eq. 1 of to the normalized absorption (dP/P_N) is shown. P_N is the absorption above T_c with reference to that at low temperatures and t is the normalized temperature.

It has been reported earlier that in the microwave absorption study of the same sample [15] the " additional loss ", compared to the two fluid fit, in the zero field absorption below $t < 0.95$ (the tail region) is attributed to the intergranular effects. Such an additional loss, however, is not observed **at** radio frequencies. This is due to the fact that the rf screen depth (which is related **to penetration depth)** is much higher than the microwave screen depth. In other words, **the** junctions present in the surface of the superconductor alone participate in microwave absorption whereas at rf a variety of junctions (mostly grain boundary junctions) present deep inside the surface contribute to the power absorption. At microwave frequencies $\lambda_0 = 0.1$ μm. Though the expected London penetration depth is of the same order, this value cannot be identified with λ_L. It is interesting to note that powder BSCCO sample (though the amount of sample used is same as that of the pellet) does not show any measurable power absorption through transition. This reiterates **that at** radio frequency the loss arising from grain boundaries is predominant.

3.2.3. Field dependent absorption

Since the lower critical field H_{c1} of the weaklinks is orders of magnitude smaller (~ 0.1 Oe) than that of the grains, the magnetic penetration is more facile into the junctions than into the grains. And hence, the change in the power absorption at low fields can be understood from the behavior of the Josephson junctions in small magnetic fields, studied theoretically by de Gennes for insulating junctions [18]. The limiting cases of Josephson junction behavior in a magnetic field are (a) very weak magnetic fields where the field decays exponentially along the junction **and** (b) strong fields where the field completely penetrates the junction. Weak field behavior holds

for fields

$$H << H_{c1}^{Jos} = \phi_0/2\lambda\delta$$

where ϕ_0 is the flux quantum and $6 = (hc^2/16\pi e I_c\lambda)^{1/2}$ is the characteristic penetration depth of the weak fields into the junction with I_c the zero field critical current density through the junction. The magnetic field within the junction decays as H(y)=H exp(-y/k) where y=0 corresponds to the intersection of the junction and the grain surface. For strong fields with $H >> H_{c1}^{Jos}$ the junction currents become periodic with wavelength / = $\phi_0/2\lambda H$ and are given by

$$I_y = I_c Sin[2\pi(y - y_0)/l]$$

with each period carrying one quantum of flux. The maximum current through the Josephson junction varies as

$$I_c(H) = I_c(0)Sin(\pi H/H_0)/(H/H_0)$$

where H_0 is the field at which the junction contains one quantum of flux. Magnetic field reduces the critical current of the Josephson junction following the above Eq. We find that the field induced absorption (discussed in detail in the following sections) goes as the inverse of $I_c(H)$ averaged over a large number of junctions with a

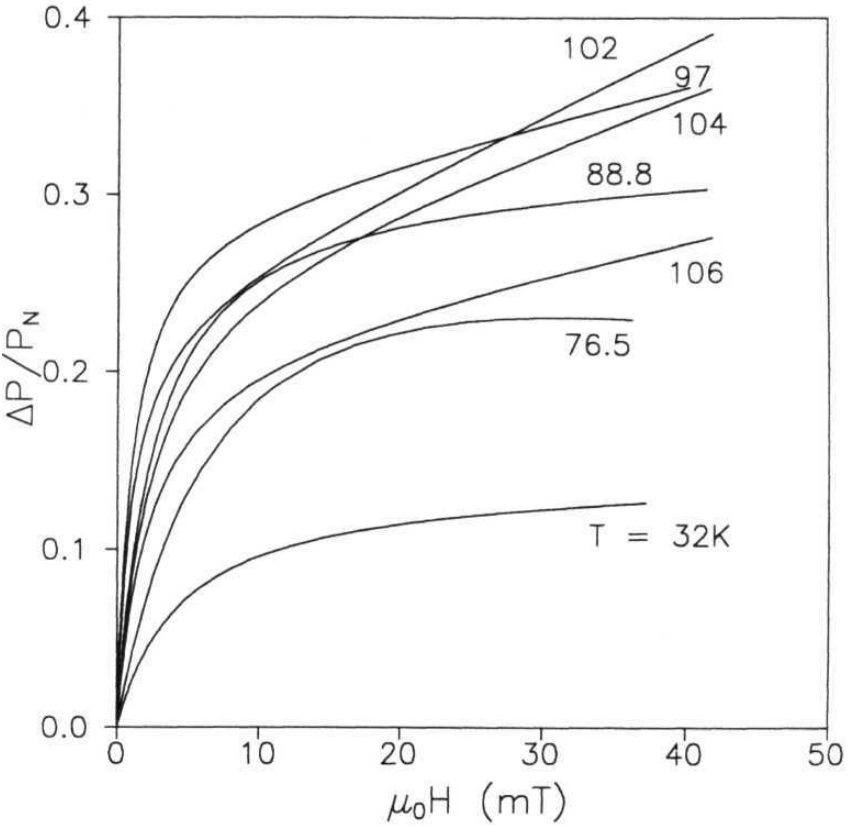

Fig. 2 Field dependence of power absorption at various temperatures below T_f.

distribution in H_0 . Experimentally, H_0 is the field at which power absorption is half the maximum.

The magnetoabsorption recorded at several temperatures between 32 K and 106 K are shown in Fig. 2. It can be seen from the figure that at low fields absorption increases monotonically with field and saturates at higher fields. However, at higher temperatures absorption tends to be linear at higher fields. To represent the data over the entire temperature range we use the empirical equation proposed, initially, to describe microwave absorption data in the same sample (15).

$$p(H,t) = \frac{\Delta P}{P_N} = \frac{\alpha(t)}{1 + \frac{H_0(t)}{H}} + \beta(t)H^n \qquad \textbf{(2)}$$

where p(H,t) is the normalized magnetoabsorption. P_N is the absorption above T_c, $\alpha(t)$ is the ratio of the change in magnetoabsorption *AP* as the field is increased from 0 to the saturation region to P_N. $\beta(t) = dP/d(\mu_0 H)$ is the slope of the linear part of the virgin curve at higher temperatures and fields and n=1. All the virgin curves are found to be following the Eq. 2 reasonably well. A typical fit at 32 K is shown in Fig.3

Some authors [19] attributed the loss to the dephasing of the junctions with the application of magnetic field. The two basic assumptions are 1) the junctions decoupled by the application of magnetic field offer a series resistance to the rf current and hence contribute to the loss and 2) the decoupling probability of a junction depends exponentially on the magnetic field. The field dependent absorption is expressed as

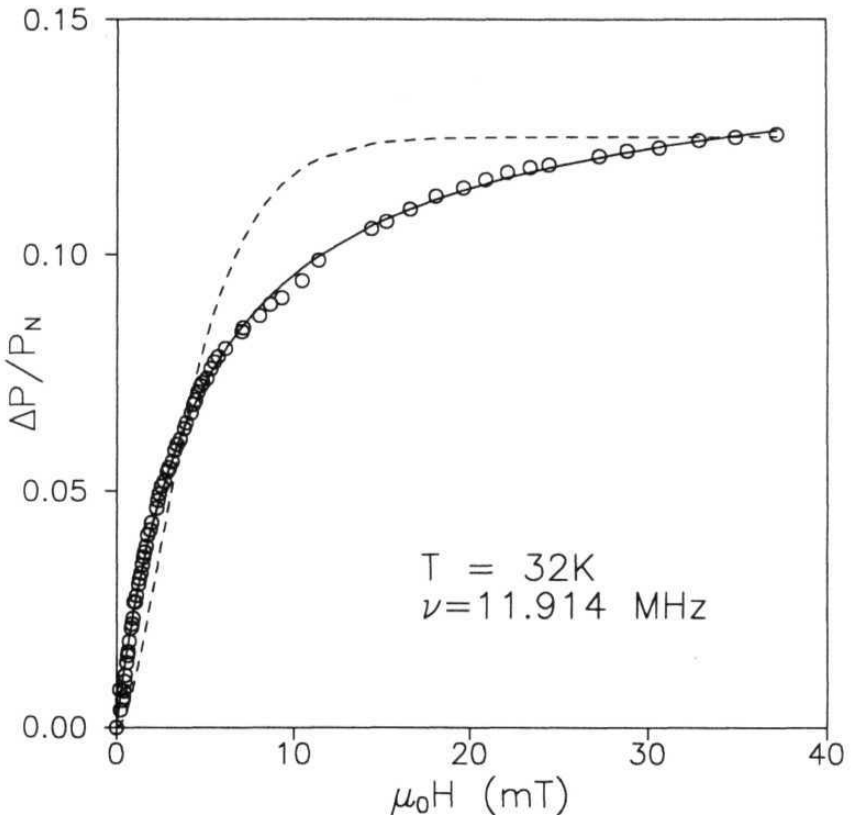

Fig. 3 Squares represent the rf magnetoabsorption of BSCCO at 32K. Solid line is a fit to the RSJ model (Eq. 2). Dashed line is a fit to Eq. 3. The excellent fit to Eq. 2 suggests that the magnetoabsorption is dominated by the reduction in the junction current than the resistance offered by junction decoupling.

$$\Delta P(H) = \Delta P_0[1 - e^{-H/H_d}(\frac{H}{H_d} + 1)] \quad \textbf{(3)}$$

where ΔP_0 and H_d are the saturation absorption and dephasing field, respectively. However, as shown in the Fig. 2 the losses increase gradually with magnetic field with the largest loss increment at low fields, i.e. in the coherent state of the junctions. Therefore, we find that such an interpretation cannot be used in the present case as we show in Fie. 3 that Eq 3 cannot describe the experimental data.

(i) $\alpha(t)$

Fig. 4 gives the variation of $\alpha(t)$ with normalized temperature, $t = T/T_c$. It can be seen from the figure that $\alpha(t)$ gradually increases with t, exhibits a peak at t=.93 and then drops off. Low field absorption is dominated by large weaklinks and the number of such weaklinks depends on the superconducting energy gap at the superconductor - insulator (S-I) or superconductor - normal (S-N) interfaces. At the interfaces energy gap decreases dramatically, thus producing a tunneling barrier. This process is possible because of short coherence lengths observed in HTSCs. At low temperatures the gap at S-I or S-N interface would return to the bulk value A(0) by proximity effect and hence the number of junctions would be reduced.

The parameter $\alpha(t)$ at GHz frequencies, in contrast, does not decrease at low temperatures but rises to an approximately constant value as shown in the inset of Fig. 4. Some other groups [20] have also observed a similar result. Presumably, the reason is that there is not much change in the number of weaklinks and the Josephson current in the surface layer as the temperature is increased. Whereas in LFRA, since

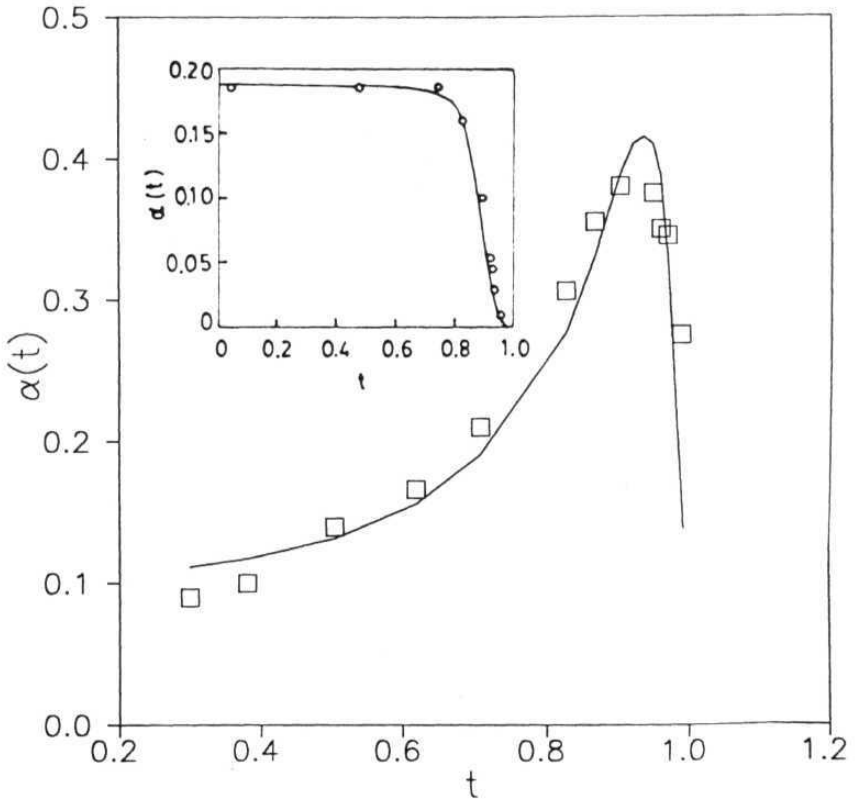

Fig. 4 Temperature dependence of $\alpha(t)$ obtained from the magnet oabsorption data (squares) at various temperatures. Solid line is a fit to the Eq. *4.* In the inset $\alpha(t)$ variation at 9.9 GHz (ref. 15) is shown.

the weaklinks in bulk of the sample contribute to the loss, an increase in their number would result in a gradual rise in loss as t is increased. The Eq. 2 does not contain any information on the number of weaklinks, and since we do not have a priori knowledge of the temperature dependence of the number junctions N(t) and their effective areas, we try an empirical model for $\alpha(t)$ of the type

$$\alpha(t) = \frac{\alpha(0)}{(1 + b[I_c^0]^{-2})} \frac{1}{(1 - t^2)} \qquad (4)$$

where b is a sample dependent parameter and $1/(1 - t^2)$ represents the variation of N(t). It is reasonable to think that the number of junctions depends on E_J (coupling energy), A (t), $\backslash(t)$ and hence one naturally expects a complex temperature variation of N(t). However, Eq. 4 fits well to the experimental results, for $b/(I_c^{00})^2 = 3.18X10^{-3}$. The I_c^0 (t) in Eq. 4 can have two different temperature dependencies, one is SIS type where $I_c^0(t) = I_c^{00}(1 - t)$ and the other SNS type where $I_c^0(t) = I_c^{00}(1 - t)^2$. Incidentally, Eq 4 fits well to both SIS and SNS variations and cannot give any specific information on the type of weaklinks in the sample. In the forthcoming discussion we show that the junctions responsible for absorption at radio frequency are of SIS type. It is important to note that at 77K the observed value of the initial slope , α/H_0, is about 100 T^{-1}. This is several orders of magnitude larger than the value predicted by flux flow loss [11,21], providing yet another support to the RSJ picture.

(ii) $\beta(t)$

As can be seen from the Fig. 2 the low field absorption is linear at high temperatures and high magnetic fields .The values of $\beta(t)$ at various temperatures are shown

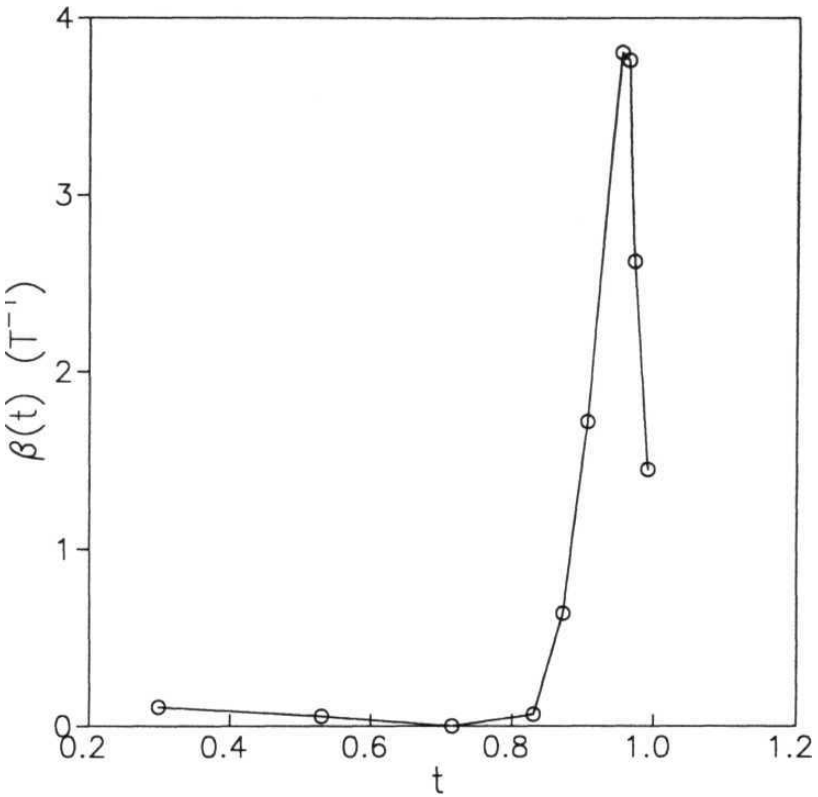

Fig. 5 Variation of $\beta(t)$ obtained from the fit to the RSJ model (Eq. 2). $\beta(t)$ is almost neglegible at low temperatures and shoots up only at 10K below T_c suggesting that the weaklinks responsible for absorption in this temperature range are strongly coupled intragrain junctions. Solid line is a guide to the eye.

in Fig. 5 against normalized temperature t. It can be seen that the **value of** $\beta(t)$ is more or less constant at low temperatures and shoots up above t = 0.85 forming **a peak** at t =0.955. A similar change in $\beta(t)$ has been observed in this sample at microwave frequencies [15]. But, at the present frequency of 11.914 MHz, the onset of the rapid rise of $\beta(t)$ takes place at a lower temperature than that at 9.98 GHz. We **also** find that at these temperatures there is no hysteresis in the magnetoabsorption. Such a change can be attributed to a very different kind of weaklinks (intragrain) operating at these temperatures. Since the magnetoabsorption response is close to being linear at higher t, one can write *fi(t)* = $dP/d(\mu_0 H)$ as is expresssed at microwave frequencies [15].

It can also be seen from Fig. 5 that the value of $\beta(t)$ (= .00038 T^{-1}) at T_{pk} is twice as much as that of *ft(t)* at 9.98 GHz [15]. Such a high value can only be explained qualitatively invoking more number of junctions in this region at rf than at microwave frequencies, since rf penetration depth is larger. The peak in *fi(t)* is reminiscent of high field (H = 1T) losses observed in some bulk [20] and thin film [21] HTSCs. In both cases absorption is attributed to viscous losses due to fluxons. The results were expressed as

$$\frac{dP}{d(\mu_0 H)} = \frac{\delta}{\lambda}\frac{1}{B_{c2}}F \qquad \textbf{(5)}$$

where $F = e^{-U/kt}$ and

$$F = [1 + (\frac{k}{\eta\omega})^2]^{-1} \qquad \textbf{(6)}$$

where U is pinning energy, k and η are temperature dependent pinning force constant

and fluxon viscosity per unit length, respectively, and other parameters have their own usual meanings. The observed magnitude of $\beta(t)$($\sim 4T^{-1}$) is much larger than that would be expected from either Eq. 5 or Eq. 6 (for a detailed discussion ref. to 15). Therefore, the present results make viscous losses an unlikely explanation for the LFRA phenomenon. There is a possibility that $\beta(t)$ is mostly due to strongly coupled weaklinks in the grain region. These weaklinks are sensed only near T_c because of rapid increase in the penetration depth in this region. So, the high temperature LFRA is again due to weaklinks modeled as RSJs with $\beta(t) = \alpha/(H + H_0')$ which is approximately equal to α/H for $H << H_0'$. The junction areas in the grain weaklinks are much smaller compared to that of intergrain weaklinks, which cause the large initial LFRA. And accordingly, one can expect large H_0' values for intragrain weaklinks as can be inferred from Eq. 7. The drop in *ft(t)* above t_{pk} is due to the fact that as $t \rightarrow 1$ all RSJ must disappear. It is quite appropriate to think that t_{pk} gives the onset of junction disappearance in the sample.

(iii) $H_0(t)$

Experimentally, it is found that H_0 decreases with increase in temperature as shown in Fig. 6. It is shown [2] that

$$H_0(t) = \frac{x_0(t)}{< A(t) >} \qquad (7)$$

with $x_0(t) = b\eta_0 I_c^0(t)$ and $< A(t) >= \lambda(t)d, d$ is the average junction thickness. Variation of H_0 therefore comes from that of A and I_c^0 .As already mentioned above $I_c^0(t)$ varies as (1-t) or $(1 - t)^2$ depending on whether the junctions are SIS or SNS type, respectively. In the Fig. 6 two fits for $H_0(t)$ corresponding to SIS and SNS

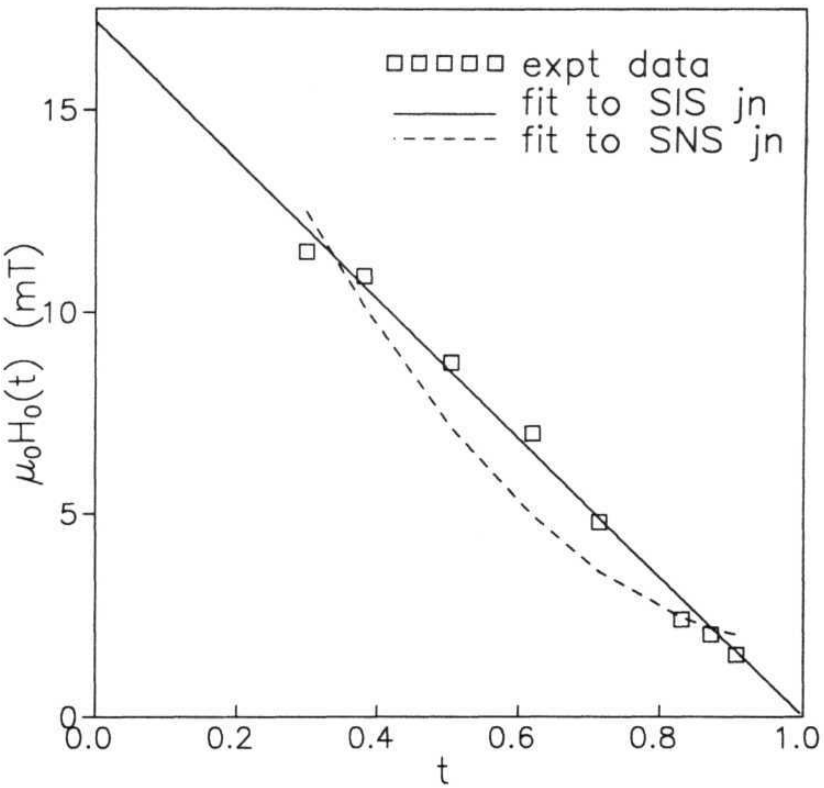

Fig. 6 $H_0(t)$, (squares) the field at which each weaklink on the average is expected to have one flux quantum in it, as a function of normalizex temperature t. Solid and dashed lines are the fits to the Eq. 7 for SIS and SNS type of $I_c^0(t)$,respectively. A very good fit to the SIS type is evident.

variations are shown. The excellent fit to SIS type temperature dependence of $I_c^0(t)$ confirms that the junctions are of SIS type. It is worth noting that a roughly linear decrease of $H_0(t)$ vanishing as $t \rightarrow 1$ is observed in the case of YBCO sample [2]. Such a temperature dependence is consistent with having SIS junctions. Another point to note is the higher values of H_0 in LFRA than that in LFMA [14]. At 77K, $H_0^r = ArnT$ whereas $H_n^{mw} \sim 1mT$. Since the number of junctions participating in the absorption at rf is more and the average I_c^0 of the grain boundary weaklinks is much higher than that of the surface defects, the higher value of H_0^r is not surprising, though the average area of the grain boundary junctions which contribute to the loss at rf is marginally larger than that of the surface defects which contribute to the loss at GHz [2,15]. This picture, higher value of H_0^r , also substantiates the increase in $\alpha(t)$, and $\beta(t)$ at radio frequencies.

It is worth noting that magnetoabsorption gives an indirect estimate of the critical Josephson current variation [31]. A Josephson junction subjected to micorwave current can be modelled by an inductance L and a shunt resistance R [32], giving microwave losses

$$P = \frac{P_N}{1 + (R/\omega L)^2} = \frac{P_n}{1 + [(2eR/\hbar\omega) I_c(H) cos\phi_0]^2}$$

$$1 + (R/\omega L)^2 \quad 1 + [(2eR/\hbar\omega) I_c(H) cos\phi_0]^2$$

$I_c(H)$ is given by the diffraction reduction discussed above, in the case of many junctions with distribution in junction areas it is given by $I_c(0)H_0/(H + HQ)$. And thus the reduction in $I_c(H)$ is what decides the magnetoabsorption. Therefore, in principle, one can obtain the $I_c(H)$ response from the magnetoabsortion response.

3.3. Power Absorption in GdBCO Superconductor

3.3.1. Experimental

Single phase sintered $GdBa_2Cu_3O_7$ (GdBCO) superconductor made by the well known solid state route is used for **the present** study. Sample is characterized to be single phase by XRD and transition to zero resistance is observed at 91.5 K. Low field radio frequency absorption (LFRA) measurements are carried out after cooling the sample to the required temperature in zero field and then applying an external dc field in steps upto about 50 mT.

3.3.2. Temperature dependent absorption

Change in the power absorption as a function of temperature is shown in Fig. 7. The transition is characterized by smooth rounding at the onset **and a** tail at $T < T_c^{rf}$. For the analysis in this report $T_c^{rf} = 91\text{K}$ is considered the critical temperature of the sample. As can be seen from the inset of Fig. 7 the London's two fluid equation (Eq. 1) fits very well to the experimental observation. At 11.914 MHz, the frequency used in the present experiments, with $\rho_n = 15\mu\Omega - m$ the λ_0 obtained (λ_0^{eff}) is 81 μm. Assuming $\lambda_0 - 0.4\mu m$ the reduction factor of screening, g, works out nearly to 200 μm which is one order of magnitude larger than that found in YBCO at microwave frequency [16]

3.3.3. Field induced absorption

In Fig. 8 magnetoabsorption variation of GdBCO sintered pellet at **various tem-**

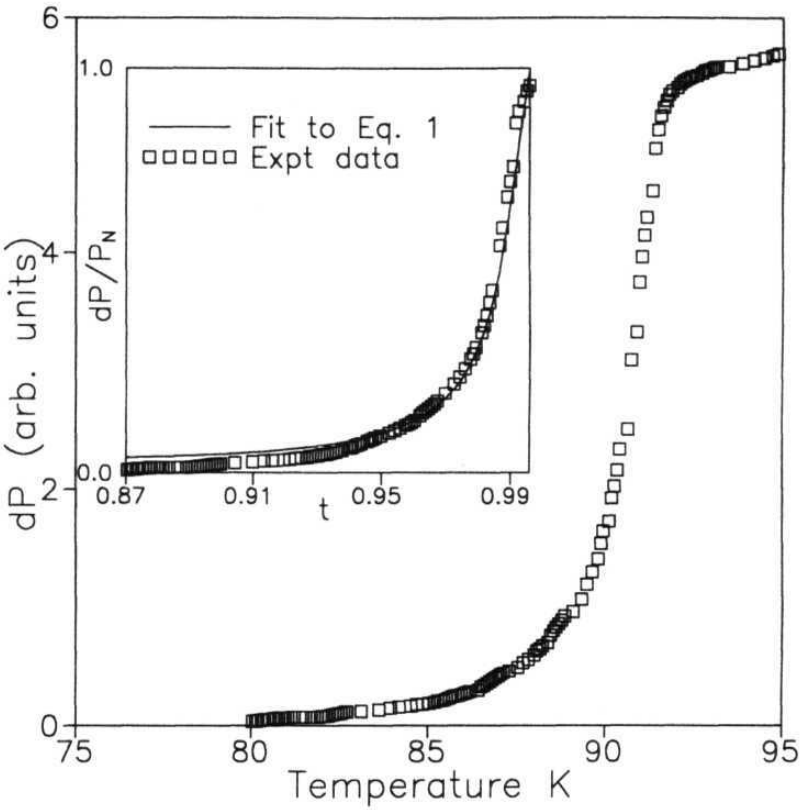

Fig. 7 Temperature dependent rf absorption in GdBCO. Shown in the inset is the change in absorption normalized to P_N versus the normalized temperature, t.

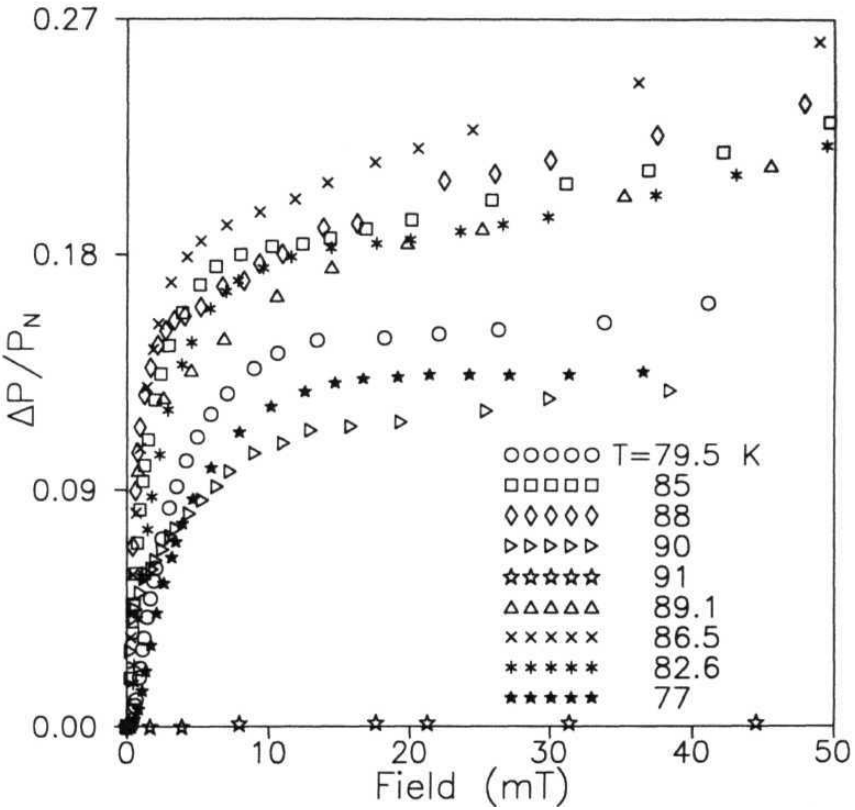

Fig. 8 Change in the magnetoabsorption at various temperatures below T_c^{rf}. The normazed values on y-axis give an estimate of the total magnetoabsorption with respect to the absorption through transition.

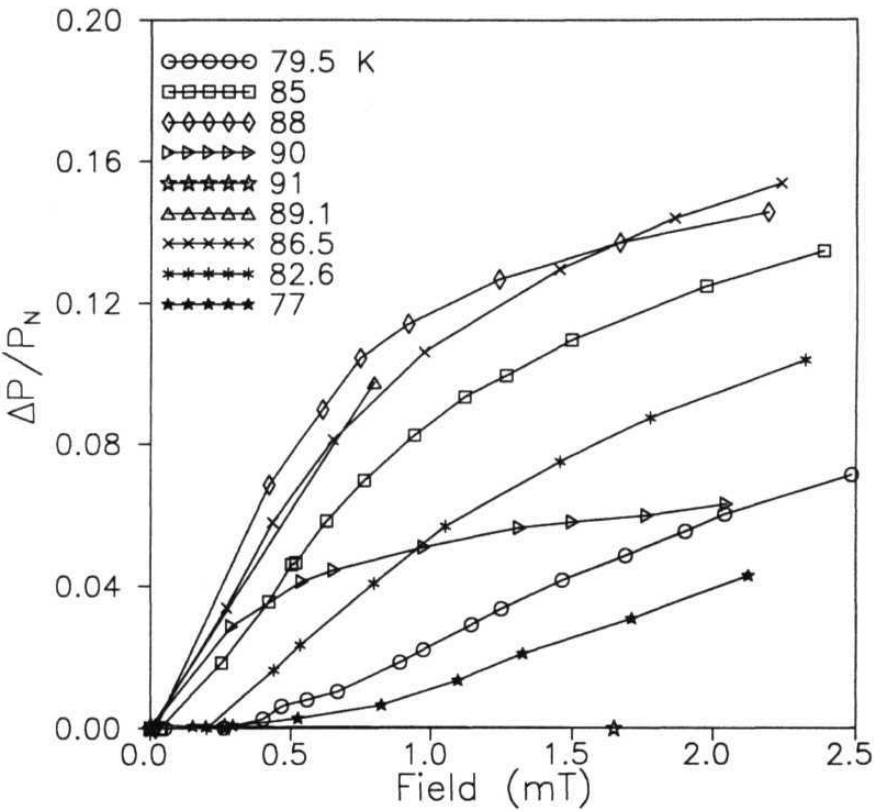

Fig. 9 Magnetoabsorption (Fig.8) expanded to show the slow initial rise with field.

peratures below T_c is shown. It can be seen that the overall absorption increases monotonically with field and saturates at high fields. However, a close look at Fig. 9, which is an expansion of the Fig. 8 at low fields, reveals many subtle features which can be interpreted in terms of inter and intra grain weaklinks operating in different temperature regions.

Firstly, at 77K, no measurable change in magnetoabsorption is observed up to about 0.5 mT. We define this field as the average lower critical field, H_{c1J1} of the intergranular Josephson junctions. At higher temperatures as can be seen from the Fig. 9, H_{c1J1} decreases as; 0.3 mT at 79.5K, 0.1 mT at 82.6K, 0.05 mT at 85K and above this temperature the initial slow rise disappears and the magnetoabsorption increases monotonically with field. The decrease in the H_{c1J1} with temperature is shown in Fig. 10a. As the temperature is increased the junction coupling energy E_J reduces as the thermal fluctuations dominate, allowing more and more junctions to be decoupled. And hence at higher temperatures $T > 86K$ absorption starts increasing as the field is increased above zero. From the Fig. 10a we obtain a temperature $T_{cJ} = 86.5K (< T_c)$ above which the contribution to the magnetoabsorption from the decoupled junctions ceases.

Secondly, the saturation in the magnetoabsorption observed at higher applied fields at 77K is not persistent at higher temperatures. One can see a clear deviation, a linear increase with field, from the saturation starting at 31.3 mT at 77K. This is attributed to the effective lower critical field H_{c1J2} of a second set of weaklinks, probably the intragranular weaklinks, at which the magnetic flux begins to have a measurable influence on them. Fig. 10b shows the reduction in $H_{c1J2}(t)$ as a function

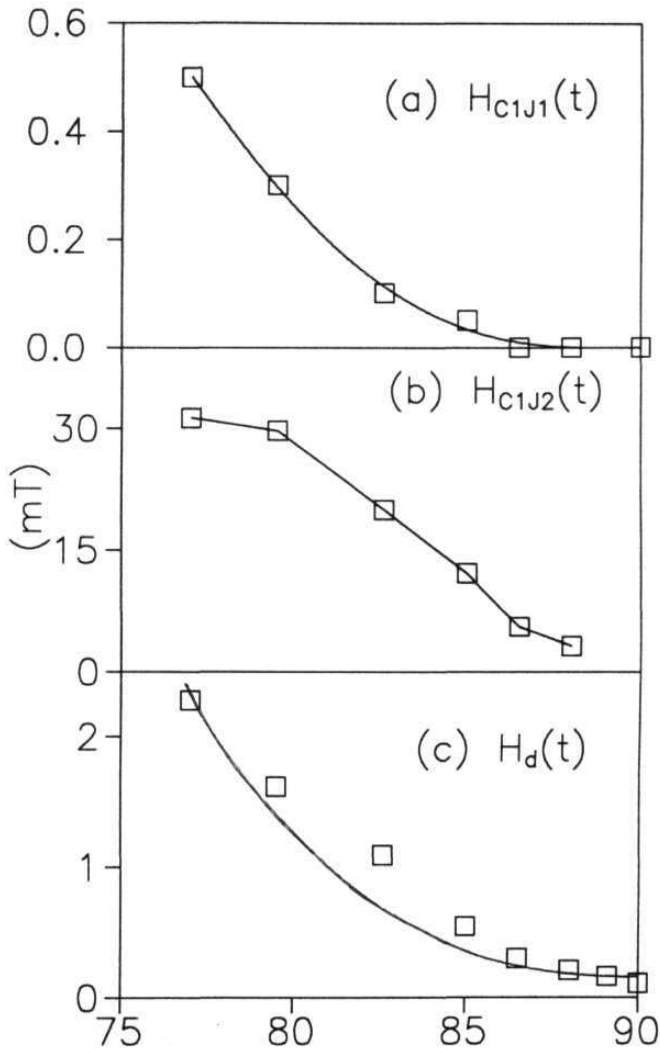

Fig. 10 Values of the characteristic (a) lower critical field of the intergrain region, (b) effective lower critical field of the intragrain junctions and (c) dephasing fields as a function of temperature.

of temperature. Yet another feature is the initial increase in the saturation magnetoabsorption value and a drastic reduction of the same as a function of temperature, as shown in Fig. 11.

To describe the magnetoabsorption fully we have made an attempt to invoke the existing RSJ model [2-6,15] as in the case of BSCCO but found that such a simple model cannot account for the magnetobsorption observed in this sample. In this model, at a fixed temperature the r.f. current becomes dissipative in the junction when the magnetic field exceeds a certain value depending on the junction geometry. And as a consequence, the resistive part of the junction increases until the junction is completely decoupled. Therefore the magnetoabsorption increases with field and when the junctions are decoupled it saturates. On the contrary, Guira's group suggested a decoupled junction model [7] to explain the magnetoabsorption. The basic assumptions in this model are a) the junctions decoupled by the application of field offer a series resistance to the rf current and b) the decoupling probability of a single junction depends exponentially on the magnetic field. As the field is increased more and more number of junctions are decoupled due to the distribution in the coupling strengths of the junctions and so an increase in the magnetoabsorption is expected. When all the junctions are decoupled the absortpion saturates. We find that even this model fails to account fully for the magnetoabsorption at all temperatures observed in the present sample, though a reasonably good fit (Fig. 11) to the experimental data is obtained at 77K.

In a sintered sample where there is a possibility of a number of paths for the rf current, it is hard to know whether the current flows through an RSJ, avoiding the

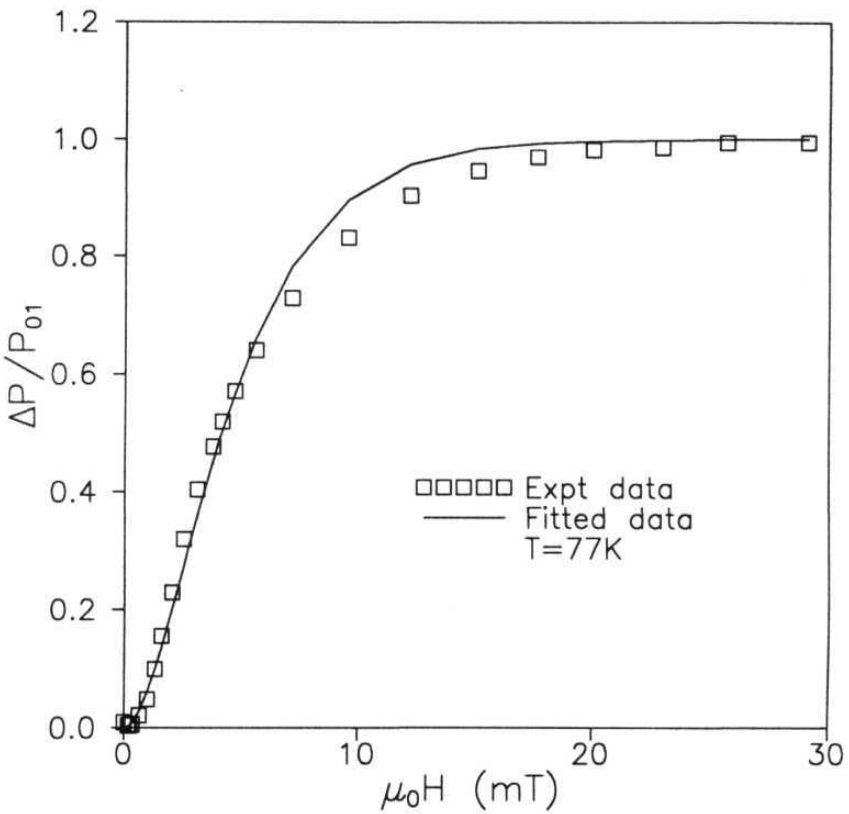

Fig. 11 Fit to the magnetoabsorption data using the first term in Eq.8.

decoupled junctions, or through a decoupled junction if there is no other low resistive RSJ path. Therefore, it is appropriate to consider that both the mechanisms discussed above contribute to the loss and whether the RSJ response dominates or the decoupled junction response dominates depends on the $H_{c1J1,2}$ and the temperature. To explain the nonlinear behavior of the magnetoabsorption at low fields and a slow linear increase at high fields we propose a model, which has contributions from both the RSJs and decoupled junctions, expressed as

$$\Delta P = P_{01}[1 - e^{-H/H_d}(\frac{H}{H_d} + 1)] + \frac{P_{02}}{1 + \frac{H_0}{H}} + \beta H \qquad \textbf{(8)}$$

where P_{01} and P_{02} are the saturation magnetoabsorption values in the decoupled junction and the RSJ model, respectively, H_d is the average dephasing field, H_0 is the field at which each weaklink on the average has one flux quantum in it and β is the slope, $\Delta P/d(\mu_0 H)$, of the higher field region of the magnetoabsorption at higher temperatures. Here, the first term represents the contribution from the decoupled junction model [Eq. 3] and the second and third terms the RSJ model [Eq. 2], which are used, independently, to explain the magnetoabsorption in various HTSCs. Figs. 12(a) and (b) show reasonably good fits to Eq. 8 at all temperatures. The parameters of concern here are the $H_d(t)$ and $\beta(t)$. From Figs. 10 (a) and (c) one can observe a similarity between $H_{c1J1}(t)$, obtained from the experimental data, and $H_d(t)$ obtained from the fit. As in the case of $H_{c1J1}(t)$, the T_{cJ} from $H_d(t)$ is again found to be 86.5K above which the change in $H_d(t)$ is minimal. The average $H_{c1J1}(t)$ being zero above 86.5K indicates that the loss coming from intergranular junctions starts decreasing rapidly. And hence the change in $H_d(t)$ above T_{cJ} is minimal.

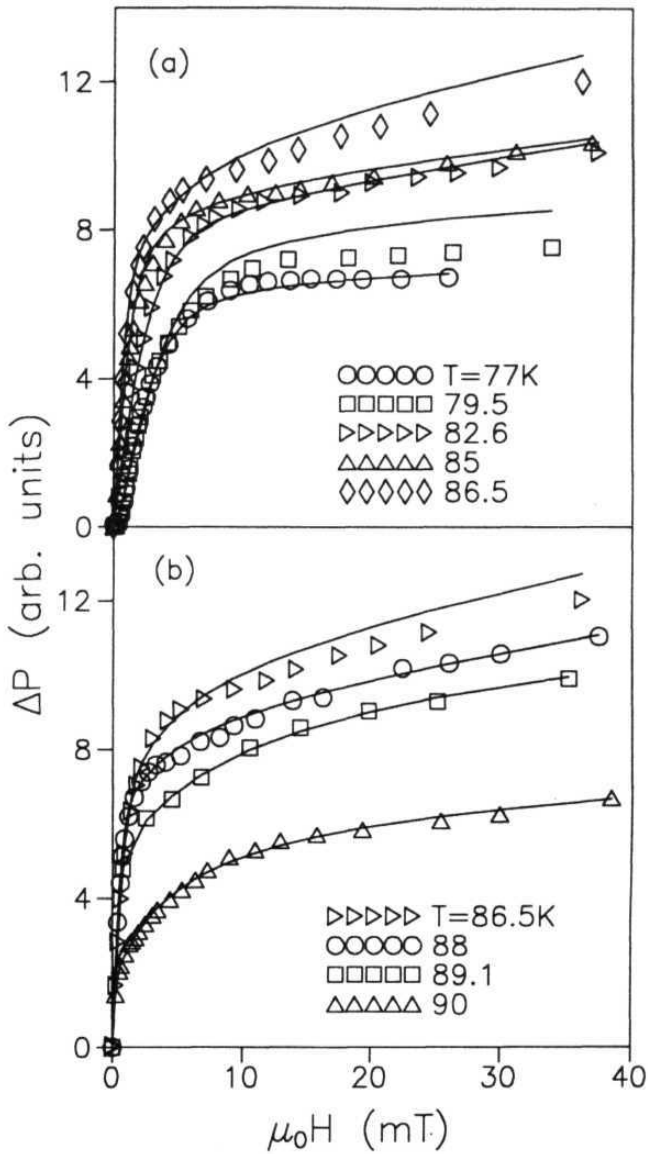

Fig. 12 Magnetoabsorption data fitted (solid lines) to Eq.8. A good fit suggests that the magnetoabsorption is both due to RSJs and the decoupled junctions.

Fig. 13 shows the variation of *ft(t)* with temperature. The linear variation in the magnetoabsorption at high temperatures and high fields can be explained to be originating from a different set of intragranular weaklinks. These strongly coupled weaklinks operate at high temperatures a few degrees below T_c^{rf} and probably have their origin in the intragrain region. There is a possibility that the linear rise at higher temperatures is due to the loss arising from the viscous motion of the vortices (flux flow). In the case of HTSCs the depinnig frequency, ω_0, is in the microwave frequency range (GHz) [22]. Since the present study is in the MHz range we rule out the depinning of the vortices by the high frequency currents and the attendant flux flow loss. However, thermally activated flux flow (TAFF) may contribute to the loss at high temperatures. The field induced absorption at high fields is often ascribed to the viscous motion of the intergranular hypervortices [23] or vortices in intragranular weaklinks[24]. Analysis of the viscous vortex motion [25-27] yields

$$P(B) = \frac{P_N B}{\sqrt{2B_{c2}B_z}} \qquad B << B_z$$

$$P(B) = P_N\sqrt{\frac{B}{B_{c2}}} \qquad B >> B_z$$

where B is the local intergranular flux density , $B_z = \mu_0\omega\eta\lambda_J^2/\phi_0$, ω and P_N are the rf angular frequency and the normal state loss, μ is the effective intergranular permeability, $\lambda_J = (\phi_0/2\pi\mu a J_c)^{1/2}$ the intergranular penetration depth [28], B_{C2} and J_c are the intergranular upper critical field [29] and the critical current density respectively.

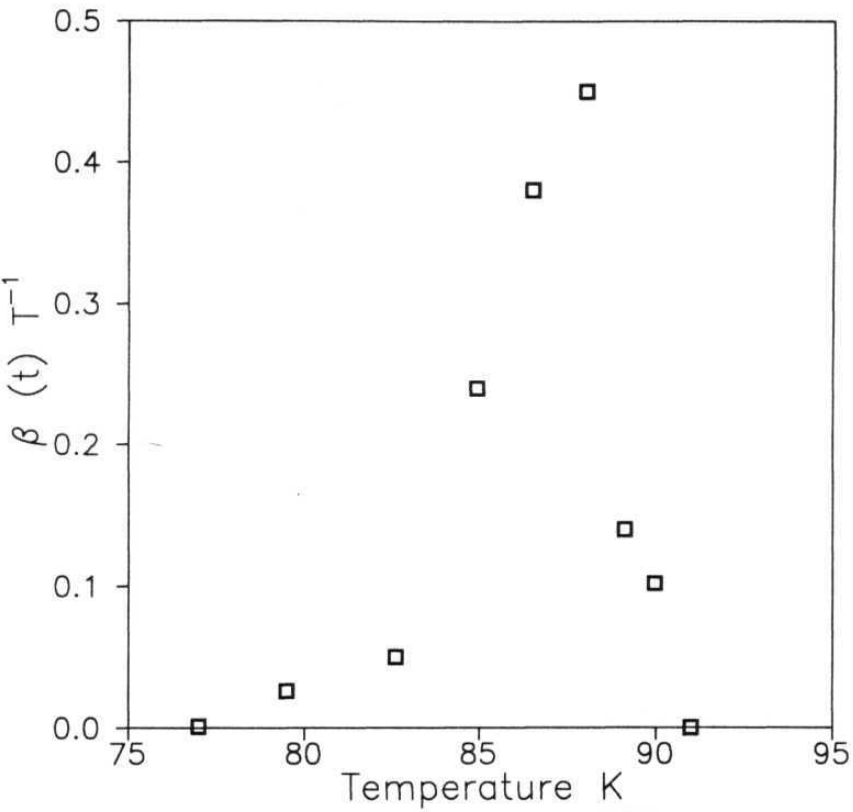

Fig. 13 $\beta(t)$ versus temperature. It can be seen that *f3(t)* shoots up at $T \simeq 85K$ suggesting that the strogly coupled weaklinks operate above this temperature. The sudden drop above 88K indicates the disappearance of the junctions as T approaches

rprf

a is the average grain dimension, ϕ_0 is the elementary flux quantum and η is the viscosity coefficient. For hypervortices $\eta = \phi_0^2/(2\pi\rho_n a^2)$. For $\rho_n \sim 15\mu\Omega -$ m and $a \sim 5\mu m$ an estimate of B_z gives $B_z \sim 10mT$. That means if the apparent linear rise, which takes place at high fields (> $10mT$) is due to flux flow it should vary as $\sqrt{B}$. In fact, we have separated this part from the remaining part of the magnetoabsorption and found no $\sqrt{B}$ variation. Secondly, a Josephson vortex model would require the existence of long Josephson junctions [30]. Taking the average grain diameter a as the maximum junction length, and the junction critical current density $J_{cJ} < 10^3 A/cm^2$, the requirement for a long Josephson junction (λ_J << a) is rather unrealistic. Hence, we conclude that the model for viscous vortex motion (flux flow) cannot describe the linear rise in this sample. Hence, the high temperature magnetoabsorption is again due to intragranular RSJs as is argued in the case of a BSCCO in the last section. From Fig. 13 it can be seen that below 85 K the response from such weaklinks is more or less negligible and that above 88K *fi{t)* decreases rapidly, which can be explained, in terms of rapid dephasing of intragranular weaklinks as T_c is approached.

At this juncture it is worth noting that BSCCO sample (section 3.2) does not show any slow exponential kind of rise at low fields in the magnetoabsorption. The different responses in GdBCO and BSCCO could be due to different grain fractions and porosities in these two samples. From the SEM analysis it is found that the average grain size of BSCCO is 5 μm and that of GdBCO is 10-12 μm. The density of GdBCO is found to be 93 % whereas for BSCCO it is 50% only. The initial slow rise of the magnetoabsorption in GdBCO can be understood in terms of higher density in this sample which leads to strongly coupled grain matrix with higher coupling energies for the Josephson junctions. Whereas, the loosely coupled grain matrix in

BSCCO leads to only weakly coupled Josephson junctions with very low lower critical fields causing a steep increase in magnetoabsorption even at very low fields. This could be one reason for not observing any dephasing effects in the BSCCO.

References

[1] M.Cardona, J.Gittleman and B.Rosenblum, Physics Letters, 17, 92 (1965), and J.I.Gittleman and B.Rosenblum, ibid, 20,453 (1966), J.I.Gittleman and B.Rosenblum, Phys. Rev Lett 16, 734 (1966).

[2] J.S.Ramachandran, M.X.Huang, S.M.Bhagat, K.Kish and S.Tyagi, Physica C, **202**, 151 (1992)

[3] E.J.Pakulis and T.Osada, Phys. Rev. **B,** 37, 5940 (1988)

[4] A.Dulcic, R.H.Crepeau, J.H.Freed, L.F.Schneemeyer and J.V.Waszczak, Phys. Rev **B,** 42,2155 (1990)

[5] B.Czyzak, Physica C, **243,** 327 (1995)

[6] M.Mahel, R.Adam, M.Darula, S.Chromnik and S.Benaka, Physica C, **202,** 243 (1992)

[7] R.Marcon, R.Fastampa, M.Guira and C.Matacotta, Phys. Rev B, 39, 2796 (1989).R.Fastampa, M.Guira, R.Marcon and C.Matacotta, Europhys. Lett, 6, 265 (1988). M.Guira, R.Marcon and R.Fastampa, Phys. Rev. **B,** 40, 4437 (1989).

[8] J.Wosik, L.M.Xie, J.Halbritter, R.Chau, J.C.Wolfe, V.Selvamanikam and K.Salama, IEEE Trans on Appl. Supercon, 3, 1432 (1992)

[9] K.W.Blazey, A.M.Portis and J.G.Bednorz, Solid State Communications, 65, 11153 (1988)

[10] M.W.Coffey and J.R.Clem. Phys. Rev. Lett, **67,** 386 (1991)

[11] L.Ji, M.S.Rzchowski, N.Anand and M.Tinkham, Phys. Rev **B, 47, 470** (1994)

[12] H.A.Blackstead, D.B.Pulling, M.Paranthaman and J.Brynestad, Phys. Rev. **B,** 51, 3783 (1995)

[13] V.Seshu Bai, S.Ravi, T.Rajasekharan and R.Gopalan, Journal **of Phys. 70,** 4378 (1991)

[14] V.G.Fleisher, V.I.Kozub and Yu.P.Stepanov, Physica C, **206,** 305 (1993)

[15] V.Seshu Bai, P.V.Patanjali, S.M.Bhagat and S.Tyagi, Journal of Superconductivity,**8**, 299 (1995)

[16] S.Sridhar, C.A.Shiffman and H.Hamdeh, Phys. Rev. **B,** 36, 2301 (1987)

[17] D.Sen, S.K.Ghatak, K.L.Chopra, G.Markandeyulu and D.Bhattacharya, Solid State Commun. 79, 935 (1991)

[18] P.G.De Gennes, Superconductivity of Metals and Alloys, Benjamin, New York, 1966, p. 234

[19] R.Fastampa, M.Guira, R.Marcon and E.Silva, Studies of High Temperature Superconductors, Nova Science, NY, ed by A.V.Narlikar, Vol 17, 115 (1996)

[20] M.Guira, R.Marcon and R.Fastampa, Phys. Rev. B, 40 4437 (1989)

[21] M.X.Huang, S.M.Bhagat, A.T.Findikogulu, T.Venkatesan, M.A.Manheimer and S.Tyagi, Physica **C,** 193, 421 (1992)

[22] F.Zuo, M.Salamon, E.D.Bukowski, J.P.Rice and D.M.Ginsberg, Phys. Rev. B, 41, 6600 (1990), A. Rastogi, Y.S.Sudershan, S.V.Bhat, A.K.Grover, Y.Yamaguchi, K.Oka and Y.Nishihara, Phys. Rev. **B,** 53, 9366 (1996)

[23] E.B.Sonin and A.K.Tagantsev, Phys. Lett **A, 140,127 (1989)**

[24] A.M.Portis and K.W.Blazey, Solid State Commun 68, 1097 (1988)

[25] A.M.Portis, K.W.Blazey, K.A.Muller and J.G.Bednorz, Europhys Lett, 5,467 (1988)

[26] M.W.Coffey and J.R.Clem, Phys. Rev. Lett, 58, 1143 (1991)

[27] R. Marcon, R.Fastampa, M.Guira and E.Silva, Phys. Rev **B, 43,** 2940 (1991)

[28] J.R.Clem, Physica **C, 153-155,** 50 (1988)

[29] A.S.Khenfets and A.I. Veinger, Physica C, **177,** 289 (1991)

[30] M.Mahel, M.Darula and S.Benacka, Supercond. Sci. Technol.**6**, 122 (1993)

[31] J.S.Ramachandran, M.X.Huang and S.M.Bhagat, Physica C, **234,** 173 (1994)

[32] J.D.Franson and J.E.Mercereau, J. Appl. Phys. **47,** 3261 (1976)

Chapter 4

HIGH FIELD MICROWAVE ABSORPTION IN SINTERED AND MELT TEXTURED HTSCs

4.1.Introduction

In the last Chapter the low field absorption in sintered BSCCO and GdBCO has been discussed in terms of Josephson junction models. However, at high fields since all the Josephson junctions are broken the effects of granularity are not observed and the superconductor goes into a critical mixed state with a periodic Abrikosov Lattice. In a type II superconductor, a transport current can give rise to flux flow dissipation because of the Lorentz force acting on the flux line or the flux line lattice. The direct and alternating current methods are effectively used to determine the flux flow resistivity. The dc method presents some disadvantages, namely the large transport current (greater than the critical current) used to overcome the strength of the pinning centres, produces a heating of the sample and a self field which bends the vortex lines. In the ac methods, generally in the microwave range, the microwave currents produce motion of the vortex lines at current densities much smaller than the J_c, provided that its frequency is higher than the depinnig frequency.

A phenomenological model proposed by Gittleman and Rosenblum [1] is generally used in the literature to study the high frequency absorption connected to the flux-flow dissipation. Assuming the current density J to be directed along the y-axis and **the** applied field along the z-axis, the equation of motion for the unit length of a

single vortex is

$$m\frac{dv}{dt} + \eta v + kx = J\phi_0, \qquad (1)$$

where, v = dx/dt is the fluxon velocity with x being the vortex displacement along the x=axis; m, η and k are the fluxon effective mass per uint legth, the viscosity coefficient and the pinning force constant, respectively. Since the displacement of the vortex lines is more or less the same and unidirectional at a given point of time, the forces they exert on each other due to displacement is negligible.

In this chapter the results and analysis of the field induced microwave absorption of various HTSCs are presented. From the results the important parameters of the mixed state like the pinning force constant and the critical current density are determined.

4.2 Experimental

In the present study sintered BSCCO and GdBCO, press sintered BSCCO and melt textured GdBCO with varying percentages of $Gd_2Ba_1Cu_1O_5$(211) samples are used. The four melt textured samples used are of the following compositions; GdBCO+0 mol % 211 (Gd-0), GdBCO+10 mol % 211 (Gd-10), GdBCO+20 mol % 211 (Gd-20) and GdBCO+30 mol % 211 (Gd-30). Preparation of the press sintered and melt textured samples is given elsewhere [chap.2, 2,3]. The transition to zero resistance of the press sintered BSCCO and the GdBCO melt textured samples are found to be at 106K and 92K (±0.2). Bruker ESR spectrometer, described in Chapter

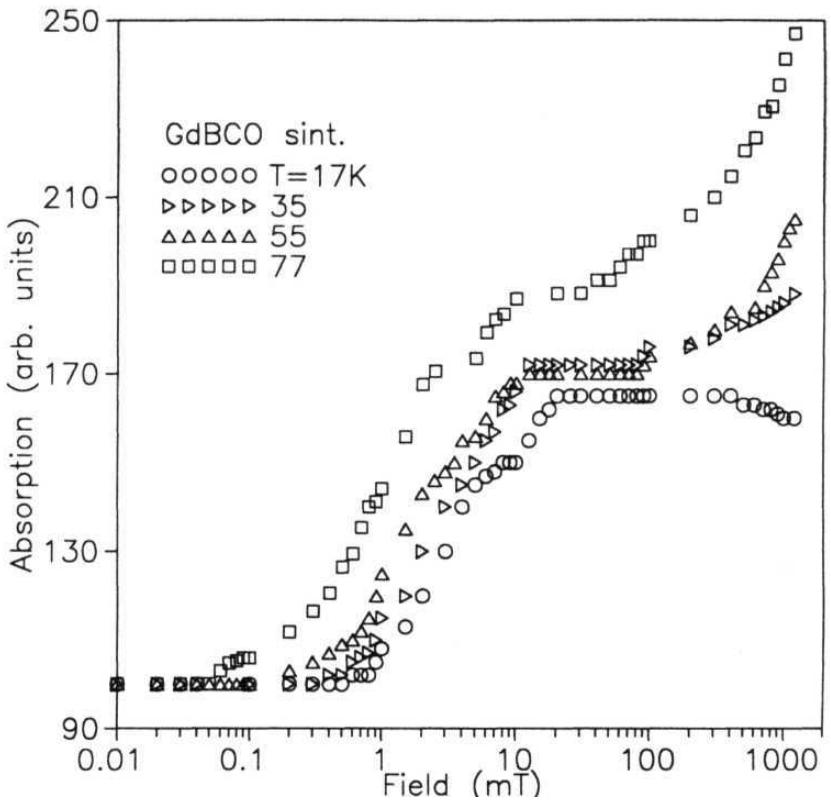

Fig. 1 Field induced microwave absorption of GdBCO sintered sample at various temperatures below T_c.

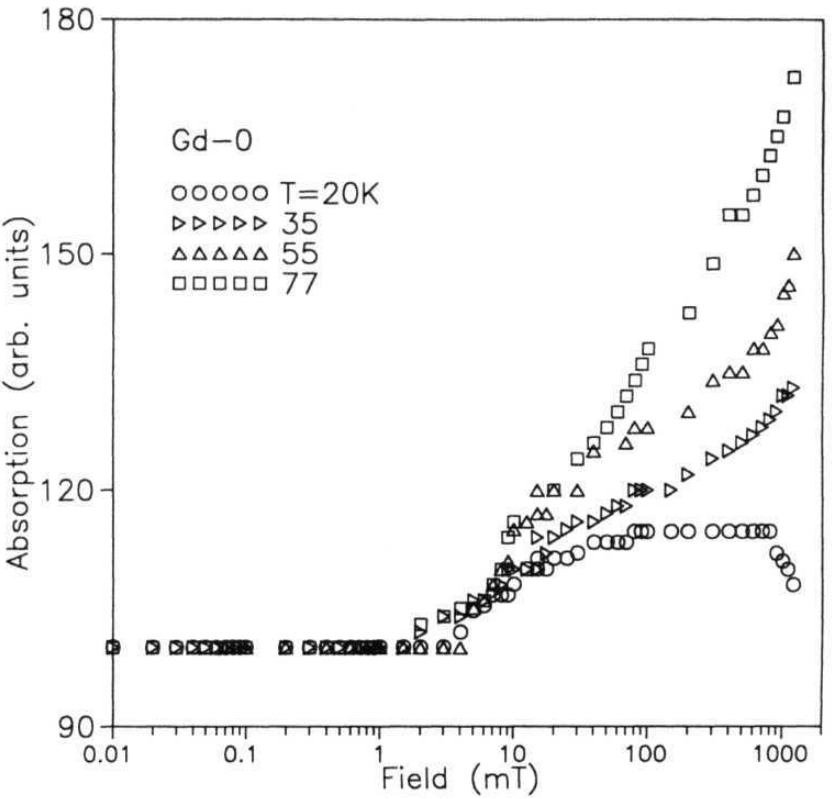

Fig. 2 Field dependent absorption of Gd-0 melt textured sample.

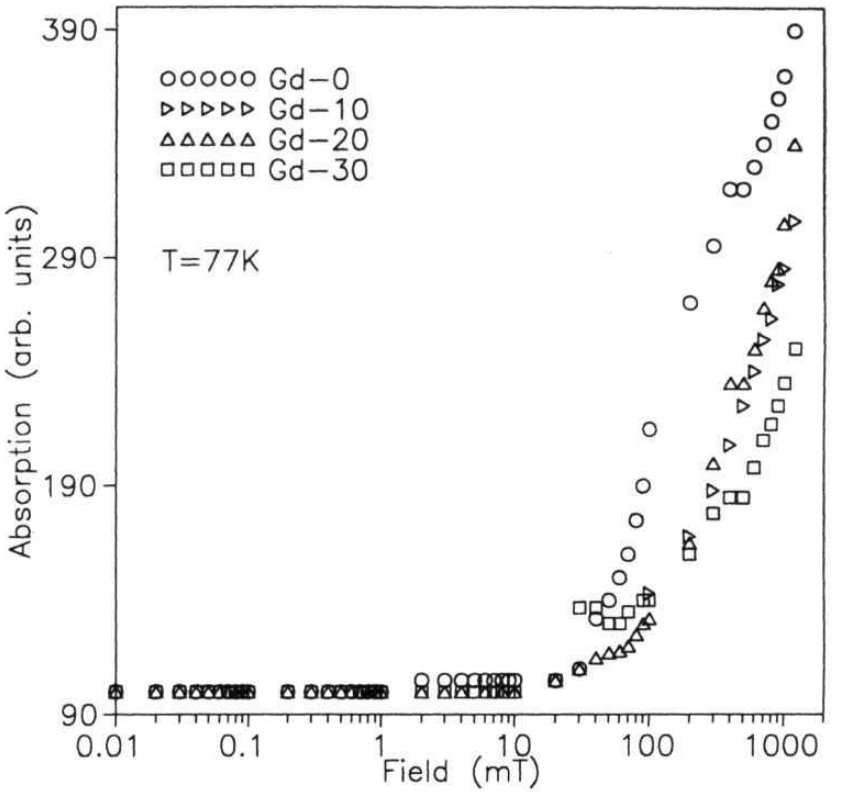

Fig. 3 Field dependent absorption of melt textured samples with varying percentages of 211.

II, is used to carry out the present experiments. Field induced absorption is recorded on zero field cooled samples at various temperatures below T_c.

4.3 Results

Fig. 1 shows the field induced absorption of the GdBCO sintered sample at various temperatures. It can seen that at low temperature, 17K, there is no measurable absorption upto about 0.6 mT, above this field the absorption keeps incresing monotonically and begins to saturate at about 20 mT. Beyond this field, interestingly, there is no change in the absorption upto about 0.8 T and above this field the absorption decreases upto the maximum field applied, 1.2 T. At higher temperatures (35, 55 and 77K) change in the absorption starts at lower fields (0.4, 0.1 and 0.05 mT), so also the saturation (9, 6 and 5 mT). As described in the last chapter the field at which there is a measurable change in absorption at low fields is described as the H_{c1J1} of the intergrain region. At higher temperatures the saturation region ends at about 0.1 T and above this field there is again an increase in the absorption, as can be seen from the Fig.1.

In the case of Gd-0 (melt textured) sample the values of H_{c1J1} are found to be 4 mT, 2mT, 1.5mT and 1mT at 20K, 35K, 50K and 77K, respectively. Fig. 2 shows the magnotoabsorption of this sample at various temperatures. As in the case of GdBCO sintered sample above 0.8T there is a decrease in the absorption at 20K. Such a decrease is seen only in these two samples at low temperatures. Figs. 3 and 4 show the magnetoabsorption of the melt textured GdBCO (Gd-0, Gd-10, Gd-20 and Gd-30) and, sintered and press sintered BSCCO samples, at 77K. From Figs. 1-4

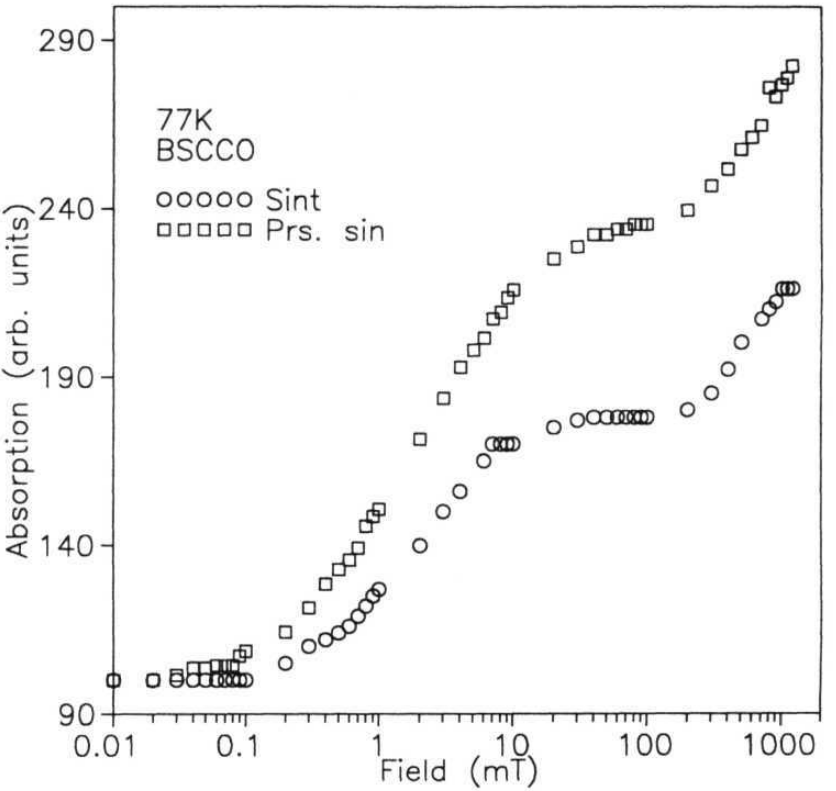

Fig. 4 Field dependent absorption of BSCCO sintered and press sintered samples.

the high field (> $0.1T$) absortion is separated from the low field absorption **and** is shown in Figs. 5-8. For comparison of the results on various samples the high field absorption at 0.1 T is made equal.

4.4 Analysis and Discussion

(i) Low field absorption

In the last chapter the low field (< $50mT$) absorption at radio frequency is well discussed in terms of the RSJs and the decouled junctions. At microwave frequency we find that the Eq. 8 [chapter 3] represents the data very well. A typical fit of the data obtained on sintered GdBCO is shown in Fig 9. The drastic reduction in the low field loss in melt textured samples (Figs. 2 and 3) is due to the elimination of intergranular weaklinks by melt processing.

(ii) High field absorption

For spaciaily constant harmonic time dependent electromagnetic field Eq. 1 gives for the absorbed power per unit volume, the expression **[1,4,5]**

$$\frac{P(\omega)}{P(0)} = \frac{\eta^2\omega^2}{(k - m\omega^2)^2 + \eta^2\omega^2}$$

Neglecting the effective mass of the vortex the interplay between elastic and viscous forces determines the depinning frequency which can be written as f_0 = fc/77 =

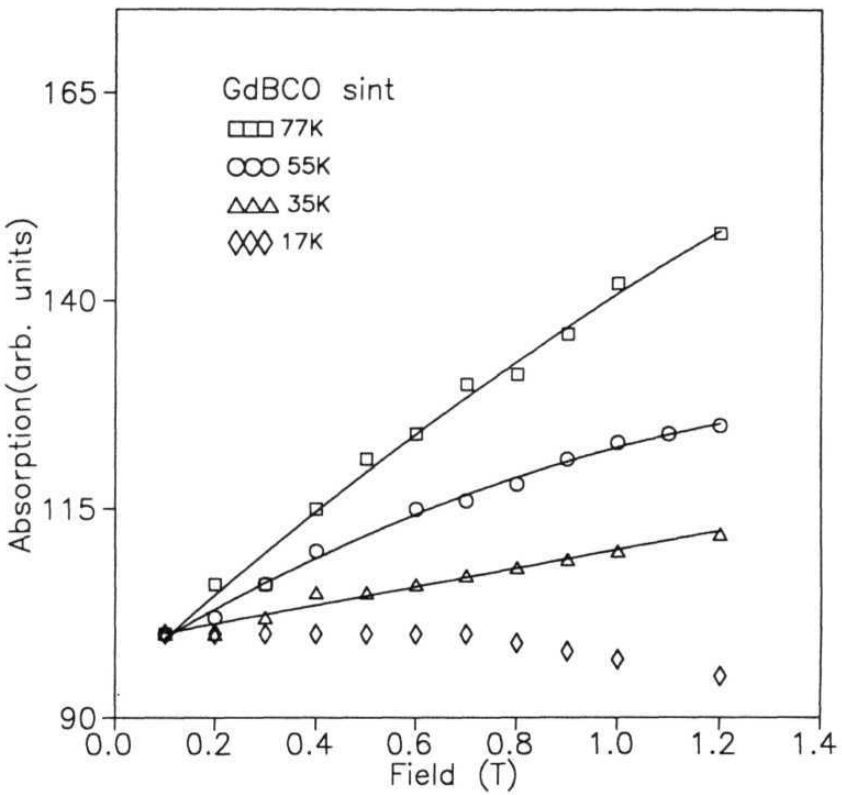

Fig. 5 High field absorption of sintered GdBCO. The solid lines are fits to Eq. 4.

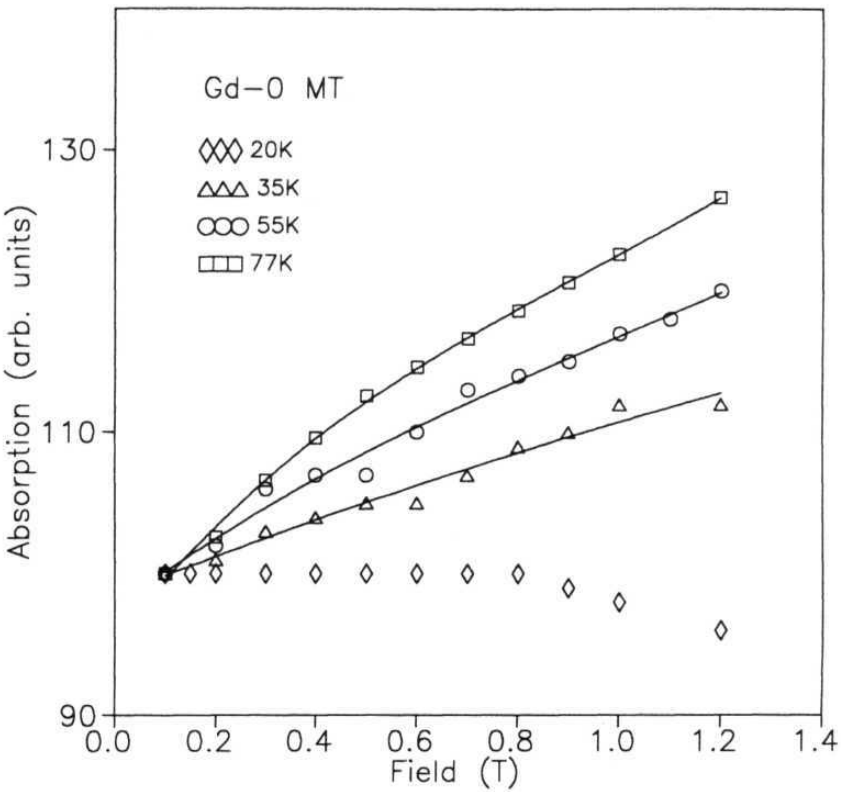

Fig. 6 High field absorption of melt textured Gd-0. Solid lines are fits to Eq. 4.

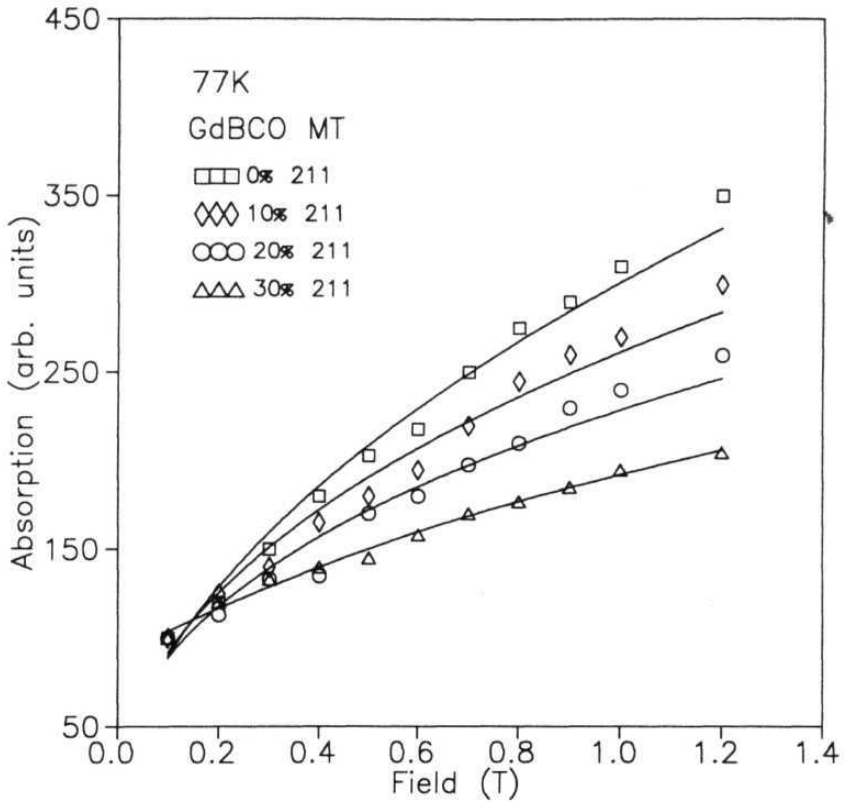

Fig. 7 High field absorption of melt textured samples with varying percentages of 211. Solid lines are fits to Eq. 4.

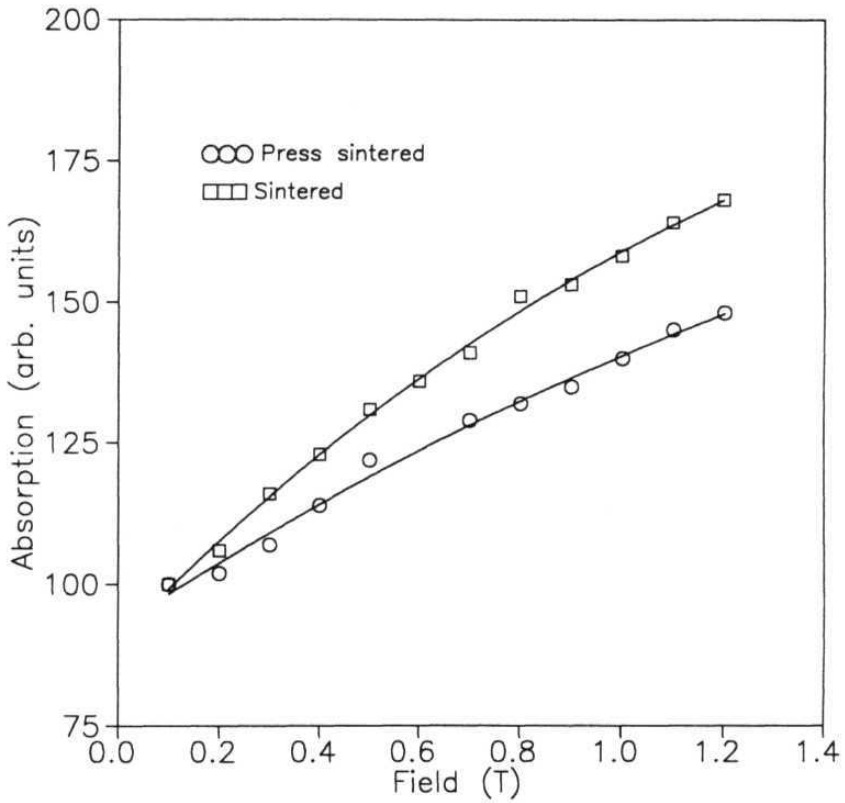

Fig. 8 High field absorption of sintered and press sintered BSCCO. Solid lines are fits to Eq 4.

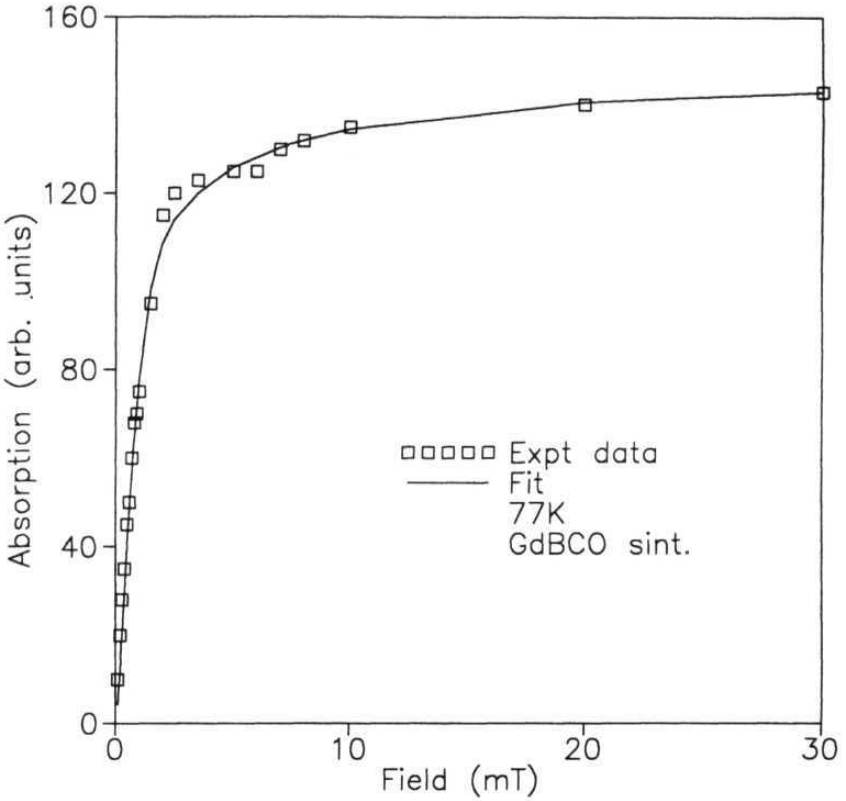

Fig. 9 Low field absorption of GdBCO sintered sample. Solid line is a fit to Eq. 8 of chapter 3.

$k\rho_n/\phi_0 B_{c2}$ where, ρ_n is the normal state resistivity and B_{c2} is the upper critical field. In the case of conventional superconductors the pinning force constant, k, is in the range $10^4 N/m^2$which gives the depinning frequency in the range 10^{8-9} Hzs [1]. However, in the case of high temperature superconductors the depinning frequency is estimated to be in the range > 10^{10} Hz [6,7]. The present operating frequency of 9.98 GHz is close to but lower than the depinnig frequency. But, due to the proximity of the operating frequency to the depinning frequency some fluxons may get depinned which cause loss in the material. At high temperatures most of the loss is expected from the thermally activated flux flow (TAFF). If f is the fraction of the free fluxons the number of unpinned fluxons is (1-f). Let $U(T,B,\omega)$ be the activation energy of the pinned fluxons then the fraction of the thermally activated fluxons F can be written as [8]

$$F = (1 - f)exp[-U(t, B)/k_B T] \quad \textbf{(2)}$$

In the complete flux flow state f=1, so F=0. Considering the thermally activated flux creep model [5], in which the activation energy varies as $(1-t)^{3/2}$, for U(t,B) we write

$$U(t, B) = U(0)(1 - t)^{3/2} g(B) \quad \textbf{(3)}$$

where, g(B) is a fuction which represents the field dependence of the activation energy and U(0) is the activation energy at t=0.

Coffey and Clem [9] have presented a detailed phenomenological treatment of the microwave surface impedance in terms of complex penetration depth A as a function of temperature, magnetic field and frequency. However, a simpler and more transparent method is proposed by Portis et.al [10] which describes the complex surface

impedance of a superconductor subjected to a static magnetic field and incident upon by the microwave radiation. For B far from the upper critical field B_{c2} and temperature not close to T_c, the surface resistance R_s connected to the flux flow dissipation using Eq.2, (including the fraction of thermally activated fluxons, F) can be written as

$$R_s(B) = Re[Z_s] = 2^{1/2}\omega\mu\lambda\sqrt{-1+\sqrt{1+(\frac{\phi_0(f+F)B}{\omega\mu_0\lambda^2\eta})^2}} \quad \textbf{(4)}$$

In the low magnetic field limit, the above equation gives a linear field dependence for R_s and at higher fields a square root behavior.

The solid lines in the Figs. 5-8 show the good fits of the experimental data obtained on various samples to Eq. 4. For the calculations we considered temperature dependence of η and A. For η, the Bardeen-Stephen equation $\eta = \phi_0 B_{c2}/\rho_n$, where ρ_n is the resistivity in the normal state and $B_{c2}(t) = B_{c2}(0)(1 - t^2)(1 + t^2)$ [9], and $\lambda(t) = \lambda_0(1 - t^4)^{-1/2}$. U(t,B) is the fit parameter in the calculation. The fits (Figs. 5-8) seem to have dominant linear behavior which is due to high values of B_{c2} in HTSCs. whereas, conventional superconductors follow $B^{1/2}$ behavior. Assuming a sinusoidal potential well $U(x) = (-U_0/2)cos(\pi x/L_y)$, where L_y is the well dimension, one can relate pinning force constant to the activation energy as [6],

$$U(t,B) = 2k(t,B)L_y^3/\pi^2 \quad \textbf{(5)}$$

Equating the maximum pinning force to the maximum Lorentz force, one gets

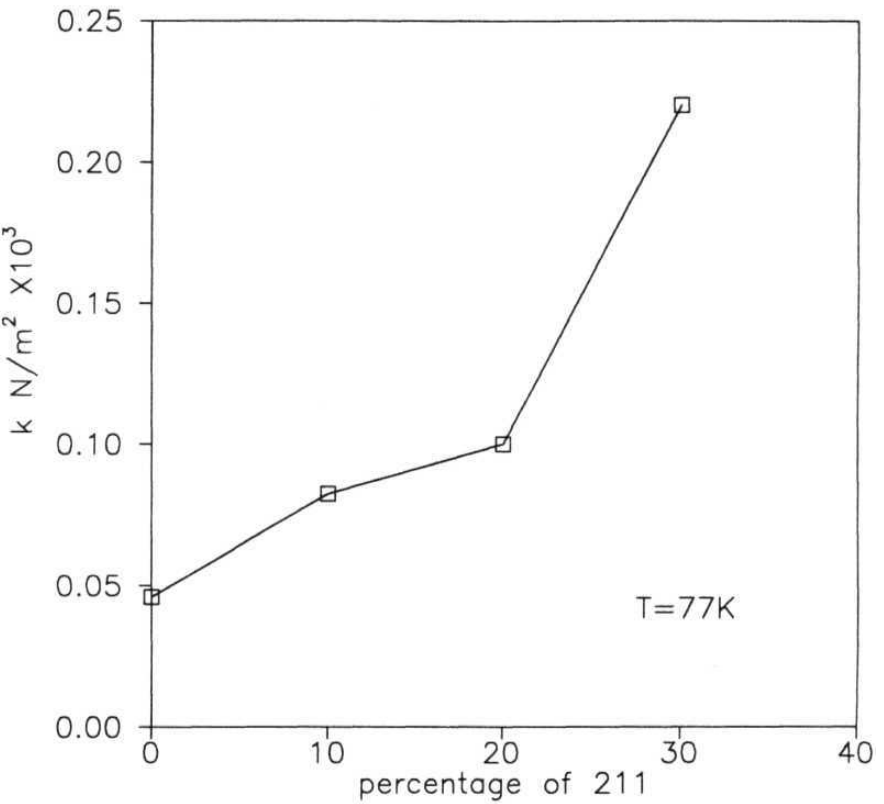

Fig. 10 Variation of pinning force constant with 211 percentage in melt textured GdBCO.

Table I.

Sample	Temp K	U(t) e.V.	k $\times 10^3 N/m^2$	$\times 10^9$	*Jc(t)* *Amp/m*^{2}
GdBCO	35	0.37	0.8		0.89
	55	0.14	0.33		0.36
	77	0.01	0.02		0.03
Gd-0	35	0.73	1.7		1.9
	55	0.34	0.78		0.87
	77	0.02	0.046		0.052
Gd-10	77	0.035	0.082		0.09
Gd-20	77	0.043	0.1		0.11
Gd-30	77	0.095	0.22		0.21
BSCCO					
sint	77	0.016	0.038		0.043
prs. sint	77	0.022	0.05		0.056

$$J_c = \frac{L_y k}{\pi \phi_0}. \qquad (6)$$

Using Eqs. 5 and 6 with $L_y \sim 0.07 \mu m$ [11] we get the pinning force constant, k, **and the** critical current density, J_c. Fig. 10 shows the variation of k with the 211 percentage at 77K. In table 1 values of both k and J_c of **all** the samples studied are given. The present values are well in accord with those determined from the magnetization measurements [12] and reported in the literature on various HTSCs [13-15].

In the case of both sintered GdBCO and Gd-0 samples, the gradual reduction in k(t) (Table 1) with the increase in temperature can be explained to be due to the depinnig of the vortices by the thermally assited flux flow (TAFF). Point here to note is the absence of high field loss in these two samples at low temperatures ($\simeq 20K$) (Figs 5 and 6), which indicates that the TAFF is absent at these temperatures. The reduction in the absorption at low temperatures in these two samples above ~ 0.8T could be due to some unknown mechanism which causes an enhancement in the effective pinning of the vortices. However, the same mechanism does not seem to have any effect at higher temperatures.

The decrease in the relative absorption with respect to the increase in the 211 percentage (Fig. 7) is due to an increase in the number of pinning centres created by the 211 which is evidenced by the increase in the pinning force constant (Fig. 10). This point also suggests that the sample is not in complete flux flow state, where all the flux lines are depinned, even at 77K. The pinning centres are formed at the interface (in the 123 lattice) of the 211 and 123 matrices as the strain developed at the interface causes secondary defects to form in it. The addition of 211 reduces the

average GdBCO platelet size and the crack width between the platelets and thereby improves the mechanical strength and critical current density.

References

[1] J.I.Gittleman and B.Rosenblum, Phys. Rev. Lett. **16,** 734 (1966)

[4] M.Rabinowitz, J. Appl. Phys, **41,** 88 (1971)

[5] N.C.Yeh, Phys. Rev. **B, 43,** 523 (1991)

[6] Dong-Ho Wu and S.Sridhar, Phys. Rev. Lett, **65,** 2074 (1990)

[7] F.Zuo, M.B.Salamon, E.D.Bukowski, J.P.Rice and D.M.Ginsberg, Phys. Rev. **B, 41,** 6600 (1990)

[8] A.Rastogi, Y.S.Sudershan, S.V.Bhat, A.K.Grover, Y.Yamaguchi, K.Oka **and** Y.Nishihar Phys. Rev. **B,** 53, 9366 (1996)

[9] M.W.Coffey and J.R.Clem, Phys. Rev. Lett. 67, 386 (1991)

[10] A.M.Portis, K.W.Blazey, K.A.Muller and J.G.Bednorz, Europhys. Lett. 5, 493 (1988)

[11] A.P.Malozemoff etal., Strong Correlations and Superconductivity, ed. by H.Fukuyama et. al, Springer Verlag, Heidelberg (1989)

[12] E.Sudhakar Reddy and T.Rajasekharan, (private commun.)

[13] M.Murakami, S.Gotoh, H.Fujimoto, K.Yamaguchi, N.Koshizuka and S.Tanaka, Supercon. Sci. Technol, 4, S49 (1991)

[14] J.W.Farmer, X.Ding, D.L.Cowan and D.C.Bardford, Phys. Rev. **B, 54,** 637 (1996)

[15] S.Sengupta, P.Mc Ginn, N.Zhu and W.Chen, Physica C, **171,** 174 (1990)

Chapter 5

ANOMALOUS MICROWAVE ABSORPTION: π JUNCTION AND THE PARAMAGNETIC MEISSNER EFFECT

5.1 Introduction

One of the characteristic properties of a superconductor is to become diamagnetic and expel magnetic field when cooled to below its transition temperature. For a superconductor with defects present the flux may be pinned at these defect sites causing the field cooled magnetization to be less diamagnetic. However, some HTSC materials, when cooled in a small magnetic field acquire a net paramagnetic moment [1-10]. This paramagnetic moment increases as the sample is cooled to about 10K below T_c and then saturates. In some samples the onset of paramagnetism occurs a few degrees below T_c even when the T_c is reduced by 20K by altering the oxygen concentration [3]. The paramagnetic moment seems to be superimposed on a conventional Meissner diamagnetism and is found to be frozen in if the external field is removed at low temperature. The possibility of this unusual paramagnetic moment originating due to paramagnetic impurities is ruled out on the grounds that no significant paramagnetism is observed in the normal state even at 1 Tesla^2 and the onset of paramagnetism always occurs a few degrees below T_c. The effect is well established and is known as paramagnetic Meissner effect (PME). Various explanations for the origin of the PME in these granular HTSCs have been proposed, including the spontaneous orbital currents due to π junctions [2,11-15] and vortex pair fluctuations

combined with pinning[1]. Of the possible mechanisms suggested the idea that HTSCs for some reason exhibit an array of loops containing π junctions and the attendant **orbital** moments seems to be more appropriate.

Bulaevskii *et. al* [16] have shown that if the Josephson junction has magnetic impurity it can then produce elastic tunneling associated with the spin flip process and the current tunneling through the junction becomes negative. In the tunneling process of the supercurrent over the impurity state there appears one permutation of two fermions, which gives the negative sign. In such a case the phase difference across the junction would not be zero, as usual, but π. The phase difference depends on the inductance of the current loop and on J_c. A spontaneous flux exists if $\frac{2\pi L|J_c|}{\phi_0} > 1$. The state of lowest energy of such a loop in zero applied field is doubly degenerate with a trapped flux equal to approximately $\pm\phi_0/2$. Such a state with spontaneous orbital moments is called[14,15] a new condensed matter state with a critical field H_{c0}. A π junction can in principle create vortex - anti vortex pair [15] in the plaquettes on either of the junction. If one of the vortices is pinned the other dilutes away into the system, the single vortex can then give rise to the PME. It is shown [14] that for a π junction the magnetic response below T_c should be diamagnetic and paramagnetic currents appear when the J_c reaches a certain value. Thus a cross over from paramagnetic to diamagnetic behavior of π junction is expected as the temperature is increased. An alternative mechanism for generating an intrinsic π-phase shift in a Josephson junction is based on the idea of existence of an unconventional, $d_{x^2-y^2}$, order parameter symmetry [17-19]. Sigrist and Rice interpreted the paramagnetic response of the BSCCO compounds as an indirect observation of d-wave superconductivity in these materials.

The signature of the PME is observed in the second harmonic susceptibility [20] and in microwave absorption [2,3,21] as anomalous responses. In the absence of any external field there exist spontaneous orbital currents in the network of π junctions. The application of microwave field will induce additional microwave currents. If the vector sum of the spontaneous orbital current and microwave current is larger than the critical current then the additional current flows as a result of Giaver tunneling and thus with dissipation [3]. Another way to look at the dissipation in π junction is to invoke the hysteretic behavior of the junction when the condition $2\pi LJ_c/\phi_0 > 1$ is satisfied. The hysteretic dependence of the J_c on H_{mw} may lead to the appearance of spontaneous magnetization and to the absorption of microwave power by the loop in the absence of the external field [17]. As the field is increased the spontaneous orbital currents are reduced and the attendant absorption decreases. Thus in the microwave absorption samples which show PME give rise to a finite absorption at zero field and a reduction as the field is increased. However, in general, the field dependent (low fields) microwave absorption in HTSCs is minimum in zero field and increases with the application of field since it is caused by dissipation in ordinary weaklinks without spontaneous currents. Lack of adequate experimental support is one of the reasons for the ongoing ambiguity about the origin of the PME. In this report we present the microwave absorption results of GdBCO superconductor and provide experimental evidence for the change in the behavior of π junctions from para to dia state as a function of temperature. We also discuss various possible origins of π junctions.

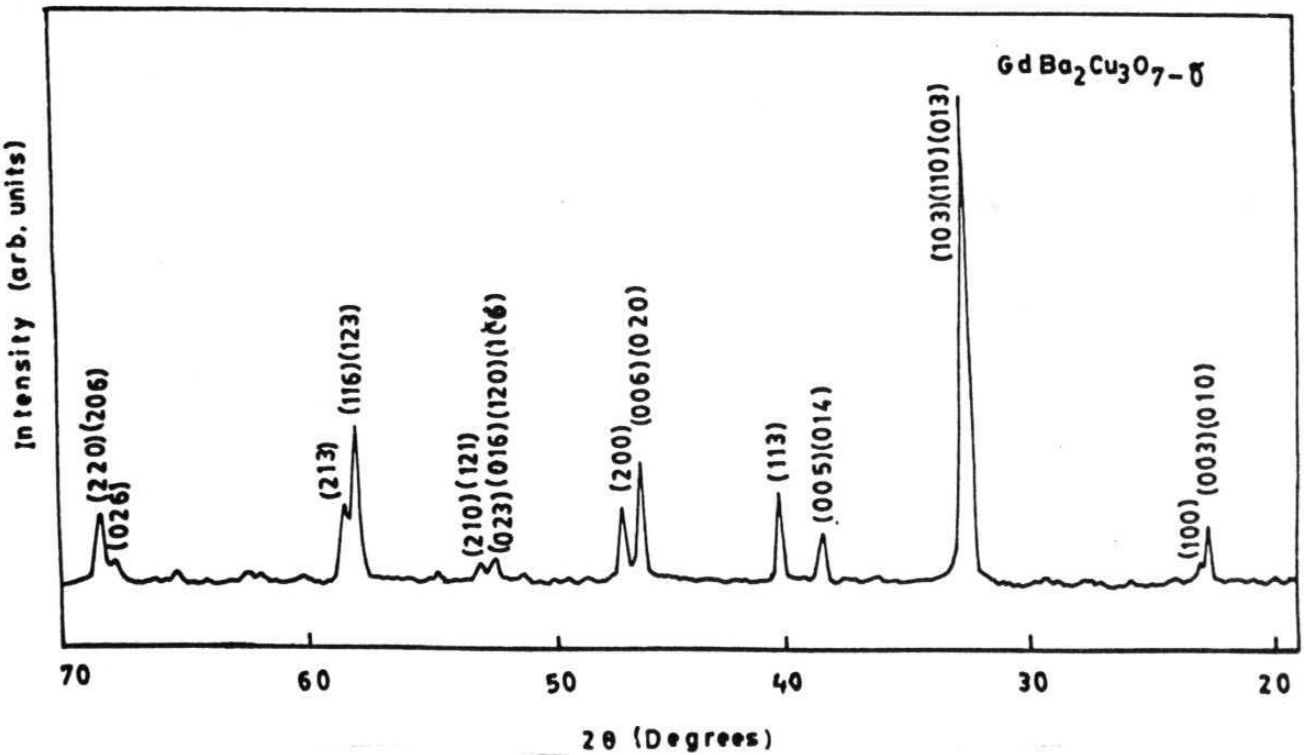

Fig. 1 X-ray diffraction pattern of powder GdBCO showing orthorhombic 123 phase without any impurity phases.

5.2 Experimental

$GdBa_2Cu_3O_7$(GdBCO) sintered superconductor is made through solid state route. Part of the sample was used as a pellet and the remaining part is crushed into powder with particle size < $30\mu m$. The powder particles are well separated by suspending them in GE varnish. Both the samples when characterized by XRD showed single GdBCO orthorhombic phase without any impurity phases (Fig. 1). Pellet sample showed zero resistance transition onset at 92K. The nonresonant microwave absorption (MWA) spectra were recorded using a Bruker ESR spectrometer which has a facility to vary field from -5 mT to 1.2 T. Field modulated microwave absorption (FMMWA) signals were recorded in the derivative form using phase sensitive detection. For all the experiments carried out using the phase sensitive detection, the internal phase of the lock-in is set to zero. The temperature of the sample is varied using a closed cycle refrigerator.

5.3 Results

Fig. 2 shows FMMWA signals recorded at 100 mOe modulation field as the dc field is scanned between ± 5 Oe, on the zero filed cooled (ZFC) GdBCO powder at various temperatures below T_c. The phase of the derivative signal at low temperatures is same as that of the Gd^{3+} EPR signal observed at 3.5 KOe (inset Fig. 3). Hence, for the sake of convenience we call the signals which have the same phase as that of the Gd^{3+} EPR signal the in-phase signals and those with opposite phase the out-of-phase signals. The in-phase signal (Fig. 2) is the anomalous signal and represents the PME response with maximum absorption in zero field followed by minima

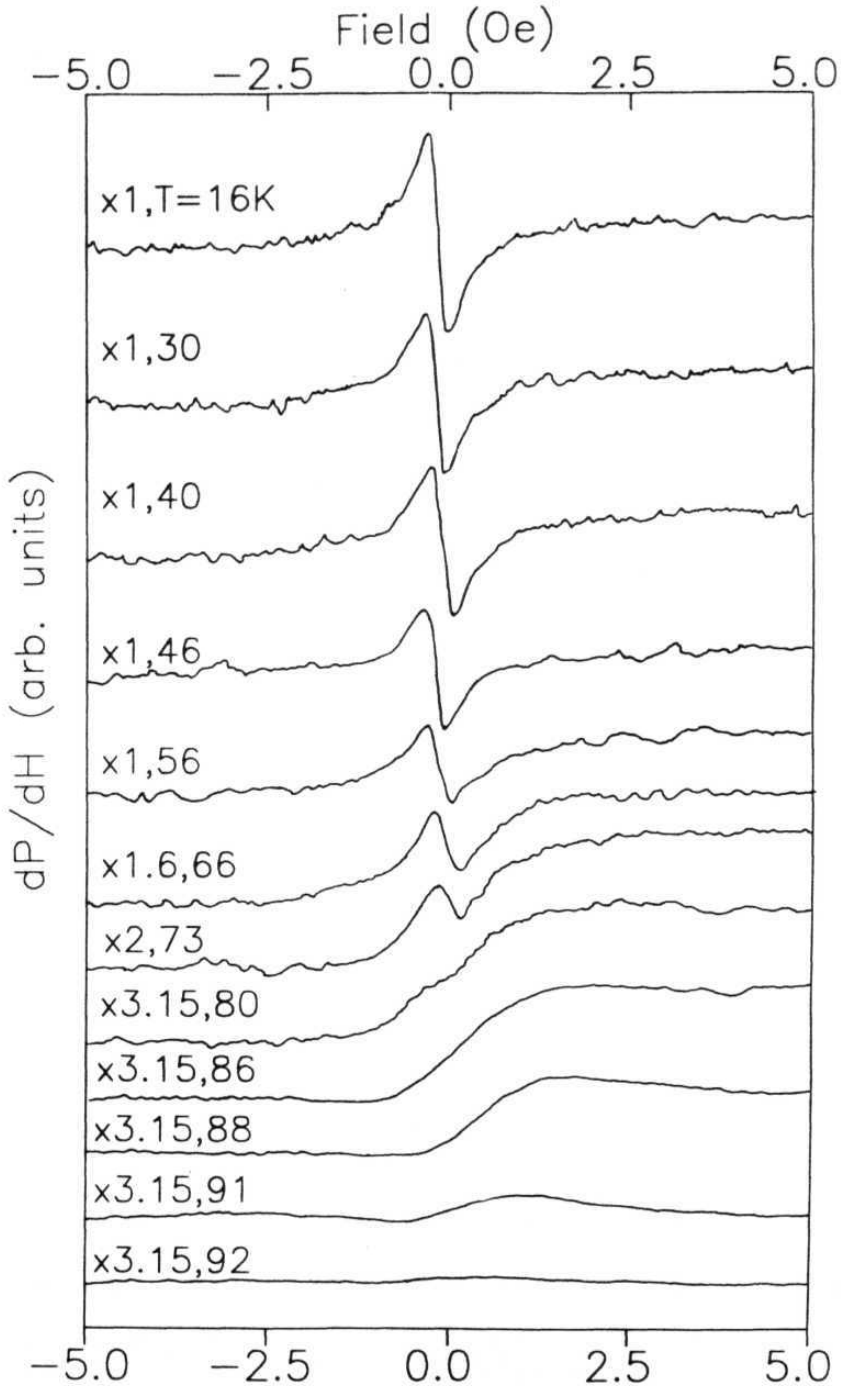

2 FMMWA signals of the ZFC Gd BCO powder recorded when the dc field is

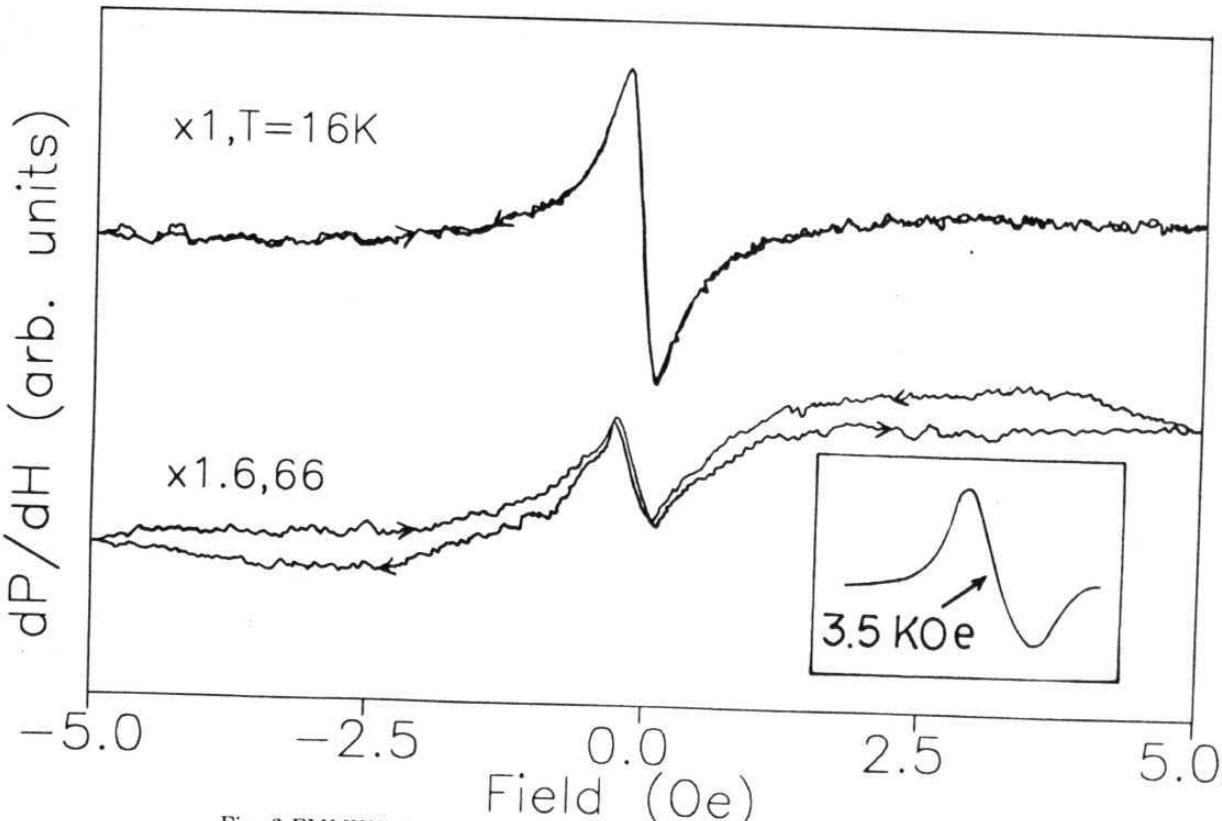

Fig. 3 FMMWA signals when the field is cycled between ± 5 Oe. In the inset Gd^{3+} EPR signal is shown.

at ± 0.6 Oe. The flat base line above this field represents a nearly linear increase in the direct absorption (P(H)). As the temperature is increased the intensity of the in-phase signal reduces and at about 56K the signature of the out-of-phase signal, which is representative of the absorption due to dissipation in the usual Josephson junctions and is also the usually observed derivative signal, starts dominating. With further increase in the temperature the out-of-phase signal initially grows in intensity and eventually dies of as T_c is approached. In the intermediate temperatures there is a coexistence of both the in-phase and out-of-phase signals. During field cycling, at low temperatures (T < 56A'), no hysteresis is observed in both the signals. But, at higher temperatures the out-of-phase signal develops hysteresis, which could be due to the trapping of flux at the normal junctions, while no hysteresis is observed in the in-phase signal as shown in Fig. 3. This clearly shows that the in-phase signal actually comes from a different origin altogether.

When 1 Oe modulation field is set while recording FMMWA the anomalous in-phase signal is not observed, however, a weak out-of-phase signal whose intensity increases with increase in temperature is observed. As in the earlier case this signal also disappears as T_c is approached. The anomalous in-phase signal is not seen in GdBCO sintered pellet. We have confirmed this observation at various modulation fields and temperatures. We have carried out the FMMWA measurements on powder at various microwave power levels (63 mW to 0.63 μW) and have always observed the in-phase signal. The ratio of the in-phase to the out-of-phase signals is found to be constant throughout the range of microwave power levels.

Fig. 4 shows the in-phase signal recorded at 15K on GdBCO powder at various

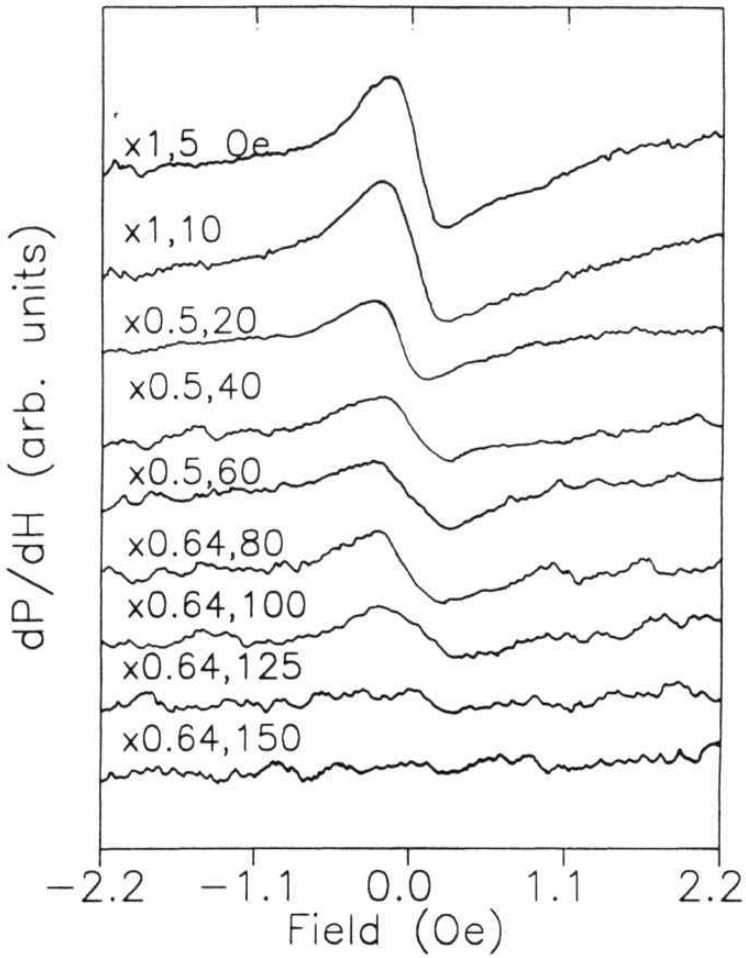

Fig. 4 FMMWA in-phase signals of the ZFC GdBCO powder recorded at 15K when the field is scanned between -5 Oe to +5 Oe (the response is shown between ± 2.2 Oe).

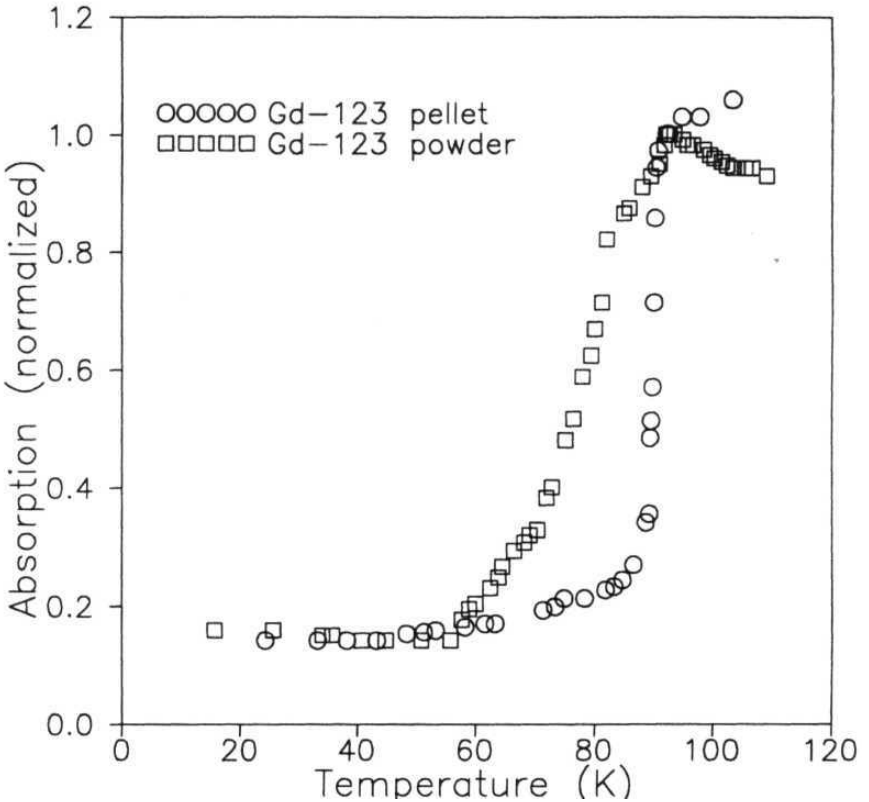

Fig. 5 Change in the direct MWA as a function of temperature of GdBCO pellet and powder. Powder sample shows three different slopes in the transition region suggesting oxygen deficiency in it.

flux trapped states. To record the signal first a certain dc field (given in the Figure) was applied on the ZFC sample and withdrawn. FMMWA response was then recorded between ± 5 Oe. From the figure one can see that there is a overall reduction in the intensity of the signal and disappearance at a flux trapped state corresponding to 125 Oe. In Fig. 5 changes in the direct MWA through transition for both GdBCO powder and pellet are shown. The broad transition width in the case of powder could be due to loss of oxygen. The three different slopes in the transition region are reminiscent of three different slopes - a plateau in high temperatures, a fall and another plateau in the low temperature region - in the oxygen content dependent T_c variation curve of a typical 123 system [22,23).

We have also carried out field induced direct MWA (which is less sensitive than the FMMWA) at various temperatures in both pellet and powder. In the case of pellet we have observed a monotonic increase in absorption at low fields (0-0.3 KOe), a saturation in the intermediate fields (0.3-1 KOe) and a linear increase at high fields(l-10 KOe). These three segments are well explained [24] by invoking resistively shunted Josephson junction (RSJ) (at low and intermediate fields) and flux flow (at high fields) models, respectively. In the case of powder no appreciable change in absorption is observed up to about 30 mT. But, at high fields an intense Gd^{3+} EPR response is observed. It is worth noting that the change in absorption in the low field region in pellet is almost 1000 times that of powder. Such a great reduction is possible due to the elimination of a large number of grain boundary weaklinks on powdering.

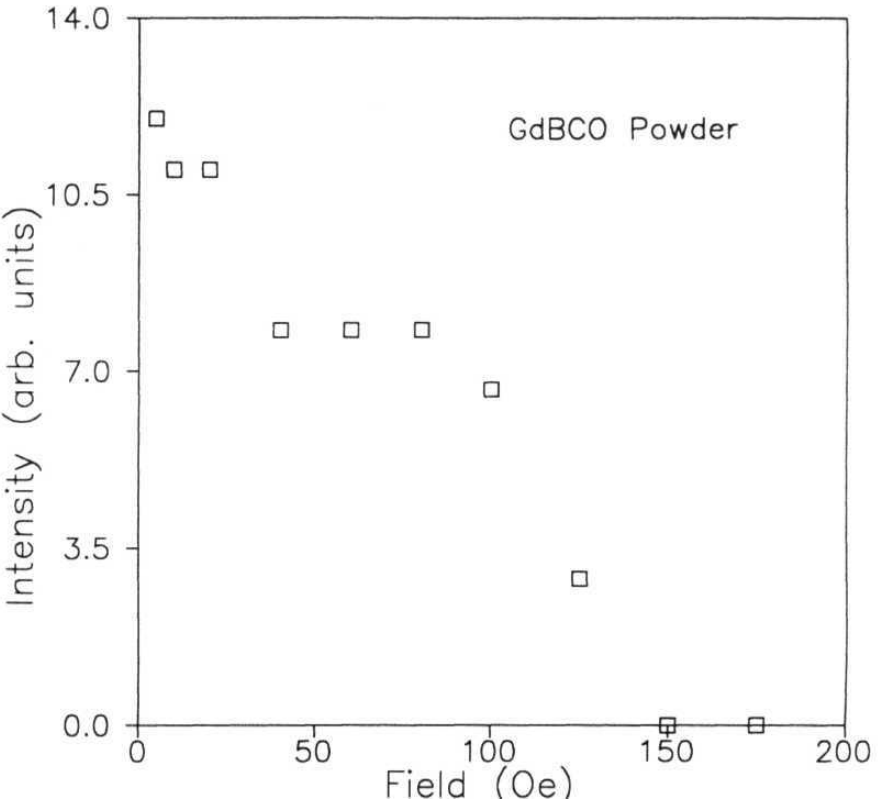

Fig. 6 Intensity of the in-phase signal (obtained from Fig. 4) at various flux trapped states.

5.4 Discusion

As already mentioned above in the magnetization studies the PME is observed **in field** cooled samples **alone.** The reason being in the ZFC sample the spontaneous orbital moments are oriented randomly giving rise to zero net magnetization. In the field cooled samples these moments are polarized to give paramagnetism. However, in the microwave absorption the sample need not be field cooled to observe the PME, because irrespective of the orientation of the orbital currents and the associated moments it is the total dissipation in the *TT* junctions which contributes to the observed in-phase signal. In other words high frequency absorption techniques, namely, field modulated rf and microwave absorption, are best suited to study the virgin π junction response not only for the reason stated above but also owing to their high sensitivity. In fact, any application of field reduces the PME. We have shown this effect in Fig. 4 by exposing the sample to different magnetic fields before recording FMMWA. The overall reduction in the intensity of the absorption (Figs. 4 and 6) with higher flux trapping can be understood in terms of gradual destruction of orbital moments. And the disappearance of FMMWA at 125 Oe field exposed suggests that the trapped field inside the sample is more than H_{c0}, the crossover field from para to dia state of the junction. The origin of the step like behavior observed in the range 40-80 Oe is not fully understood. However, it could be because of a cross over from one level to a different level of critical state where in weaklinks of two different kind operate.

The absence of in-phase signal in the pellet could be for two reasons. Firstly, the π junction response is overshadowed by a very strong dissipation in the normal Josephson junctions which are very large in a pellet. Secondly, the current in a junc-

tion network is decided by the weakest possible junction which has the lowest J_c. Whereas, the condition $\frac{2\pi L|J_c|}{\phi_0} > 1$ for a π junction demands that the product $L|J_c|$ be high enough, which is improbable in a pellet. This point is further validated by the fact that PME is reported in melt textured, single crystal and powder samples only [1-12]. J_c in all these three varieties of samples is much higher than in sintered samples.

It has been shown [15] that the critical field of the orbital glass state is

$$H_{c0} = \frac{\phi_0}{2S}$$

where ϕ_0 is the elementary flux quantum and S is the area of the current loop. In the present sample with H_{c0} = 0.6 Oe, the value of S is found to be $16.6 \times 10^{-12} m^2$ which corresponds to a square loop with a side of $4\mu m$. Such a loop is quite possible within a grain of $10\mu m$ size. So, it is justifiable to say that the π junctions are, in fact, intragranular contacts with high $J_c s$. Also for a junction with coupling energy E_j, the temperature at which the orbital moments are destroyed is $T_0 \simeq \frac{E_j}{n^2}$, n is the number of π junctions [14,15]. (Incidentally, to create a spontaneous orbital moment it is necessary to have a loop with odd number of junction. On the ring with n=1 the orbital moment is not created at all as the quantum fluctuations destroy it. Hence, the minimum number of π contacts is three.) Since we do not have any a priori knowledge of E_j and n, it is only appropriate to say that depending on the distribution of E_j and n, T_0 has a distribution. Once the orbital moment is destroyed the π junction behaves as an ordinary Josephson junction. Keeping this in view and the fact that

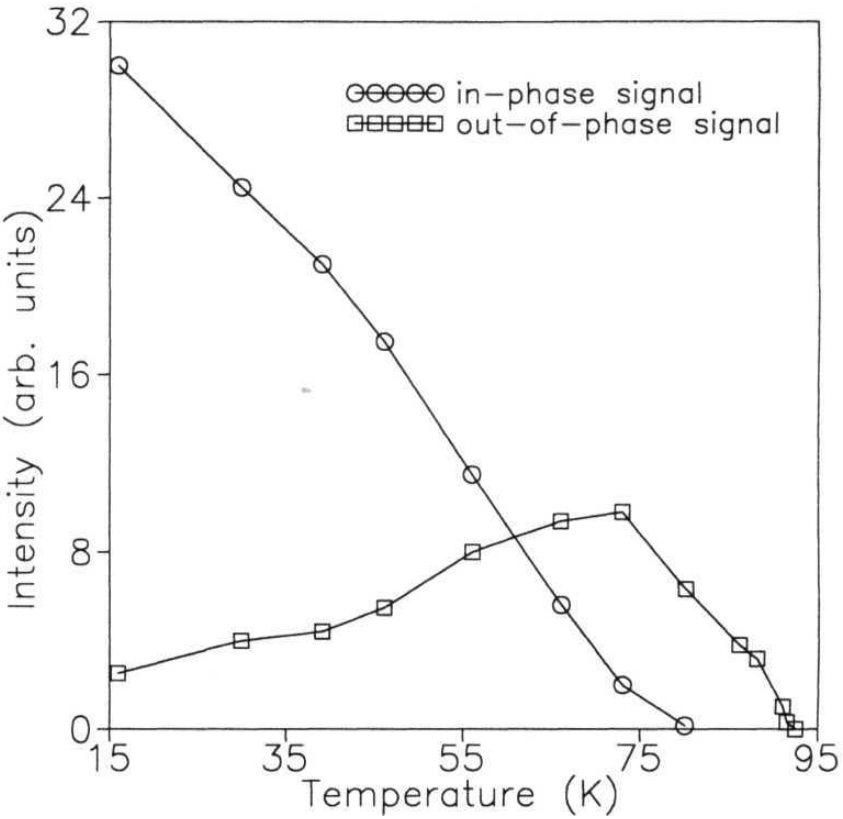

Fig. 7 Variation in the intensities of the in-phase and out-of-phase signals as a function of temperature. The development of the out-of-phase signal at the expense of the in-phase signal clearly suggests a cross over from para to dia state of the π junctions.

the out-of-phase signal develops at the expense of in-phase signal (Figs. 2 and 7) it is reasonable to say that the phase reversal observed could be due to a change in the behavior of π junctions from para to dia state. Another note worthy point here is the gradual, almost linear, increase in the intensity of in-phase signal with the decrease in temperature (Fig. 7), which can be understood in terms of increase in the average J_c and the number of the π junctions operating.

The reason for the PME or the origin of the π junction formation is not yet clear and remains to be a subject of speculation. However, some of the explanations present in the literature, though intriguing, can be ruled out on the following grounds. Bulaevskii et. al [25] argue that in layered superconductors with moderate anisotropy the spontaneous creation of thermally induced vortex-antivortex lines should occur above a certain temperature $T_s < T_c$. Many experimental results [1-5] do show the positive magnetization developing a few degrees below T_c. In order to explain the PME Koshlev and Larkin [26] propose flux compression caused by inhomogeneous cooling as a possible origin. If the PME is thought to be due to the trapping of one of the vortices of the vortex-antivortex pair or due to the compressed flux, it can be cross checked by low field microwave absorption study. Any such flux trapping or compressoin is not expected to give anomalous microwave absorption. Instead, the microwave current induces Lorentz force on the vortex lines and may cause dissipation if the Lorentz force is greater than the pinning force. The application of the external field (in the FMMWA) induces diamagnetic currents on the surface of the superconductor which generate a field opposite to the external field. So, when the field is applied the trapped flux lines try to orient in the direction opposite to the applied field because of the field on the surface of the sample. Since the microwave

induced current is perpendicular to the applied field, these flux lines experience maximum Lorentz force when they are oriented fully. Thus absorption increases with the increase in the applied field as more and more number of flux lines involve in the process of orientation. Therefore, normal microwave absorption alone is observed. Hence, from the present MWA study, one can rule out the vortex-antivortex pair formation leading to the PME.

Qualitatively, the assumption of the existence of the spontaneous orbital currents and the associated fluxes is enough to explain the present experimental observation. With regard to the microscopic origin of π junction in GdBCO powder, one possibility is that Gd^{3+} ion acts as magnetic impurity thereby forming a π junction, if there is tunneling. Another possibility is Cu^{2+} itself acting as impurity. In GdBCO powder the broad transition (Fig. 5) is due to oxygen deficiency and the oxygen content may vary from O_7 to $O_{6.6}$. The oxygen sites associated with the deficiency are the chain oxygen atoms in the charge reservoir layer [23]. The dominant effect of this variation in oxygen content is to change the oxidation state of chain copper atoms. And hence there is always a possibility of a finite concentration of impurity Cu^{2+} ions with local moments (unpaired spins). In powder particle with randomly oriented grains the supercurrent that flows through Cu-0 planes may be compelled, because of alignment of two adjacent grains, to tunnel across the chains containing the local moments Gd^{3+} and/or Cu^{2+}, forming a π junction.

Yet another possibility for π junction formation is the grain boundary contact of unconventional pairing, $d_{x^2-y^2}$ [17-19]. In this case the internal phases of the order parameter which depend on the relative orientation of the two grains in contact de-

termine the sign of J_c, so that for some particular orientations $J_c < 0$, thus forming a π junction. Though our experimental results give evidence to the existence of π junctions in powder sample, it is not clear whether they originate due to paramagnetic impurities or $d_{x^2-y^2}$ symmetry expected in HTSCs. Estimation of the strength of paramagnetism or in-phase signal for both impurity moment and $d_{x^2-y^2}$ symmetry considerations of the π junction may be considered important to resolve the ambiguity and for further understanding of this aspect. In summary, we have presented here the results of experimental study of anomalous microwave absorption in GdBCO powder. The analysis of field and temperature dependence allows us to conclude that the anomaly in the microwave absorption has a common origin with the PME and is caused by the presence of π junctions in the sample. It is suggested that microwave absorption is a better tool to investigate the π junctions in the superconductors. Thermally induced vortex-antivortex pair formation or the compressed flux cannot account for the anomalous microwave absorption and hence are ruled out as a possible mechanisms for the paramagnetic Meissner effect.

References

[1] P.Svedlindh, K.Niskanen, P.Norling, P.Nordblad, L.Lundgren B.Lonnberg and T.Lundstrom, Physica C, **162-164,1365** (1989).

[2] **W.** Braunisch, **N.Knauf, V.Kataev,** S.Neuhausen, A.Grutz, **A.Kock B.Roden,** D.Khomskii **and** D.Wohlleben Phy. Rev. Lett. **68,1908** (1992).

[3] W. Braunisch, N.Knauf, G.Bauer, A.Kock, A.Becker, B.Freitag, A.Grutz, V.Kataev, S.Neuhausen, B.Roden, D.Khomskii and D.Wohlleben Phy. Rev. **B,48,** 4030 (1993).

[4] B.Schliepe, M.Stindtmann, I.Nikolic and K.Baberschke, Phy. Rev B **47,** 8331 (1993).

[5] S.Thoming, J.Kotzler, M.W.Pieper and A.Spirgatis, Verh. Dtsch. Phys. Ges. VI 27, 912 (1992).

[6] N.Knauf, W.Braunisch, G.Bauer, A.Kock, A.Becker, **B.Freitag, V.Kataev, B.Roden and** D.Khomskii, Physica **B 1940196,** 2229 (1994).

[7] W.H.Lee, Y.T.Huang, S.W.Lu, K.Chen and P.T.Wu, Solid State Commun. 74, 97 (1990).

[8] S. Riedling, G.Brauchle, R.Lucht, K.Rohberg, H.V.Loneysen, H.Claus, A.Erb and G.Muller-Vogt, Phys Rev B 49, 13283 (1994).

[9] M.D.Lan, J.Z.Liu and R.N.Shelton, Phys. Rev B 43 12989 (1991).

[10] **Yusheng He,** C.M.Muirhead and W.F.Vinen, Phys **Rev B,53,12441** (1996).

[11] D.Khomski, J. of Low Temp. Phys, 95, 205 (1994).

[12] D.X.Chen and A.Hernando, Europhys. Lett, 26, 365 (1994).

[13] D.Dominguez, E.A.Jagala and C.A.Balserio, Phys. Rev. Lett, **72,** 2773 (1994).

[14] F.V.Kusmartsev, J. Superconductivity, 5,463(1992).

[15] F.V.Kusmartsev, Phys Rev. Lett. 69, 2268 (1992).

[16] L.N. Bulaevskii, V.V.Kuzii and A.A.Sobyanin, JETP Lett.25, 290 (1977).

[17] M.Sigrist and T.M.Rice, J. Phys. Soc. Jpn.**61**, 4283(1992).

[18] M.Sigrist and T.M.Rice, Rev of Modern Phy, 67, 503 (1995).

[19] V.B.Geshkenbein et al. JETP Lett 43, 395 (1986).

[20] Ch.Heinzel, Th. Theilig and P.Ziemann, Phys Rev **B,** 48,3445 (1993).

[21] S.V.Bhat, A.Rastogi, N.Kumar, R.Nagarajan and C.N.R.Rao, Physics **C,219**, 87 (1994).

[22] R.J.Cava, A.W.Hewat, E.A.Hewat, B.Batlogg, M.Marezio, K.M.Rabe J.J.Krajewski,W Jr, L.W.Rupp Jr, Physica C, **165,** 419 (1990).

[23] J.D.Jorgensen, Physics Today, 34, June (1991).

[24] P.V.Patanjali, V.Seshu Bai, R.M.Kadam and M.D.Sastry, (unpublished).

[25] L.N.Bulaevskii, M.Ledvij and V.G.Kogan, Phys. Rev. Lett. 68, 3773 (1992).

[26] A.E.Koshelev and A.I.Larkin, Phys. Rev. **B,** 52, 13559 (1995).

Chapter6

TEMPERATURE AND FIELD DEPENDENCE OF RADIO FREQUENCY SHIFT OF HTSCs

6.1 Introduction

While there have been numerous studies of the HTSCs using traditional probes such as magnetization, specific heat, tunneling, resistivity, etc. there have been relatively few which directly probe the order parameter and dynamics of vortices. The behavior of penetration depth is an area of much investigation in HTSCs as it is expected to reflect the order parameter symmetry of the wave function [1-3]. Moreover, the measured effective penetration depth reflects the pinning, flux creep and flux flow contributions to the vortex dynamics in the mixed state [4]. With the idea of studying the penetration depth and surface reactance of HTSCs as a function of field and temperature at radio frequencies, we have built a marginal oscillator (detailed description of the construction of the oscillator is given in chapter 2). The frequency change of the oscillator as temperature or field is varied is expected to give information on these two parameters [5-7]. This technique has been validated through precise measurements in the cuprate superconductors of the non-linear Meissner effect and of vortex parameters such as H_{c1} and pinning force constants [7,8]. In this chapter the results of frequency shift of various HTSCs are presented. The difficulties that arise when the present technique is used to determine the penetration depth or surface reactance of granular HTSCs and the possible analysis of frequency shift taking into consideration the kinetic and geometric inductances are also discussed.

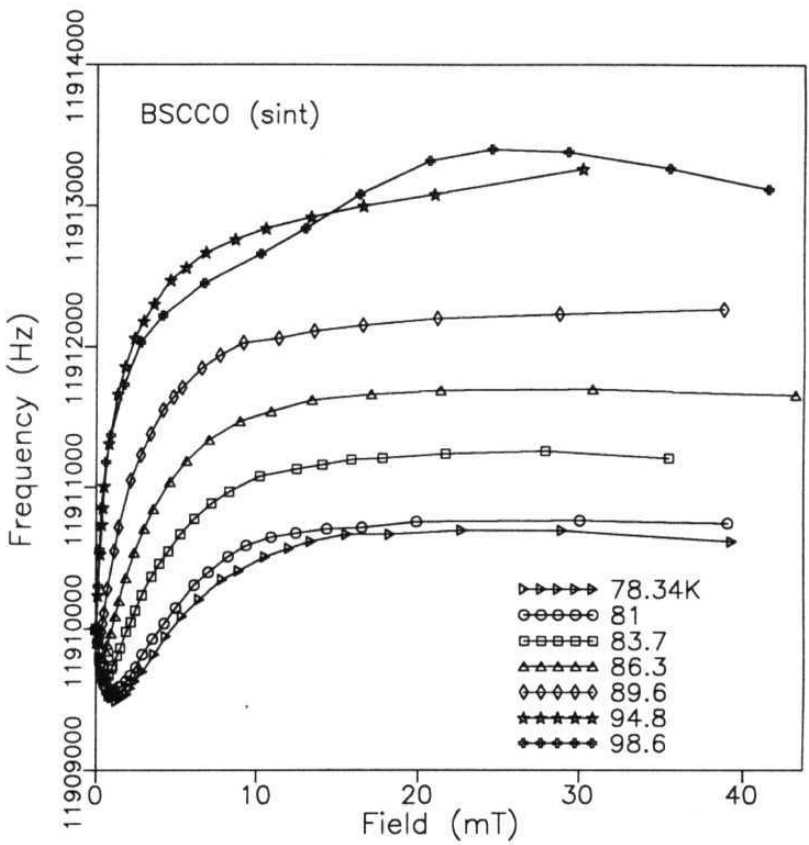

Fig. 1a. Frequency variation with field of sintered BSCCO pellet at various temperatures.

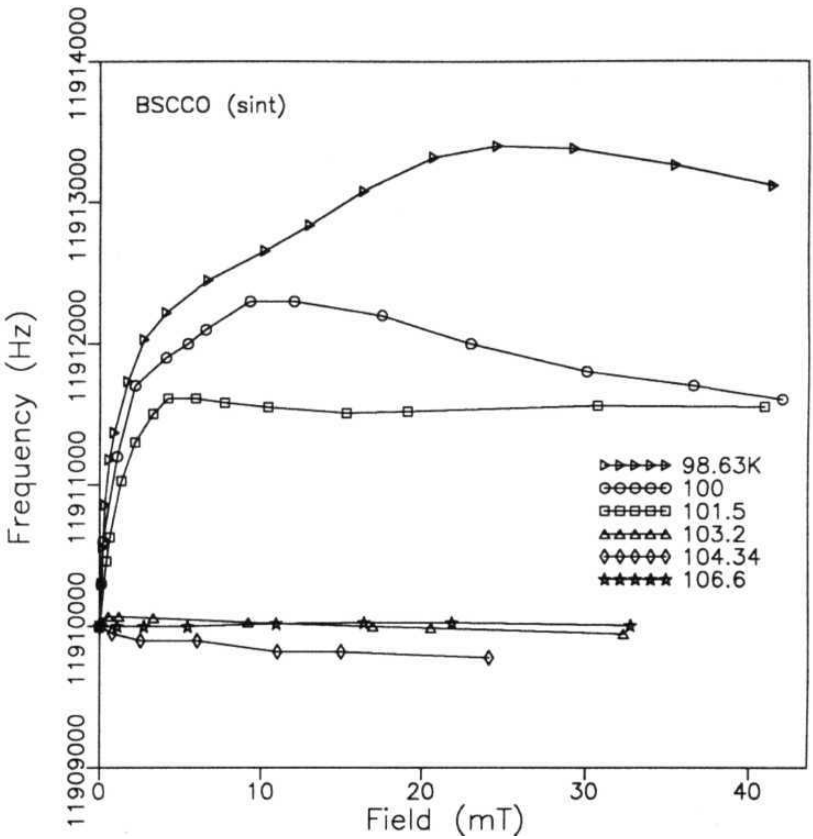

Fig. 1b. Frequency variation with field of sintered BSCCO pellet at various temperatures.

6.2 Experimental

For the present study the marginal oscillator described in chapter 2 is used. The change in frequency is monitored by a counter from the signal sensed across the tank coil using a pick up coil assembly. The samples used are sintered and press sintered BSCCO, and sintered and melt textured GdBCO and sintered DyBCO. Preparation of these samples is given in chapter 2. Virgin field induced frequency shift is recorded after cooling the samples to a required temperature below T_c in zero field .

6.3 Results

Figs. 1 (a) and (b) show the frequency shift of the oscillator when the field is increased from 0 to about 40 mT. The field induced frequency shift is recorded between 77K and T_c = 106.6K. It is to be noted that at low temperatures (T < 89.6K) (Fig. la) the frequency initially decreases and starts increasing at a characteristic field H_p, the full penetration field (the justification of H_p is discussed in the next section). At higher fields the change in the frequency saturates. At higher temperatures (T > 89.6K) the frequency increases monotonically (no decrease is observed) and saturates at higher fields. At still higher temperatures (Fig. 1b) the frequency can be seen to be decreasing again. And it continues upto the temperature 104.3K above which no change in frequency is observed at any magnetic field. The corresponding field at which the frequency starts decreasing second time is considered the H_{c1g} of the grains.

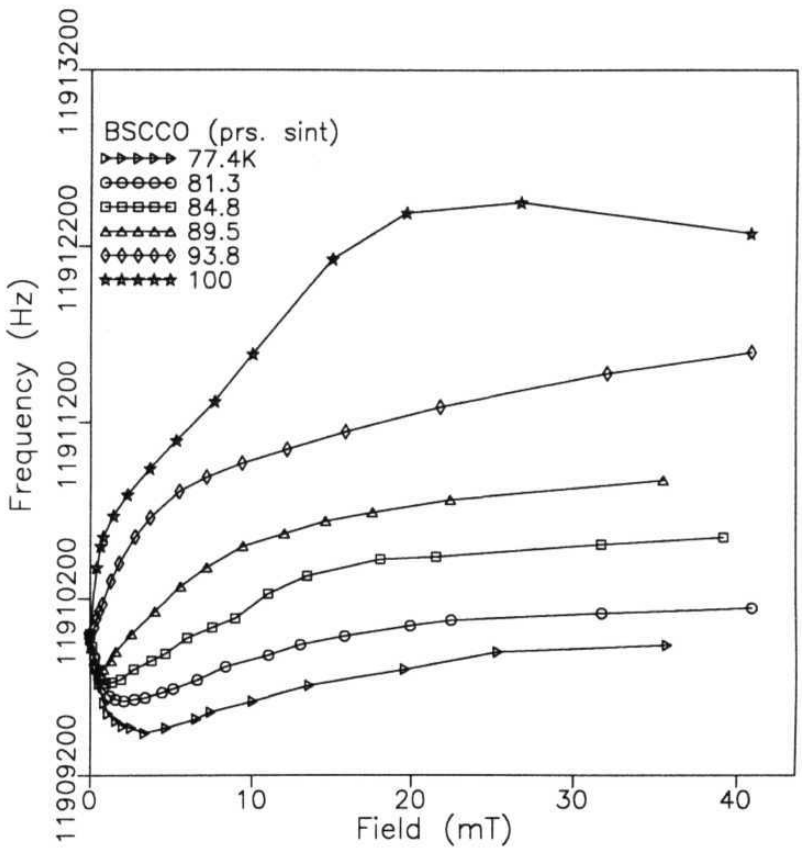

Fig. 2a. Frequency variation with field of press sintered BSCCO pellet at various temperatures.

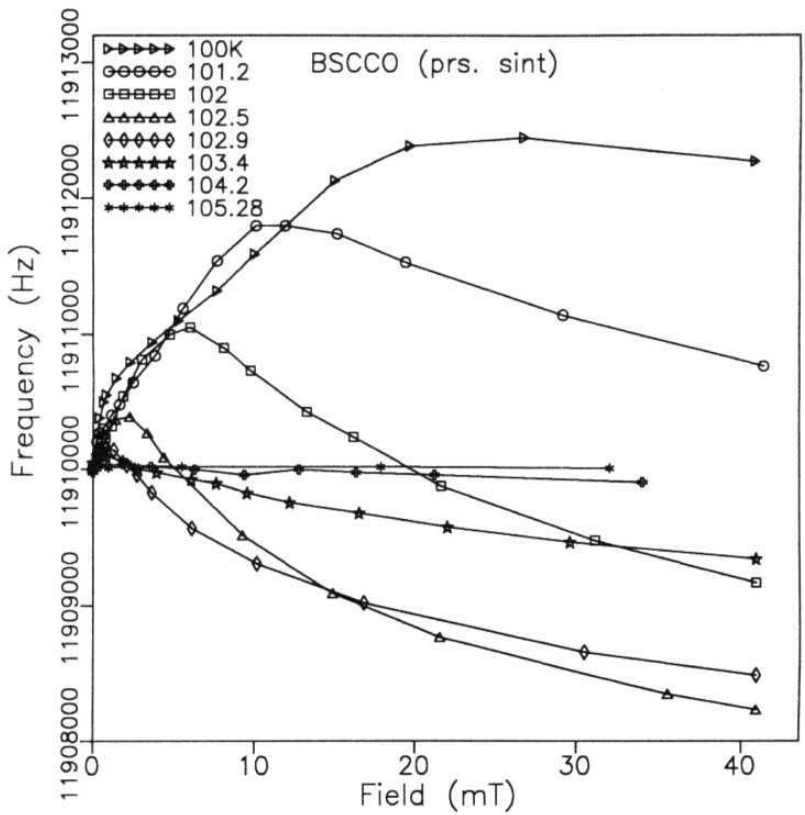

Fig. 2b. Frequency variation with field of press sintered BSCCO pellet at various temperatures.

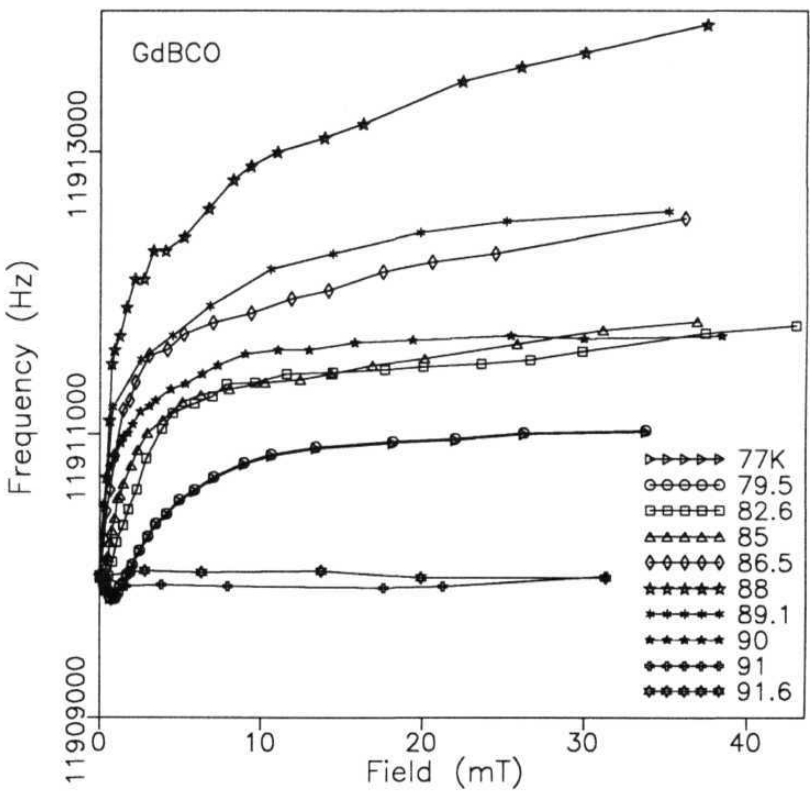

Fig. 3. Frequency variation with field of sintered GdBCO pellet at various temperatures.

In Figs. 2 (a) and (b), and 3 the frequency shift as a function of field of press sintered BSCCO and sintered GdBCO are shown, respectively. The salient features of these curves are almost same as that of sintered BSCCO, described above. However, in the case of GdBCO (Fig. 3) the decrease in frequency at higher temperatures is not observed.

Fig. 4 shows the change in frequency of the sintered BSCCO through the transition at various field cooled states. It can be seen that when H=0 mT as the temperature is increased the frequency initially increases, forms a peak and decreases rapidly above T=103K. The transition temperature of the sample is determined from the intersection of the extrapolated regions in the superconducting and normal states. The T_{cf}^{rf} is determined to be 107K which is found to be equal to the T_{cp}^{rf} determined from the power absorption measurement [chapter 3]. It is worth noting that while the change in power absorption in the normal state just above T_{cp}^{rf} is minimal [chapter 2], the decrease in frequency above T_{cf}^{rf} is unusual. Such a decrease in frequency above the transition is not observed in ReBCO samples (Figs. 5 and 6). Another noteworthy feature is the second peak observed when the frequency change through transition is recorded in the presence of field (inset Fig. 4). It can be seen that the second peak shifts to lower temperatures at higher fields.

The frequency shift of sintered pellet, powder and melt textured GdBCO through the transition is shown in Fig. 5. In the case of melt textured and powder samples the frequency decreases as the temperature is increased through transition. Melt textured sample shows a sharp transition to normal state while powder sample shows a broad transition extending upto 80K. But, the pellet sample shows an unusual frequency

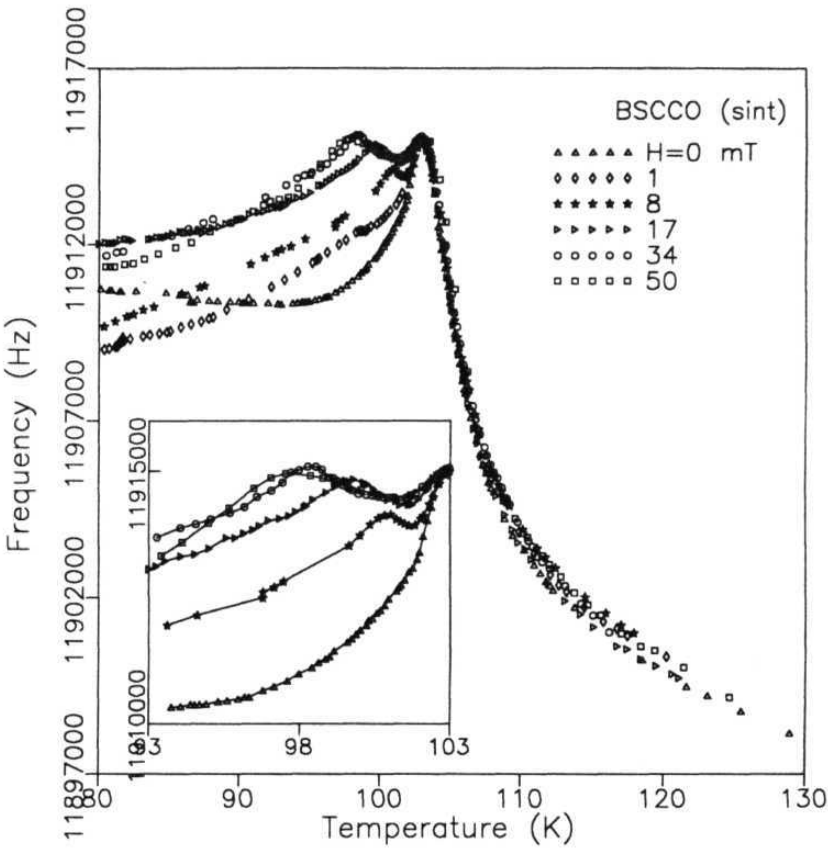

Fig. 4. Temperature dependence of frequency of sintered BSCCO sample in various field cooled states. In the inset a small portion of the response below the 'first peak' is shown.

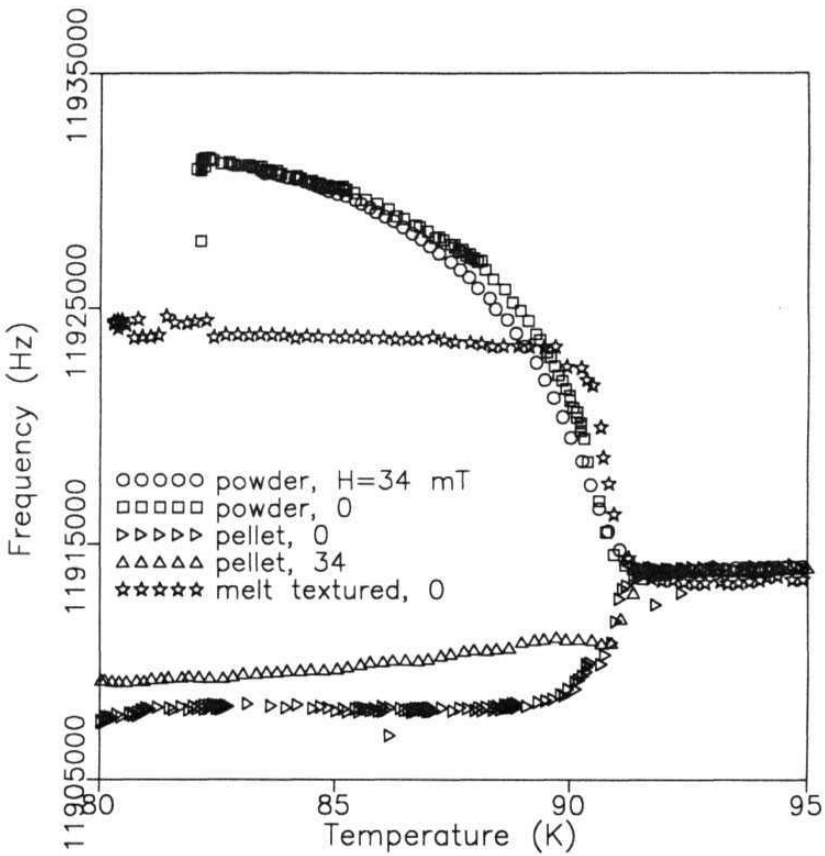

Fig. 5. Temperature dependence of frequency of sintered, powder and melt textured GdBCO samples in the ZFC and FC states.

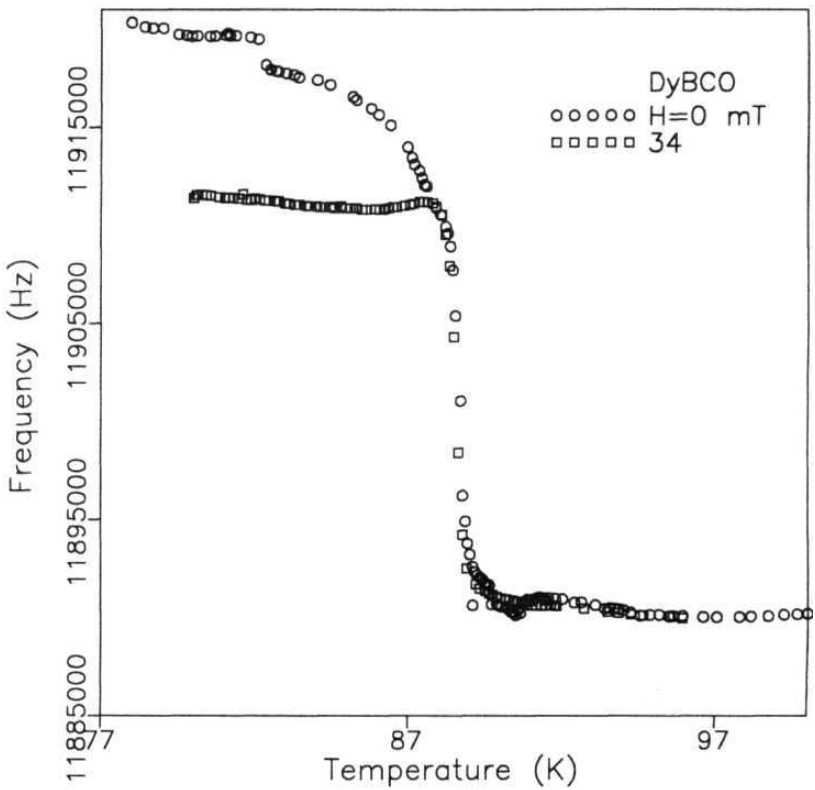

Fig. 6. Temperature dependence of frequency of sintered DyBCO sample in ZFC and FC states.

increase as the temperature is increased. In the case of powder sample there is no difference in the frequency change in ZFC and FC (H=34 mT) states. However, in the case of pellet frequency change through the transition is reduced in the FC state as shown in the Fig. 5.

Fig. 6 shows the decrease in frequency as the temperature is increased, in the ZFC and FC states of DyBCO sintered pellet. As in the case of GdBCO pellet the change in frequency in the FC state of DyBCO also is reduced when compared to that of the ZFC state, but point here to note is the opposite response of DyBCO pellet when compared to GdBCO pellet.

6.4 Analysis and Discussion

Estimation of penetration depth

In chapter 2 it has been shown that the radio frequency penetration depth can be determined from the frequency shift of the oscillator. With the change in temperature and magnetic field the inductance of the coil changes which reflects as a change in the resonant frequency. When there is no sample the inductance of the coil having area $A_c (\pi r_c^2)$ and length 1 is given by

$$L_0 = N^2 A_c \mu_0 / l$$

N is the number of turns of the coil. In the superconducting state the sample becomes diamagnetic which effectively reduces the area occupied by the flux. At $T < T_c$ the inductance of the coil with sample inside is given by

$$V = N^2 \mu_0 A_{eff}/l$$

where $A_{eff} = \pi r_c^2 - \pi[r_s - \lambda(T,H)]^2$, r_s is the radius of the sample **and** $X(T)$ is the rf penetration depth- Therefore,

$$\frac{L' - L_0}{L_0} = \frac{\Delta L}{L_0} = \frac{2\pi r_s \lambda - \pi r_s^2}{A_c}$$

where, $AL = L_s(T, H)$ is the inductance of the sample. Change in inductance with temperature or magnetic field is

$$\frac{L_{s1} - L_{s2}}{L_0} = \frac{L_1' - L_2'}{L_0}$$

The resonant frequency shift δf is given by

$$\frac{\delta f}{f_0} = -\frac{\delta L}{2L_0}$$

Therefore, the change in the penetration depth can be written as

$$\delta\lambda = -G\frac{\delta f}{f_0} \tag{1}$$

where, $G = A_c/4\pi r_s$, is the geometric factor. From the SX change in the rf reactance, δX_s can be determined by

$$\delta X_s = \mu_0 \omega \delta\lambda. \tag{2}$$

Using the above Eqs. by monitoring the change in the radio frequency, change in the penetration depth and rf reactance of a uniform superconductor can be determined. In the case of granular HTSCs which comprise of both inter and intra grain regions,

the value of r_s changes dramatically as a function of temperature or magnetic field. At low temperatures and in the absence of field, the rf currents pertain to the surface of the sample through the screening depth. When the field or temperature is increased grains get decoupled therefore rf field enters the intergrain region. In such a case the r_s changes from the radius of the sample to the average grain radius. To account for the change in r_s and the random local fields one has to invoke critical state models, which needs a detailed study.

From Eqs. 1 and 2 it can be said that an increase in frequency reflects a decrease in A and X_s and vice versa provided r_s and hence the geometry factor G are unchanged. Therefore, the initial decrease in frequency in Figs. 1,2 and 3 suggests an increase in the penetration depth as a function of field. However, the strong increase which continues upto about 20 mT seems to suggest a decrease in the penetration depth, which is not expected. The paradox is due to the change in r_s as described above. In the initial stages when there is coupling between the grains, the r_s keeps reducing with the increase in the field. When all the junctions are decoupled the field enters to the centre of the sample. Thus the initial points of inflection in Fig 1,2 and 3 possibly represent $H_p(T)$,full penetration field. In the same way the decrease in frequency at higher temperatures (Figs. 1b and 2b) may represent H_{c1g} beyond which penetration into the grain increases with field.

The second peak observed in the temperature dependent frequency change of BSCCO (Fig. 4) is due to intergranular effects and the change in the r_s as the sample is cooled below the transition. To understand the frequency change observed when the sample is cooled in the absence of field we propose a qualitative picture. If converted

into penetration depth the frequency change represents a negative λ_{eff} variation. The λ_{eff} which initially decreases through transition, appears to be increasing in the tail region as the sample is cooled. The temperature dependence of measured λ_{eff} can possibly be accounted by defining

$$\lambda_{eff}(T) \propto [A(T)\lambda_G(T) + B(T)\lambda_J(T)]$$

where, $\lambda_G(T)$ and $\lambda_J(T)$ are the grain and Josephson penetration depths, and A(T) and B(T) are the fractions of the intra- and inter grain superconducting regions. As the temperature is decreased, just below the onset of the transition grains alone become superconducting. At this stage the sample, even though a sintered pellet, is in a state of virtual powder with decoupled grains and $\backslash G(T)$ determines the change in $\lambda_{eff}(T)$ So one observes a decrease in the λ_{eff}. However, as the temperature is lowered further the coupling between the grains starts establishing making the quantity B(T) increase rapidly. It is this increase in B(T) which gives rise to the increase in λ_{eff} at lower temperatures.

The sintered GdBCO shows a frequency decrease when cooled to below the transition as shown in Fig. 5. However, the decrease in frequency starts at the onset of the transition and continues (Fig. 5), unlike the BSCCO where it starts in the tail region of the transition. The fact that such an anomalous decrease is not observed in GdBCO powder and melt textured samples (Fig. 5) suggests that it is probably associated with the Josephson currents, which are predominant in GdBCO pellet. This anomaly may be thought to be arising from the interaction of Josephson currents with the Gd^{3+} paramagnetic moments. However, the usual frequency increase observed in the case of *DyBCO* (Fig. 6), which also contains strong Dy^{3+} paramag-

netic moments, complicates the understanding of such an anomalous feature. At this stage it is not understood why GdBCO sintered sample alone shows such an anomaly among all the samples studied.

The Josephson coupling between the grains can be modeled by the standard resistively shunted junction picture [9-13]. In this model the kinetic inductance is given by $L_k = \mu_0\lambda^2$ and the geometric inductance by $L_g = \hbar/2eJ_c$. The inter and intra grain inductances, which have contributions from both L_k and L_g, play a crucial role in determining the total sample inductance. As the frequency change of the oscillator basically reflects the inductance change of the sample in the coil, the results reported in this chapter could as well be be due to an interplay of the various inductances and their variation with temperature and magnetic field. Remillard *et. al* [14] have studied the surface reactance at microwave frequencies on thin films and sintered pellets. The X_s variation with field of YBCO pellet is similar to that observed in our samples. But, in their study, no detailed independent analysis X_s is presented.

Though the results of frequency shift of various HTSCs presented in this chapter can be qualitatively explained to some extent by the interpretations given above, a rigorous analysis taking into account the critical state models and/or kinetic and geometric inductances is needed to fully comprehend all the subtle features. Further work in that direction is in progress.

References

[1] S.K.Yip and J.A.Sauls, Phys. Rev. Lett. 69, 2264 (1992)

[2] A.Maeda, Y.Lino, T.Hanaguri, N.Motohira, **K.Kishio and T.Fukase,** Phys. Rev. Lett. **74,** 1202 (1995)

[3] L.Drabeck, J.PCarini, G.Gruner, T.Hulton, Phys. Rev **B,** 39 785 (1989)

[4] M.W.Coffey and J.R.Clem, IEEE Trans. Magn. 27, 2136(1991)

[6] A.Omari and A.F.Khoder, Cryogenics **33,** 1098 (1993)

[5] A.L.Shalow and G.E.Devlin, Phys. Rev. **B, 113,** 120 (1959)

[7] S.Sridhar, D.H. Wu and W.L.Kennedy, Phys. rev. Lett. 63, 1873 (1989)

[8] D.H.Wu and S.Sridhar, Phys. Rev. Lett. 65, 2074 (1990)

[9] M.Tinkham and J.C.Lobb, Solid State Physics, 42, ed H.Ehrenreich and D.Turnbull, Academic Press, p. 91 (1990)

[10] F.Auracher and T.van Duzer, J. Appl. Phys. 44, 848 (1973)

[11] T.L.Hylton, A.Kapitulnik, M.R.Beasley, J.PCarini, L.Drabeck and G.Gruner, Appl. Phys. Lett, 53, 1343 (1988)

[12] T.L.Hylton and M.R.Beasley, Phys. Rev. **B,** 39, 9042 (1987)

[13] M.Hein, H.Piel, M.Strupp, M.R.Trunin and A.M.Portis, J. MMM **104-107** , 529 (1992)

[14] S.K.Remillard, M.E.Reeves, F.J.Rachford and S.A.Wolf, J. Appl. Phys. 75, 4103 (1994)

Chapter 7

CONCLUSIONS

The high T_c cuprate superconductors are highly anisotropic, layered type II superconductors with very short coherence lengths of the order of cell dimensions. This makes it possible for the ceramic samples to have a variety of inter- and intra grain defects which form weaklinks in these superconductors. The presence of such extrinsic but ubiquitous weaklinks makes the high frequency electromagnetic response of these materials very sensitive to the applied field and temperature. The loss that arises from such weaklinks is not fully understood yet. High frequency loss poses a serious hindrance to the technical applications of these materials. Interestingly, some of the intriguing, but unsolved, problems of HTSCs such as paramagnetic Meissner effect, order parameter symmetry, etc. could actually be understood by studying weaklinks as these properties are reflected in the unavoidable weaklinks in HTSCs. Therefore, a detailed study of weaklinks at high frequencies and vortex dynamics is essential both for scientific and technological points of view. In this thesis a detailed study of HTSCs is carried out at radio and microwave frequencies. The important conclusions that can be drawn from the work presented in chapters 2,3,4,5 and 6 are given here.

The construction of a marginal oscillator is described in chapter 2. Stable oscillations are obtained by feeding the output of the oscillator to a FET amplifier in common drain configuration, which also decouples the possible interdependence of power output and frequency. To accommodate samples of various sizes and densities a coil with varying pitch is designed. It is shown that the marginal oscillator can be

effectively used to study the radio frequency absorption, penetration depth and reactance as a function of temperature and magnetic field. The magnetically modulated radio frequency technique is developed in analogy with the MAMMA technique at microwave frequencies. This technique though more sensitive than the direct power absorption suffers from a few disadvantages and can be effectively used to detect the superconducting phase transitions.

In chapter 3 a detailed study of radio frequency (MHz) absorption in sintered BSCCO and GdBCO has been presented. It is found that London's two fluid equation for surface resistance fits very well to the experimental temperature dependent absorption in both BSCCO and GdBCO superconductors. The large effective penetration depth determined is explained in terms of reduced superelectron screening and contributions from both grain and Josephson penetration depths. The reduction factor of screening at MHz is found to be an order of magnitude larger than that at GHz frequency. The temperature variation of absorption has contributions from both inter- and intra grain regions. However, in the case of field induced absorption at low fields most of the response comes from the intergrain region.

The RSJ model presented has been shown to describe the magnetoabsorption data of BSCCO very well. In the case of BSCCO it is found that the magnetoabsorption originating from the decoupled junctions seems to be less appropriate. The higher values of the parameters of the RSJ model, $\alpha(t), \beta(t)$ and $H_0(t)$ at rf suggest that a much larger number of weaklinks participate at rf than that at microwave frequency. It is found that flux flow losses are absent at low fields in this sample. The present results when compared to the magnetoabsorption at microwave frequency suggest

that the weaklinks operative at rf are much different from that at 9.98 GHz. The junctions responsible for absorption at rf are found to be of SIS type. It is suggested that magnetoabsorption in BSCCO gives an indirect estimate of the critical Josephson current variation.

Field dependence of radio frequency absorption in sintered GdBCO sample at low fields shows a slightly different response when compared to the BSCCO and can best be described in terms of a combined response from both the RSJs and decoupled junctions. The loss arising from flux flow due to depinnig of the vortices at high frequencies and temperatures is not seen in this sample. The high temperature linear magnetoabsorption is attributed to the strongly coupled weaklinks which might be operative in the intragranular region.

The field induced microwave absorption (GHz) study on both sintered and melt textured samples of GdBCO, and sintered and press sintered BSCCO is presented in chapter 4. At low fields, as in the case of rf absorption, microwave absorption in sintered samples is also found to be describable by the Josephson junction model. Melt textured samples are found to show no measurable change in absorption in low fields which suggests that intergranular weaklinks are greatly reduced in these samples due to melt processing. The high field absorption is explained using the flux flow model. Though the depinnig frequency in HTSCs is higher than the present frequency used, 9.9 GHz, a fraction of the fluxons do get depinned due to proximity to the depinning frequency. However, thermally assisted flux flow seems to be a major source of loss compared to the depinnig of the fluxons by the high frequency currents in the samples studied. At low temperatures since thermally assisted flux flow is absent no increase

in the field induced loss is observed. The phenomenological model described in the literature is used to simulate the high field loss and it is found to fit very well to the experimental observations.

In the case of melt textured **GdBCO** samples **with varying 211 percentages,** it **is found** that the change in loss with field decreases with **the increase in the 211** percentage, at 77K. This is explained in terms of an increase in the number of flux pinning centres with an increase in the 211 percentage. The Pinning force constant and the J_c are determined for all the HTSCs studied from the activation energy, which is obtained from the fit to the flux flow model. The values of these two parameters are found to match with those determined from the magnetization measurements.

While there have been very few reports on the paramagnetic Meissner effect there have been fewer reports on the anomalous microwave absorption which is associated with π junctions and the paramagnetic Meissner effect (PME). In chapter 5 the results of field modulated microwave absorption (FMMWA) of GdBCO pellet and **powder** are presented . The signature of the π junctions is observed in GdBCO powder as anomalous microwave absorption. The absence of anomalous in-phase signal (with reference to Gd^{3+} EPR signal) of the FMMWA in GdBCO pellet is explained to be the result of overshadowing of the π junction response by a very strong dissipation in the normal Josephson junctions. The phase change observed in the FMMWA of GdBCO powder as a function of temperature gives evidence for a change in the behavior of π junctions from para to dia state. The intragrain weaklinks with high J_c **are** likely to be forming π junctions in the powder sample.

It has been suggested that high frequency absorption techniques make a better tool to investigate the π junctions in superconductors owing to their high sensitivity when compared to conventional magnetization measurements. The phenomena of thermally induced vortex-antivortex pair formation and flux compression due to inhomogeneous cooling may not be the right pictures to explain the origin of the PME as the flux trapping that is resulted by them does not give rise to anomalous microwave absorption. A cross check should be made, on samples that show the PME in magnetization measurements, using the FMMWA to say anything conclusive about the yet unsolved problem of the PME. In the wake of the on going controversy regarding the order parameter symmetry in HTSCs, whether it is the conventional s-wave or the unconventional $d_{x^2-y^2}$, the origin of the PME need be understood fully. Whatever is the mechanism eventually proved to be it has tremendous importance in solving the long standing problems related to vortex dynamics or order parameter symmetry.

The changes in frequency of the oscillator as a function of temperature and magnetic field when the tank coil of the oscillator is loaded with different HTSCs are presented in chapter 6. From the frequency shift, it is shown that, one can determine penetration depth and rf reactance of HTSCs. The difficulties that arise when this technique is used to determine penetration depth of sintered HTSCs are discussed. It has been observed that for all the samples studied the frequency increases when the sample is cooled to below its transition temperature. A decrease in frequency is observed in the tail region of the transition in the case of BSCCO sintered sample which is explained to be the result of an interplay between grain and Josephson penetration depths, and fractions of inter and intragrain regions. The anomalous decrease in the

frequency observed in the case of sintered GdBCO pellet as the sample is cooled to below its transition temperature could be due to an interaction of Gd^{3+} moments with the Josephson currents and needs further study since DyBCO does not exhibit such an anomaly. It is suggested that a detailed study is needed to comprehend all the features seen in the frequency variation as a function of temperature and magnetic field of the HTSCs studied.

List of Publications

Journals

1) Virgin response of field induced microwave absorption in the BSCCO HTSC-RSJ model
V.Seshu Bai, P.V.Patanjali and S.M.Bhagat
Solid state Commun. 90, 809 (1994).

2) Microwave magnetoabsorption - virgin curves, hysteresis and random fields in BSCCO
V.Seshu Bai, P.V.Patanjali, S.M.Bhagat and S.Tyagi
J. of Supercon. 8, 299 (1995).

3) rf surface impedance in BSCCO and melt textured YBCO superconductors
P.V.Patanjali and V.Seshu Bai
To appear in IEEE Trans. on Appl. Supercon.

4) Observation of paramagnatic Meissner effect in GdBCO powder - a microwave absorption study
P.V.Patanjali, V.Seshu Bai, R.M.Kadam and M.D.Sastry
To appear in the proceedings of the International symposium on Advances in Superconductivity - Materials, Critical currents and Devices, Sep. 17-21, 1996, TIFR, Mumbai, India.

5) Field and temperature dependence of radio frequency (MHz) absorption of BSCCO superconductor
P.V.Patanjali, V.Seshu Bai
Submitted to Physics C.

6) Anomalous microwave absorption in GdBCO powder: π junctions and the paramagnetic Meissner effect
P.V.Patanjali, V.Seshu Bai, R.M.Kadam and M.D.Sastry
Submitted to Phys. Rev B.

7) Weaklink response to the rf (MHz) absorption in GdBCO superconductor
P.V.Patanjali and V.Seshu Bai
Submitted to Physica C.

8) Field induced microwave absorption in HTSC - determination of pinning force and critical current
P.V.Patanjali, V.Seshu Bai, R.M.Kadam and M.D.Sastry
Submitted to Superconductor Sci. and Technol.

9) rf margial oscillator for surface impedance measurements of superconductors
P.V.Patanjali, N.Harish Kumar and V.Seshu Bai
To be communicated to Rev. of Sci. Instru.

10) Study of vortex dynamics in BSCCO and GdBCO from the radio frequency shift
P.V.Patanjali and V.Seshu Bai
In the preparation.

11) Anomalous frequency shift in GdBCO - Interaction of Josephson currents with the paramagnatic moments
P.V.Patanjali and V.Seshu Bai
In the preparation.

International Conferences

1) Marginal oscillator for measuring surface impedance of superconductors
P.V.Patanjali, N.Harish Kumar and V.Seshu Bai
14th World Congress on Nondestructive testing, Dec. 8-13, 1996, New Delhi, India (oral presentation)

2) Temperature and field dependent rf surface impedance in BSCCO and melt textured YBCO
P.V.Patanjaii and V.Seshu Bai
1996-Applied superconductivity Conference, Aug. 25-30, 1996, Pittsburgh, USA.

3) Observation of paramagnetic Meissner effect in GdBCO powder- a microwave absorption study
P.V.Patanjali, V.Seshu Bai, R.M.Kadam and M.D.Sastry
International symposium on ASMCCD, Sep 17-21, 1996, TIFR, Mumbai, India.

4) Observation of anomalous frequency shift in GdBCO - a study of radio frequency impedance
P.V.Patanjali and V.Seshu Bai
International Workshop on HTSC - 10 years after its discovery, Dec 17-22, Jaipur, India.

4) Study of flux pinning in HTSC using radio frequency absorption
P.V.Patanjali and V.Seshu Bai
Indo - US Workshop on Ordering Disorder Prospect and Retrospect in Condensed Matter Physics, Dec 29 1992 Jan 5 1993, Hyderabad.

5) Low field switching of hysteretic microwave magnetoabsorption in 110K phase

BSCCO superconductor
V.Seshu Bai, S.M.Bhagat, P.V.Patanjali and S.Ravi, Presented at the Applied Superconductivity Conference, 16-21 Oct 1994, Boston, USA.

National Conferences

1) Transport current density measurements in quench melt grown **YBCO samples**
P.V.Patanjali, C.S.Murthy, V.Seshu Bai, R. Gopalan and T.Rajasekharan
Proceedings of the DAE Solid State Physics Symposium, Vol 35C, pp 319, 1991.

2) Radio frequency absorption studies in BSCCO superconductor
P.V.Patanjali, N.Harish Kumar and V.Seshu Bai
Proceedings of the DAE Solid State Physics Symposium, Vol 37C, pp 372, 1994.